Wiesmair Sebastian Peter, BSc

# Megalithic Monuments in Styria

A Master Thesis
Submitted in Earth Sciences
At the Technische Universität Graz
Institut für Erdwissenschaften

Advisor:
Kurt Stüwe

# EIDESSTATTLICHE ERKLÄRUNG

Ich erkläre an Eides statt, dass ich die vorliegende Arbeit selbstständig verfasst, andere als die angegebenen Quellen/Hilfsmittel nicht benutzt, und die den benutzten Quellen wörtlich und inhaltlich entnommenen Stellen als solche kenntlich gemacht habe. Das in TUGRAZonline hochgeladene Textdokument ist mit der vorliegenden Masterarbeit identisch.

_____          _____

Datum                                                              Unterschrift

**Acknowledgements**

## Zusammenfassung

Das Gebiet rund um Vorau in der Oststeiermark/Österreich zeigt eine hohe Dichte an megalithischen Konstruktionen, die in Europa ihresgleichen sucht. Insbesondere liegt die Megalith Häufung von Vorau in einem Bereich Europas aus dem solche Bauwerke bislang praktisch unbekannt waren. Um eine gute Datenbank der Standorte zu erhalten, wurden vorhandene Daten aus früheren Kartierungen zusammengeführt und in einer Karte eingezeichnet. Danach wurden die Bereiche ohne Daten auf dieser Karte mit weiteren Kartierungen vervollständigt. Als Ergebnis wurde eine relativ vollständige Datenbank der Megalithvorkommen im Bereich Vorau entwickelt. Um das Aufstellungs-, oder Bearbeitungsalter der Menhire zu bestimmen wurde der Versuch unternommen das Expositionsalter ihrer Oberfläche mit Hilfe des kosmogen gebildeten Nuklids $^{10}$Be zu bestimmen. Dazu wurden insgesamt neun Proben von Menhiren und Abdeckplatten von Erdställen in zwei Probenahmedurchgängen genommen und dessen $^{10}$Be Gehalt gemessen. Die gemessenen Konzentrationen wurden auf die Endglieder Prozesse: (a) eines Expositionsalters und (b) einer Erosionsrate umgerechnet. Die Expositionsalter ergeben sich zwischen etwa 10000 und 55000 Jahren. Die berechneten Erosionsraten sind zwischen 12 m/Myr und 75 m/Myr. Die Expositionsalter korrelieren gut mit der letzten Eiszeit und könnten als eiszeitliches Auswittern der Gesteinsblöcke (aus denen die Menhire gebaut wurden) aus dem anstehenden Gesteinsverband interpretiert wird. Als Erosionsraten interpretiert korrelieren die gemessenen Werte gut mit anderen Messungen Holozäner Erosionsraten aus diesem Teil der Ostalpen. Im Prinzip könnten die Expositionsalter auch als Bearbeitungs- und Baualter der Menhire interpretiert werden. Jedoch wäre dies nur plausibel, wenn nachgewiesen werden könnte, dass die Menhire vor ihrer Aufstellung aus vielen Metern Tiefe unter der Oberfläche durch Menschen abgebaut wurden. Um diese Möglichkeit zu evaluieren und die Herkunft der Megalithen zu bestimmen, wurden einige Proben in Bezug auf ihre mineralogische Zusammensetzung und Textur untersucht, mit dem Elektronenmikroskop analysiert und diese Daten mit veröffentlichten petrologischen Beschreibungen der Gesteine der Umgebung verglichen. Der Vergleich zeigt, dass ein Ursprung der Menhire aus der näheren Umgebung wahrscheinlich ist (insbesondere aus dem Strallegg Komplex) und unterstützt daher eine Interpretation von natürlicher Bildung der Gesteinsblöcke aus denen die Megalithe gebaut wurden.

**Abstract**

The area around Vorau in eastern Styria/Austria features a high density of megalithic constructions, especially in Menhirs and Holed Stones. To obtain a database of their locations, existing data from earlier field mapping campaigns were collated and plotted on a map. After that, the areas without any data were complemented with further field mapping. As a result, a relatively complete database of the megalithic monuments in the Vorau region was developed. The database shows an uncommonly high density of Megaliths for this part of Europe. In an attempt to date the erection age of these monuments, their surface exposure was dated with the aid of the cosmogenic nuclide $^{10}$Be. A total number of nine samples of Menhirs and cover plates of subsurface tunnels were dated in two sampling runs. The measured $^{10}$Be concentrations were re-calculated to the inferred end member processes of: (a) an exposure age and (b) an erosion rate. The calculated exposure ages range between about 10000 and 55000 years. The calculated erosion rates are between 12 m/Myr and 75 m/Myr. The calculated exposure ages correlate well with the last glaciation period and may indicate the age when the Menhir blocks weathered from outcrop. Interpreted as erosion rates, the measured values correlate well with other measurements of Holocene erosion rates performed in this part of the Eastern Alps. The exposure ages can also be interpreted in terms of an erection age of the Menhirs. However, it is suggested here that this is only plausible, if the Menhirs were excavated and mined from at least several meters below the surface just prior to their erection by humans. In order to evaluate this possibility and to determine the origin of the megaliths, several samples were studied for their mineralogical composition and texture and analyzed by electron microscopy and these data were compared with published petrological descriptions of rocks from the region. The comparison shows that the origin of Menhirs is likely to be in the vicinity and is therefore consistent with an in situ formation of the rock boulders from which the Menhirs were built (in particular from the Strallegg Complex).

# 1. Introduction

Megalithic natural stones, which were used as a cultural symbol, were very common in prehistoric times. However, large stone monuments were also erected in medieval times for practical purposes and it is often not trivial to discern the difference. Today remnants of large stone monuments can be found in many parts of Europe and all over the world. However, knowledge of their existence in Austria is relatively new. One of the areas with the highest density of such stones is Vorau in the east of Styria. At the moment, there are very few scientific studies existing about this topic. The interest in this subject first started to get aroused with the work of Heinrich and Ingrid Kusch and the publication of their book "Tore zur Unterwelt" (2009). It was the beginning of a field mapping project that documented the distribution of these monuments in Styria. Location and other information about these Menhirs, Holed Stones and the connected subsurface tunnel*s* were collected by Dr. Heinrich and Ingrid Kusch and, later, by three Bachelor students of the University of Graz. An attempt to document the erection age of these megalithic monuments was made. The results of this work were used in the three Bachelor theses of this students and the book "Versiegelte Unterwelt" by Heinrich and Ingrid Kusch (2014). Because of this lack of scientific studies, I decided to write my Master's thesis about this topic. The intention of my work is to collect all the data from the existing field mappings of the scientists mentioned above, put them together, map the missing areas and develop a database of the locations. I also summarize in this thesis the attempts to measure the erection ages via cosmogenic isotopes method and present different possible interpretations of the results and discuss their plausibility. Finally, I present some mineralogical and petrological information on the Megaliths and compare this data to published geological information on rocks from the region.

## 2.1 Definition

The word "megalith" can be derived from the Greek words *mègas*: large and *líthos*: stone. So the translations "big stone" describes the basic architectural style of the constructions from this special kind of culture very well. Several kinds of arrangements of stones can be called megalithic construction. There are definitions for certain forms like: Menhir, *Alignement*, *Dolmen*, *Cromlechs* or *Monolith*:

**Menhir**

The word Menhir can be derived from the Breton words *men*: long and *hir*: stone. This translation "long stone" describes the basic design very well. In fact, a Menhir is an upright stone, which is longer than broad. This form is the most common megalithic construction. An important part of the definition is that the stone must be erected by humans. It cannot have formed naturally to be called Menhir. This restriction is the big difference to, for example, an erratic block from the last ice age. If just a single Menhir occurs, it is called *Monolith* after the Greek words *mono*: one and *lìthos*: stone (Kirchner, 1955). In German another common word for Menhir is *Hinkelstein*. With a height of 12 meters, the highest still standing upright Menhir is located near Plourazel in the west of Brest, Bretagne (Zylmann, 2008). But this height is an exception. In fact, the average size of a Menhir is between two and four meters (Teichmann, 1983).

**Alignement**

The word *Alignement* originates from the French language and describes a linear row, consisting of a minimum of three Menhirs. The height, thickness and morphology have no influence in the name of the construction. Due to the fact that the number of stones and the distance between them can vary, there are a lot of different possibilities how an Alignment could look like. In fact, two *Alignements*, which run parallel, are often connected to other

megalithic constructions and were used for example as a marker for a path (Teichmann, 1983).

**Dolmen**

The word *Dolmen* can be derived from the Breton words "*tol*" and "*men*" and means "table of stone". As the translated name suggests the construction looks like a table, which is built up of several upright anchored stones holding one or more cover stones. In fact, there are many varieties in size and number of the cover stones (Hoffmann, 2012).

**Cromlech**

Another construction is the Cromlech. This word can be derived from the Welsh words "*Crom*" which means crooked and "*llech*", which represents a flat and smooth stone. In fact, it means that in most cases five to sixty Menhirs are arranged in a circle, an oval or something in between. In some cases, one more Menhir or a flat-lying stone is placed in the middle of this circular construction (Teichmann, 1983; Habel, 1987).

## 2.2 History

Remnants of megalithic cultures are not just a regional phenomenon, but they are spread all over the world. Besides the famous constructions like *Stonehenge* in Wiltshire, England or the *Carnac Stones* in Bretagne, France, signs of this culture are found along much of northwest European coast from Portugal trough Spain to West-France, to the British Isles, the North-German lowlands, Denmark and even South-Sweden (Fig. 1). Other regions with remnants of this culture are: North-Spain, Apulia, Southern Greece, the Balearic Islands, Corsica, Sardinia, Sicily, Malta and Crete. But even outside of Europe, for example in the Middle East, North and West Africa, India, Japan, Oceania and America, megaliths can be found. Because of this worldwide distribution and their big varieties, it is assumed, that there existed more than just one megalithic culture (Biedermann, 1963; Korn, 2005).

Interpretations of the age and origin of the megalithic cultures are very often disputed in science (Akcar et al., 2008). Generally, it is assumed that this culture goes back to the Neolithic and the Bronze Age (Fig. 2). Through the results of the method of radiocarbon dating, it is believed that many of the European megaliths were set up before the temples of Mesopotamia and the Egypt pyramids were built. Furthermore, this interpretation excludes the idea of a centre from where the culture of megalithic constructions has spread out. The European megalithic culture is generally believed to have commenced in the 5th Millennium before present from the island of Malta to Ireland (Maier, 2005). As may be seen on Figure 1, the European megalithic monuments are known to have been built in two characteristic time periods. An older one, ranging roughly from 4800 - 3000 BC and a younger one, ranging roughly from 3000 - 1200 BC. From the independently constructed but very similar megaliths, it is concluded that all the megalithic cultures must have shared a similar economy and worldview (Maier, 2005).

It is assumed that tribes have left the front of the Orient around 6000 BC, due to scarcity of resources, leaving their home and spreading out over Europe. Traces on the Balkans leading across Europe from the Neolithic about 5500 BC were found. In 3500 BC the first settlement of megalithic cultures on the Danish islands started (Habel, 1987).

These megalithic cultures occur predominantly in Western Europe. Some regions in southern France, in the Bretagne, in south westernmost Spain and southwest England are known as the oldest centres of this culture. During the Bronze Age these cultures spread to larger regions of Europe.  But only in the west of a line reaching from the German Baltic Sea coast to Monaco (Fig. 2). On the east of this line only few remnants of the megalithic cultures occur in regions of Romania and Bulgaria. In the Alps, remnants of a megalithic culture only have been described in the Swiss foreland. In 2009 the discovery of a megalithic culture with several hundreds of Menhirs and associated subsurface tunnels in the eastern margin of the Alps around Vorau is therefore no less than a sensation (Fig. 1) (Kusch and Kusch, 2009). In view of this comparably recent discovery, it is therefore of large interest to document the time period in which they were erected and their connection to the prehistoric events of Austria (Fig. 2).
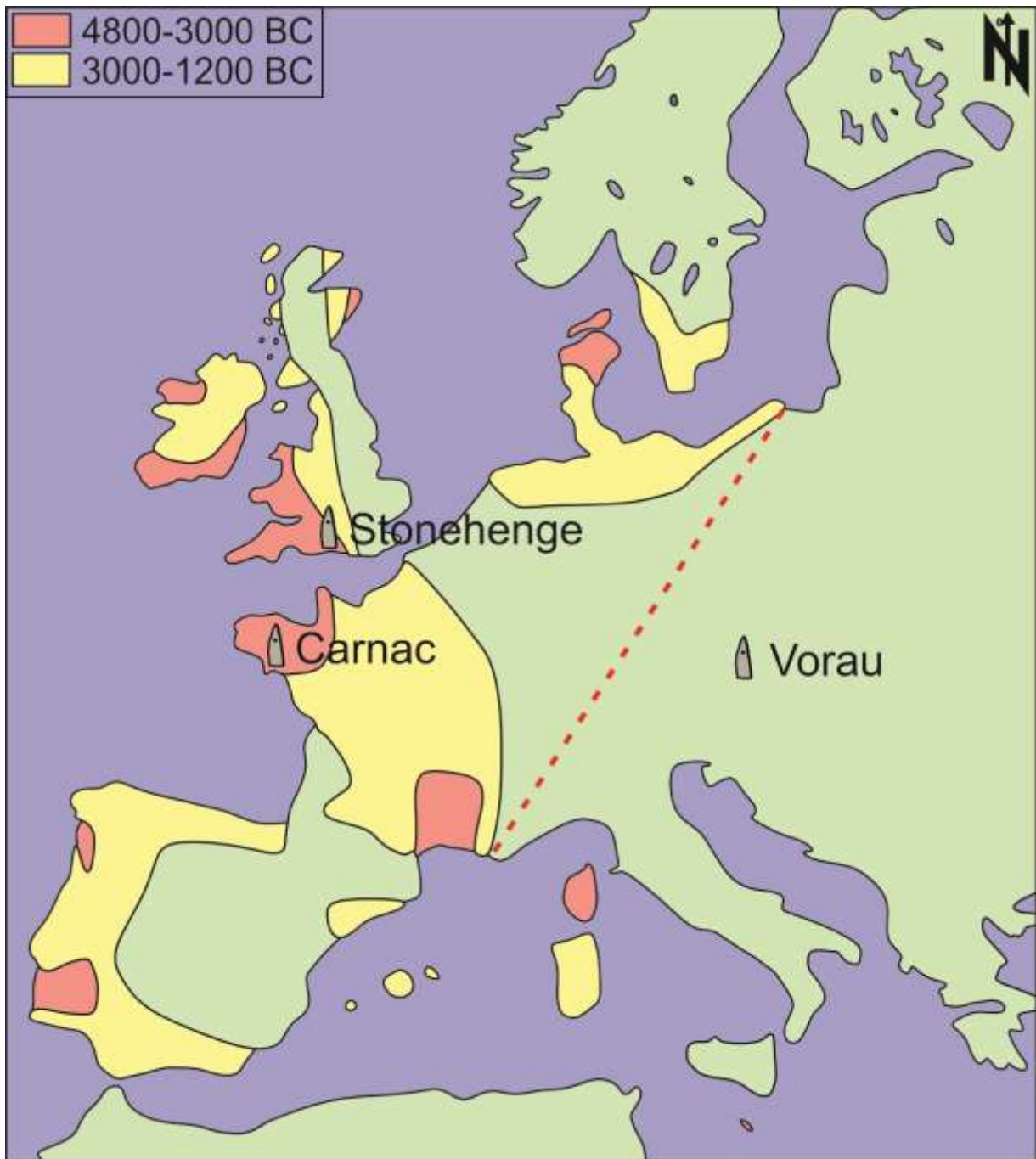
**Figure 1: Map of the Megalithic cultures in Europe with the two world famous sites, named *Stonehenge* and *Carnac*, and the new place of finding *Vorau*. The red dashed line symbolises the border between the west part of Europe, where megalithic cultures are widely spread, and the east, where megalithic cultures are virtually unknown. The different basic colours show the two different occurring ages of the megalithic cultures. The older culture is painted in red (4800-3000 BC) and the younger one in yellow (3000-1200 BC). The green colour symbolises the area with no confirmed findings until now; modified after http://www.britam.org/picturesYair/dolmen/map.jpg.**

**Paleolithic**

The first human findig in Austria was discovered in the Repolusthöhle in Styria. In fact some fireplaces and stone tools of cave bear hunters. They originatd about 30000 BC. Between 40000 y and 35000 y the Neanderthals got taken over by modern humans.
The most famous finding is the "Venus von Willendorf". This figure of a woman was made about 29500 BC.

**8000 BC**

**Mesolithic**

Findings of this time period were made in the Zigeunderhöhle in Styria.

**6000 BC**

**Neolithic**

The most famous finding is a glacial conserved mummified corpse called "Ötzi". It was found at the Tisenjoch and the death was dated to 3300 BC.

**2200 BC**

**Bronze Age**

Starts with the mastering of the bronze metallurgy in Austria

**800 BC**

**Iron Age**

Starts with the mastering of the ferrous metallurgy in Austria

**15 BC**

**Roman times**

Beginning of the Roman conquest

Figure 2: Timeline of the prehistory in Austria ranging from the beginning of the Palaeolithic to the beginning of the Roman times. Some important facts and famous findings are mentioned for each time period; data taken from Austria-Forum operated by TU-Graz.

The end of the megalithic culture took place in different regions at different points in history. The climate change led to increased violence within the population, which was triggered by food and raw material shortages (Korn, 2005). Skeletal remains of the transition period from the Neolithic to the Bronze Age report about strengthened signs of external violence by fighting. A new hierarchy in the community started and the idealized funeral changed from megalithic grave sites to grave mounds with bronze grave goods. Individual Dolmens and Menhirs still were built, but the number declined sharply until their erection terminated completely (Korn, 2005).

However, megalithic constructions continued until modern times, albeit typically as utility constructions rather than cultural monuments of symbolic character. During Roman, medieval and even up to modern times, monoliths were erected as fence posts and property markers, ice- and wine cellars were dug and earlier monuments moved and used. As such, it is not trivial to determine the original age of a given monument and it is the purpose of this study to contribute to this debate.

## 2.3 Origin and work methods

The older a Menhir is dated, the more natural it is in his appearance. Starting at 2000 BC the aniconic stone monuments were approaching increasingly the morphology of the human body until 1500 BC, when they showed the first clear outlines of Human faces. This development is supported by 84 Menhirs in Corsica, which have a pronounced nose and chin (Korn, 2005).

The origin of the rocks, which were erected as Menhirs, is mostly located in the vicinity. The methods for transporting the megaliths remain still unknown, largely because of the lack of archaeological evidence. Whether the Menhirs were transported by using a lever, or by pulling on underlying logs, or other techniques can only be guessed. It is likely that erratic boulders, which were found in the immediate vicinity, were used as Menhirs. Prehistoric mining areas with the discoveries of tools are evidence of prehistoric quarrying. By these discoveries the working methods can be reconstructed. Fist hammers and picks made out of stag antlers were common tools. They were mainly used in the processing of softer rock such as sandstone and limestone (Mohen, 1989).

In harder rocks other methods must have been used. A possibility could be the blow up of the stone by the interaction between fire and water. Furthermore, the technology of using wooden wedges, which were driven deep into the stone and after that make the holes swell by water and thus develop an explosive power, could be used (Zylmann, 2008).

In order to be able to place to origin of the Menhirs of the Vorau region into a context of the surrounding rock types, I begin with a summary of the geology of the region. Vorau is located in a gneiss and schist region at the eastern edge of the Alps at the transition of the Styrian Basin to the crystalline basement rocks of the Alps. All basement rocks in the region belong to the so called "Middle Austroalpine nappe complex" (Tollmann 1977). Going from the foot to the hanging-wall, the basement is composed in the study region by the Wechsel-, Semmering-, Strallegg-, Sieggraben-, and the Troiseck-Floning Komplex (Fig. 3). Furthermore, the so called Vöstenhof-Kaintaleck Komplex is wedged into the overlying Grauwackenzone. In the general region of Vorau, four of these complexes occur in a larger scale. Because of these complexes are close to- and similar in rock type to the Menhirs, they could be a reasonable source for the megalithic monuments of the Vorau region. It is therefore worth to describe these basement rocks a bit closer.

## 3.1 Characterization of the most import crystalline units in this area

Three different metamorphic phases are detectable in the four basement rock complexes that occur in the Vorau region (Schuster et al., 2001). The first is a Variscan metamorphic event, which is determinable in all units and shows ages around 370 Ma. The second one is a Permotriassic HT/LP metamorphic event. It shows increasing metamorphism in direction of the hanging wall in the southern part of the area. The climax of this metamorphism was about 270 Ma. The third one is the Eoalpidic metamorphic event, which has two different trends: In the northern part of the region, the metamorphic grade decreases against the hanging wall from the greenschist facies to the anchizone and the metamorphic ages rise from 80 Ma to 120 Ma. This implies a stacking of these units previous to the peak of metamorphism. In the south, it is opposite: the metamorphic grade increases from the greenschist facies in footwall to amphibolite- and granulite facies grade in the hanging wall. This implies thrusting after the metamorphic peak (Schuster et al., 2001).

**Wechsel Komplex**

The Wechsel Komplex occurs in the North-East of Vorau (Fig. 3). Several Menhirs and Holed Stones can be found close to Sankt Lorenzen am Wechsel, which is part of the Wechsel Komplex. The Wechsel Komplex overlies the Penninic of the Rechnitzer Fenstergruppe as the deepest cover belonging to the Austroalpine nappe complex (Pahr, 1977; Tollmann, 1977) and crops out in multiple tectonic windows, for example the Wechsel-, and Wiesmather Fenster (Tollmann, 1977; Kovach and Svingor, 1981). The monotones gneisses of this complex have a typical greenschist paragenesis with the following mineralogy: Ab + Ms + Chl + Qtz ± Ep ± Tur (mineral abbreviations after Kretz, 1983). The greenschists, which are integrated concordantly, consist of Ep/Czo + Chl + Qtz ± Ab ± Act (Faupl, 1970a; Müller, 1994). Retrograde, partly chlorite bearing, garnet-mica-schists, chlorite-epidote-albiteblasts schist, amphibolites and quartzites form the so called "Hüllserie". The Wechselgneise are connected across graphitic serizit-chloritegneiss with the Wechselschiefern, which are graphitic albite-phyllites. They consist out of the following progradely formed mineral paragenesis: Hgl + Chl + Qtz ± Ep ± Ab. Remnants of sedimentary structures like graded bedding as well as detrital micas are preserved especially in the hanging wall. Rb - Sr analyses of coarse-grained phengitic micas from the Wechselgneise, show ages of about 360 Ma to 370 Ma. This result represents the pressure stressed early Variscan metamorphism of the footwall of the Wechsel Komplex. The overlying Wechselschiefer had their first formative metamorphic event isochronal to a later metamorphic overprint of the Wechselgneise. An Ar - Ar dating analyses of the fine-grained paragonitic white mica from the schists and gneisses shows ages about 245 Ma and thus Permo-Triassic ages (Müller, 1999). The Eoalpidic metamorphic overprint reached conditions of the lowest greenschist-facies (300 °C to 330 °C). An Rb - Sr analyses in muscovite from a shear band shows ages about 86 ± 12 Ma (Müller, 1994). According to Korikovsky et al. (1998) the Wiesmather Fenster was exposed to higher metamorphic conditions. Analyses of zircons from the Wiesmather granite gneiss, show an age of the metamorphosis climax of about 109 ± 23 Ma, which was reached at a temperature of about 500 °C and a pressure of 10 kbar (Schuster et al., 2001).

**Waldbach Komplex**

The Waldbach Komplex occurs in Vorau and the eastern vicinity (Fig. 3). In this area, a very high density of Menhirs and Holed Stones can be found. The complex tectonically overlies the Wechselfenster in the southern part and according to Flügel and Neubauer (1984) it forms a recumbent antiform with a core of metapelites. These metapelites are overlain by the "Vorauer Serie", which consists of orthogneiss, hornblende gneiss and amphibolite. The "Vorauer Serie" has lithological similarities to the Fertöràkos Komplex on the Austrian-Hungarian border, which is considered part of the Wechsel Komplex by some authors (Kovach and Svingor, 1981; Frank et al., 1996). Furthermore, transgressive overlying Permomesozoic metasediments occur on the western edge of the Waldbach Komplex. The mica-schists occur in different units in different elevations. Phyllonitic mica-schist with albite porphyroblasts form the footwall. In contrast, the hornblende gneiss contains layers of coarse flaked garnet mica-schist, mica-schist and gneiss. Other important lithologies are orthogneiss and amphibole bearing rocks. The principal metamorphism of the Waldbach Komplex is of Variscan age. According to Faupl (1970b) this metamorphism reaches conditions of the upper amphibolite facies and locally even the anatexis. In Eoalpidic times a retrograde metamorphic overprint of the rocks took place. Ar - Ar analysis of muscovites in permoskythic quartzites gives an age about 82 Ma for this overprint (Dallmeyer et al., 1998; Schuster et al., 2001).

**Semmering Komplex**

The Semmering Komplex covers parts of Vorau and large parts of the region west of it (Fig. 3). Similar to the area of the Waldbach Komplex, the density of Menhirs and Holed Stones in the area of the Semmering Komplex is very high. From the footwall to the hanging wall the Semmering Komplex is subdivided in several partial nappes. According to Tollmann (1964) they are fold nappes with upright and inverse lying Permomesozoic sedimentary deposits and crystalline fold cores. Monotone matapelites and –psammites, which are called "Hüllschiefer" in some older studies, build up the crystalline rocks. In fact, they consist out of phyllitic mica-schist, phyllonites as well as retrograde mica-schist or gneiss (Berka, 2000). The "Hüllschiefer" can be subdivided in phyllitic mica-schists and phyllonites, which have a grey-brown to greenish-grey color with a mineral composition of $Hgl + Qtz + Chl \pm Czo \pm Tur \pm Py$, and the Ms-Chl-Grt-schist. The Ms-Chl-Grt-schists are gray to dark blue-grey with a rusty

alteration and have an older high temperature paragenesis with the mineral composition of Grt + Bt + Ms + Pl + Qtz ± Kfs and a younger greenschist paragenesis with the mineral assemblage of Ms + Chl + Qtz + Ab ± Cld ± Bt ± Grt. Large amounts of porphyric granite gneiss, called "Grobgneis" (Vacek, 1982), are interbedded. This "Grobgneise" appear as augengneiss with up to 3 cm microcline crystals and sometimes myrmecitic intergrowths on the edges. The magmatic mineral paragenesis consists of Kfs + Pl + Qtz + Bt + Ms + Zrn. Furthermore, small gabbro- metagabbro- and amphibolite bodies occur along the boundaries of the "Grobgneis" (Wieseneder, 1961; 1971). In addition, leucophyllites (Weißschiefer) are very common and are used economically (Huber, 1994). They are white, silky sparkling and thin foliated with a mineral composition consisting out of Hgl + Leuchtenbergit (Mg-Chl) + Qtz. The overthrust Semmeringer unit contains stratification from the Permoskyth to the Upper Trias. Koller et al. (2002) calculated a Permian Sm - Nd age of 246 ± 7 Ma for an olivine gabbro of Birkfeld and U - Pb ages of 270 Ma and 283 Ma for zircons of the "Grobgneise" by Kirchschlag. The Eoalpidic metamorphic overprint of the Semmering Komplex is documented by several Rb - Sr and Ar - Ar ages. The age of the crystallines are between 71 - 86 Ma with the lowest ages coming from the southern part near Vorau (Müller, 1994; Dallmeyer et al., 1998). In general, the Eoalpidic metamorphic conditions decrease from south to north (Schuster et al., 2001).

**Strallegg Komplex**

The Strallegg Komplex occurs in several different separate geographical locations, in particular in three spots of the mapped area. One spot lies in the center close to Vorau, one in the western vicinity and one in the southern vicinity (Fig. 3). All of them are overlapping with areas of more or less dense *megalithic* findings. The complex is made up of two units: The Stralleggergneise and the Tommerschiefer (Wieseneder, 1971; Koller and Wieseneder, 1981; Berka, 2000). Both occur near Vorau. In the southern edge of the region near Hartberg, Strallegg and Stubenberg the biggest occurrence of these lithologies can be found. The Stralleggergneise are biotite rich, alumosilicate bearing mica-schists, gneiss and magmatic gneiss, with a polymetamorphic development. Noticeable are their dark color and the weak distinctive schistosity. Furthermore, they show signs of an old HT/LP metamorphic event with a paragenesis of Bt + And + Sil + Pl + Qtz + Ms + Kfs. In fact, it is a Bt-And-Sil-schist. The Tommerschiefer are Ms-Chl-Grt-schists and consist of polymetamorphic garnet-mica-

schists with 10 cm long, prismatic pseudomorphosis (Berka, 2000). The rocks of the Tommerschiefer have a foliation defined by white mica and up to 1.5 mm big ilmenites. The formerly abundant biotite was converted to chlorite. Fine-coarse granites and pegmatites occur in both units. In contrast, amphibolites, calc-silicates and marble are really rare in this area. Kyanite, quartzites and leucophylittes are widespread in the Strallegg Komplex. The rocks of the Strallegg Komplex show a polymetamorphic evolution. The oldest rocks have Variscan ages around 320 ± 2 Ma (Berka et al., 1998). In addition, signs of Permian HT/LP metamorphism, a Permotriassic metamorphic event and Eoalpidic metamorphism are found (Schuster et al., 2001).
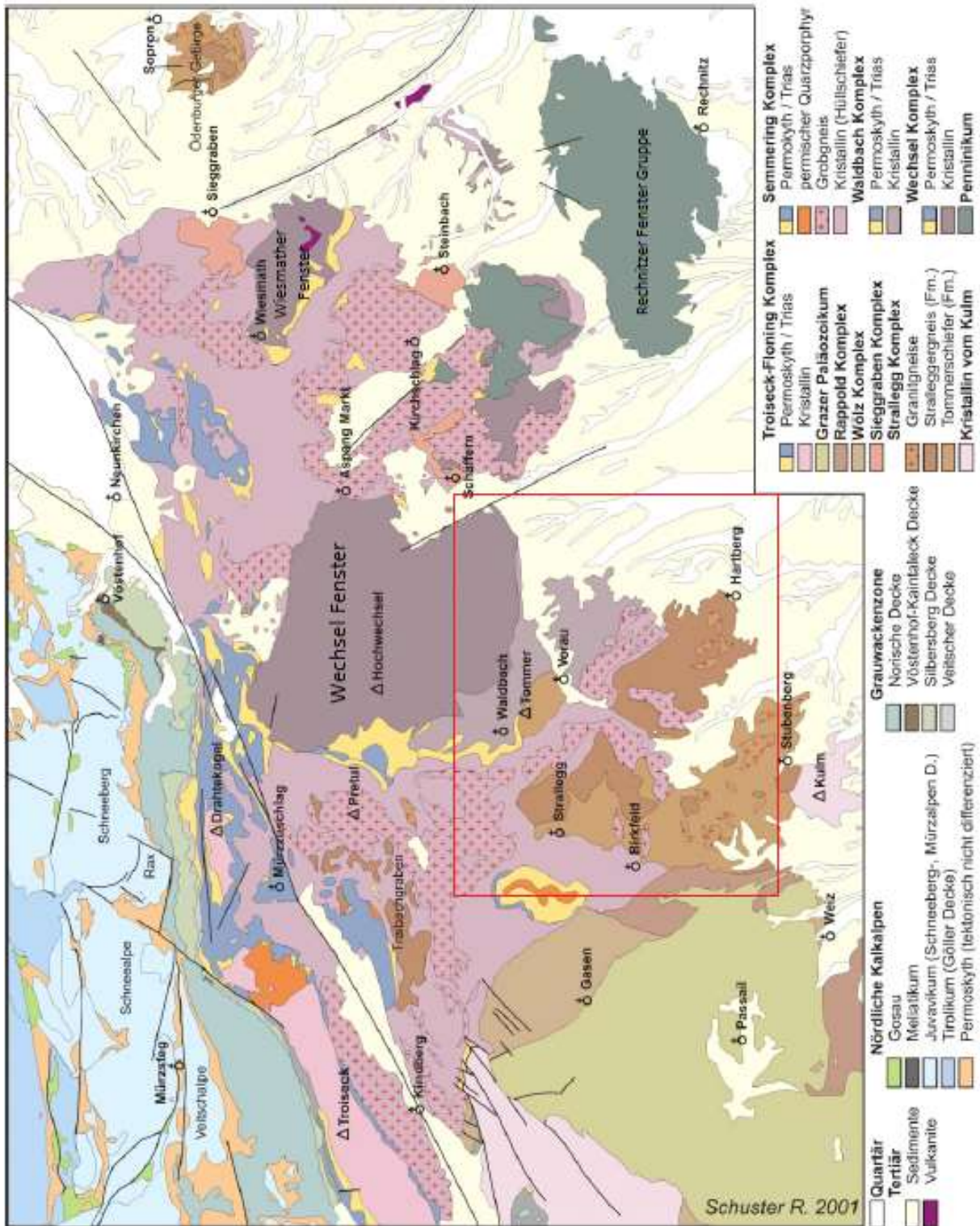
Figure 3: Geology of the Eastern Alps; modified after Schuster et al. (2001). The red rectangle marks the area of Fig. 4.
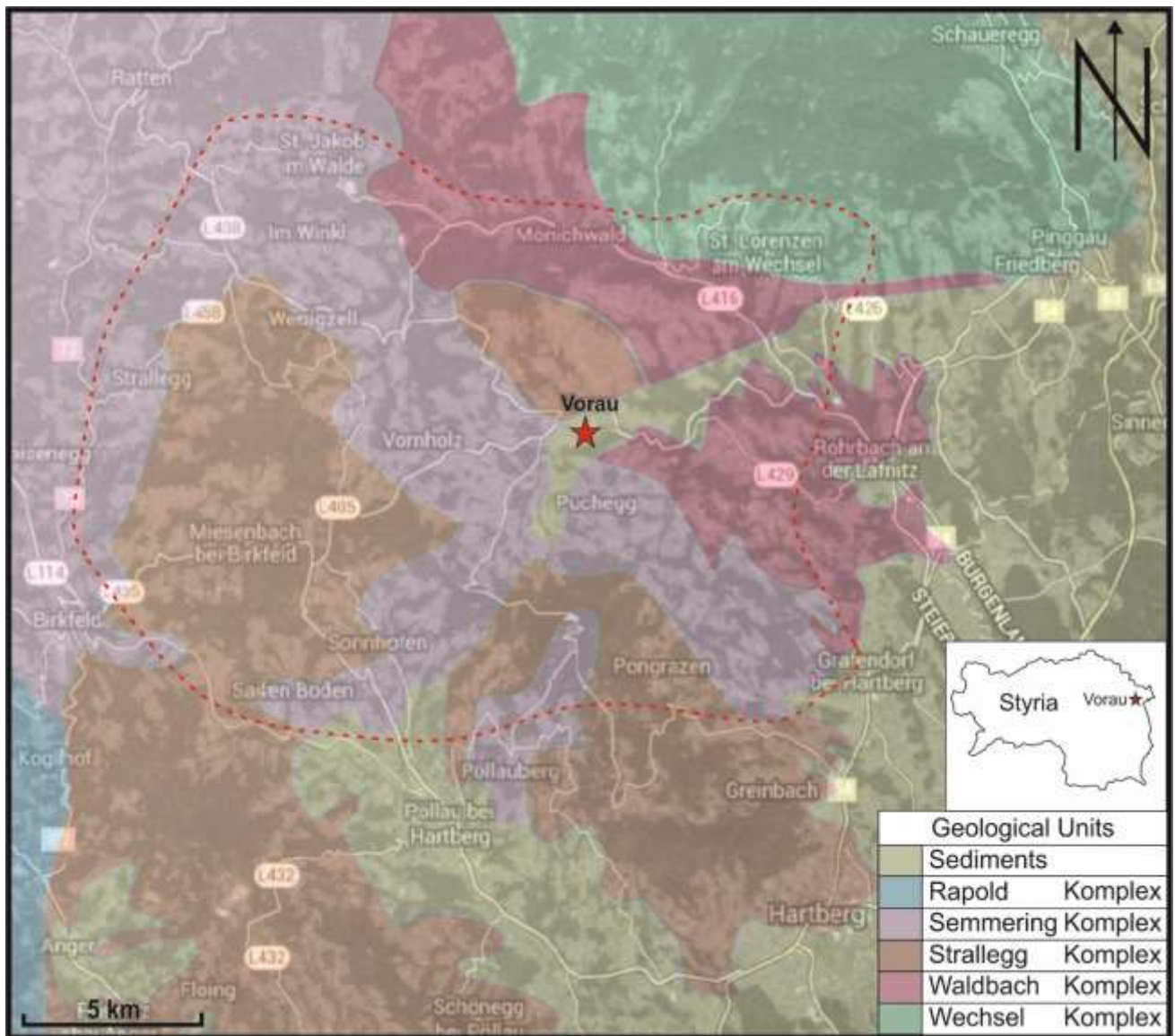
**Figure 4: Map of the geological units of Vorau and the vicinity. The geological Information is simplified to the crystalline units and the sediment. The red dashed line marks the area of the megalithic findings. Geological information, taken from Schuster et al. (2001).**

# 4. Field mapping

The intention of my field mapping was to create a full overview of the Menhirs in the region of Vorau (Fig. 5). Therefore, the data collected by Dr. Heinrich and Ingrid Kusch - who spent the last years with collecting as much information as possible about the Menhirs in this region - were combined with the data of three earlier Bachelor students, (Katharina Steinbauer Andreas Landler and Sasha Jürgen Emanuel Speil). After putting these data together, the data were plotted in Arc-Gis to get an overview about the areas which were not already investigated. After that, mapping started in the regions not yet investigated (Fig. 5). To detect the latitude and longitude as well as the sea level, the GPS device "Garmin etrex 20" was used. Additionally, the dimensions of height, width and thickness, as well as the hole-shape and size, were recorded. Furthermore, the orientation of the hole and the presence of catholic religious facilities (clerical buildings like wayside shrines, wayside crosses or churches) were noted. To judge whether a Holed Stone is "in situ", or was displaced in historic or prehistoric times, is really difficult. One clue could be information from locals. They often know about a displacement of several meters, or if it was even being fetched from a distance. Another problem are recently constructed Menhirs, which are used as an ornamental stone in the region. Evidence of the Menhir being in situ could be its location and orientation. If a Menhir is located at a heavily overgrown property and the existing hole or the wide side is parallel to an existing path, the Menhir is more likely to be in his original position. For this reason, the term "in situ" only indicates that a stone is probably in its original position. However, clearly the information on a Menhir being "in situ" based on the arguments presented above only refers to its position for the last century or so. No information on moving of stones before this time was possible to obtain.

Especially when dealing with Menhirs it should be recognized that the *Monoliths* were often excavated, were completely destroyed or were modified for other uses in the last millennia. In fact, this causes big differences in the overall picture, which has perhaps allowed other impressions and interpretations (Teichmann, 1983).

The rural area, which has a very hilly morphology, often made it very difficult to explore (Fig. 5). This is the reason why the help of the population was very important. For this reason, farmsteads and houses were systematically visited and locals interviewed. In fact, the missing areas in the map were often used for agriculture or were forested. This is the reason why the

number of the new found Menhirs is not that high. But it was a big step to a completion of the regional map. As a result, all the Menhirs were merged together in an excel sheet, which includes the most important facts like: GPS-position, sea-level, if they are expected to be in situ or not, if they are a Holed Stone or a Menhir and their dimension (see Appendix). Furthermore, they were plotted in an Arc-Gis map to get a good overview about their distribution (Fig. 5).

It should also be said that the Menhirs and Holed Stones of the Vorau region are not the only potentially prehistoric monuments in the region. Heinrich and Ingrid Kusch have found associated subsurface tunnels and several stone pits, where the Menhirs were possibly mined from, in the Vorau region (Kusch and Kusch, 2009; 2014). These tunnels and subsurface chambers may have a total length of up to several kilometres and are undoubtedly in some association with the surface structures. The most important subsurface tunnels in this area are the Strebl-Felsgang, Kandelhofer Erdstall and the Grubergang. While it is not the purpose of this thesis to investigate these other above- and below-surface monuments in any detail, it is worth mentioning, that the data base presented here will form a basis for future studies correlating the surface monuments with the subsurface monuments.
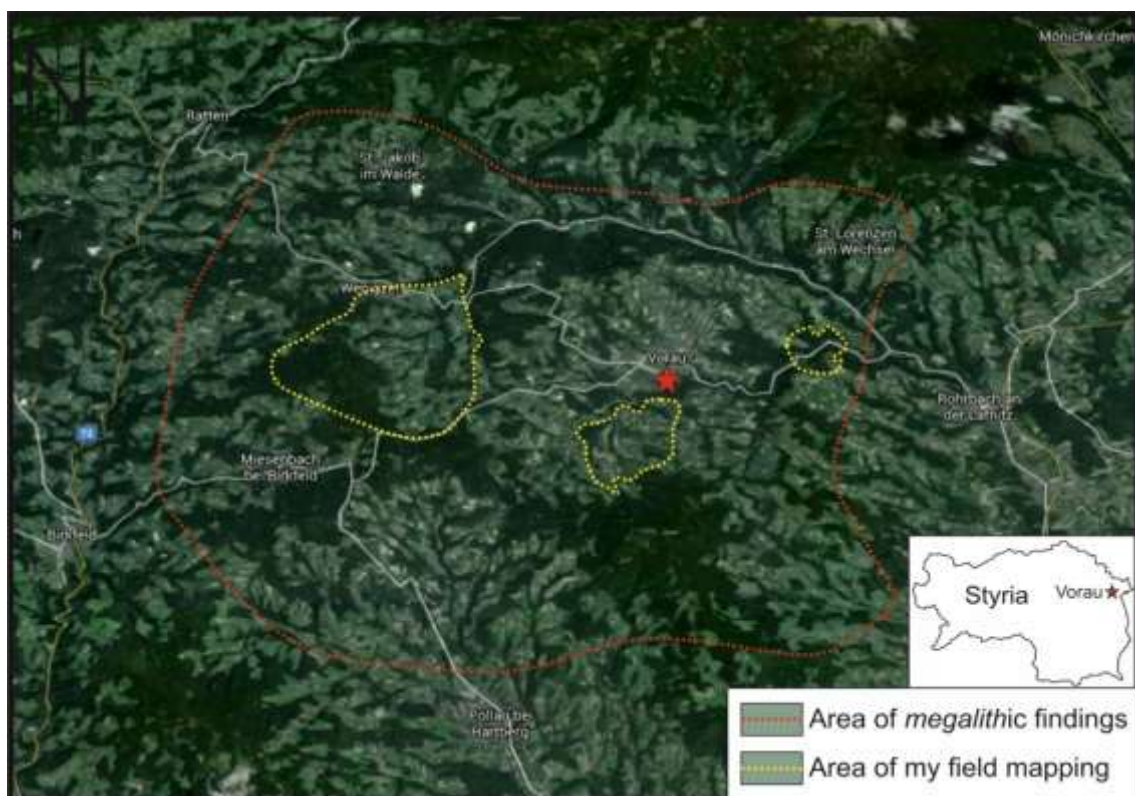


Figure 5: Map of Vorau and vicinity, including the area of megalithic findings, encircled by the red dashed lines, and the area of my field mapping, encircled by the yellow dashed lines; basic map taken from google earth.

## 4.1 Results

The results show a really high density of Menhirs in the investigated area of Vorau and its surroundings. In some areas, especially in Vorau itself and the closest vicinity, the density is extremely high and even leads to overlapping location points in the map. To get an idea about the total number of Menhirs and Holed Stones, you have to take a further look at the Excel sheet in the appendix. You can easily discover the enormous number found in this relatively small area of about 300 km$^2$. All together more than 500 locations of Menhirs and Holed Stones were documented. On average, more than one Menhir and/or Holed Stone can be found per km$^2$. The occurrence and especially the density of the Menhirs and Holed Stones are a novelty in this part of Europe. The historical meaning of these findings is discussed later and in the discussion in chapter 8. The Arc-Gis map below (Figs. 6 and 7) shows the collected data of all the field mappings done by Heinrich and Ingrid Kusch, Andreas Landler, Sasha Speil, Katharina Steinbauer and me. Every star marks a location, in which one or more Menhirs and/or Holed Stones were found. The different colours stand for the person who is responsible for collecting the detailed information on this particular find. The map includes all the findings until the summer of 2016 and shows an outline of the region within which mapping was performed. Due to the destruction and/or dislocation of Menhirs and/or Holed Stones by the population, the ultimate number and some of their locations change constantly. The ultimate number of Menhirs and/or Holed Stones also increases all the time, due to new discoveries. Therefore, this map and the Excel sheet in the Appendix are just a snapshot and show the minimum number of *megalithic* remnants located in this area. Narrations and reports suggest, that there must have been even more Menhirs and/or Holed Stones in the past. Many of them got destroyed or buried during construction works. The shape, occurrence and usage of the Menhirs and Holed Stones varied a lot from location to location (Fig. 8). Further detailed information about this and some pictures of examples of them can be found in chapter 4.2.
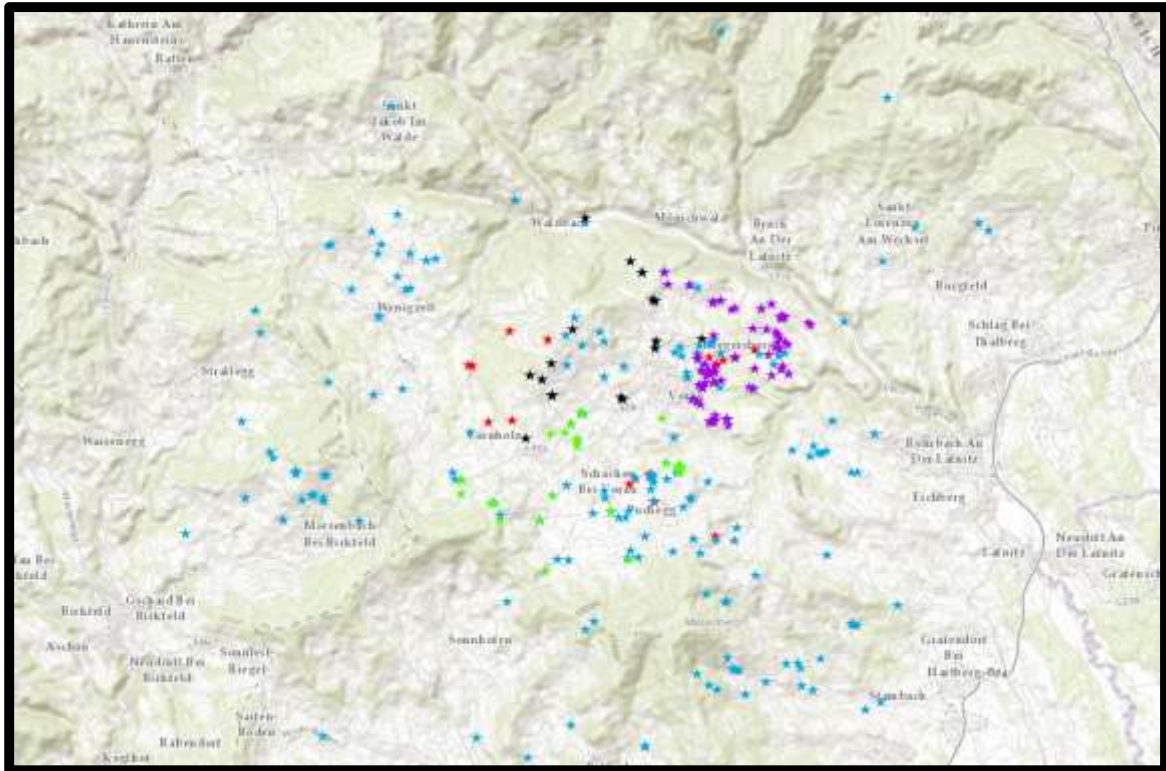
Figure 6: Arc-Gis map of Vorau with the obtained Menhir locations; the differently coloured stars stand for the respective person, who is responsible for the detailed information about them. Blue: Heinrich and Ingrid Kusch; green: Andreas Landler; black: Sasha Speil; purple: Katharina Steinbauer; red: Sebastian Wiesmair.
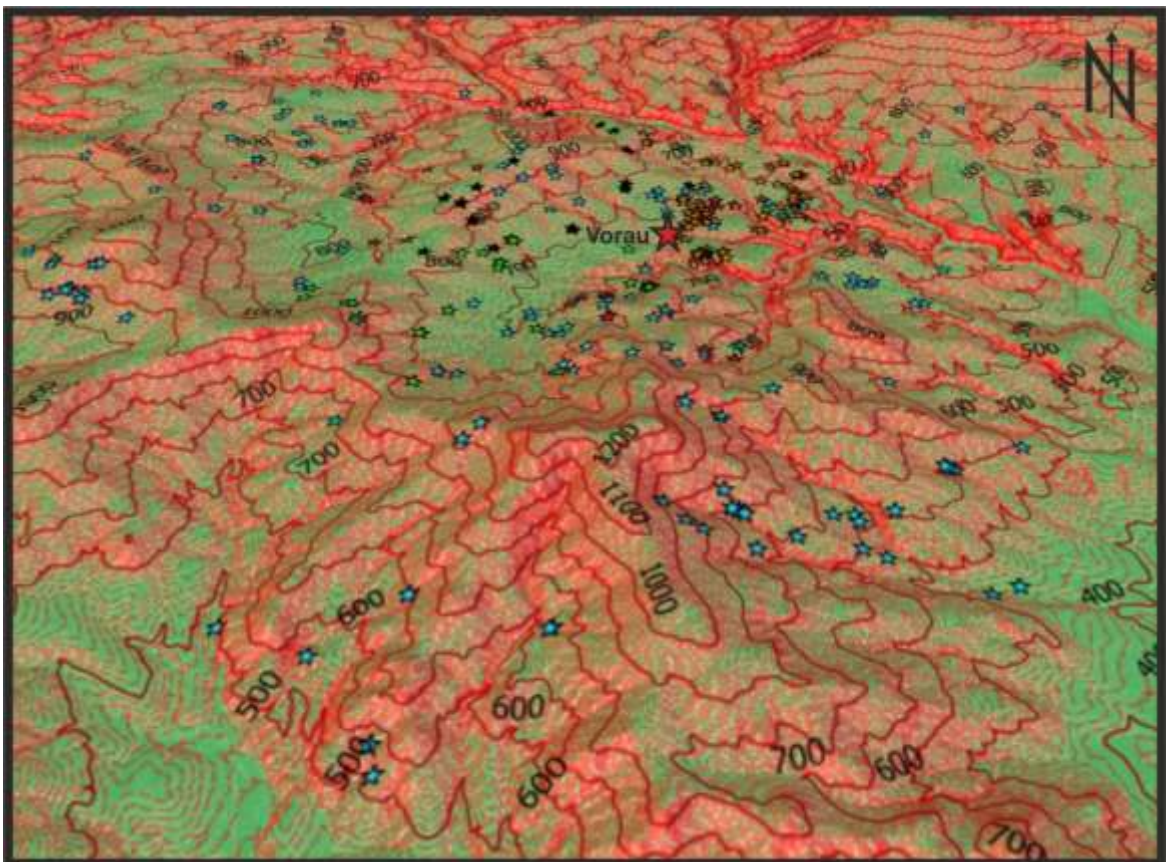


Figure 7: Digital elevation model of Vorau and the vicinity with the obtained Menhir locations; The differently coloured stars stand for the respective person, who is responsible for the detailed information about them. blue: Heinrich and Ingrid Kusch; green: Andreas Landler; black: Sasha Speil; purple: Katharina Steinbauer; red: Sebastian Wiesmair.

## 4.2 Some examples

In this section I want to describe a few illustrative examples of the Menhirs in the Vorau region to show how different their occurrence, appearance and further usage can be. As described earlier there is no particular location, where the Menhirs and Holed Stones can be found. Nowadays most of them are located besides paths (Fig. 8a), homesteads or fields. But this allocation is just a result of dislocations and removals over the last thousands of years. Many Menhirs and Holed Stones were located in unpractical places like fields or building areas. Because of the lack of interest and knowledge about their historical significance, they got removed or dislocated. There are no former studies or reports about the original locations. Due to bigger forest and agriculture tools and the construction of new buildings the number of removals was rising over the last hundred years. This movement is even enforced by trend to place Menhirs as an accessory in the yards of private houses. The last few years these Menhirs become popular and started to attract some tourists. That is the reason why a 4 km long loop road, which shows some Menhirs and Holed Stones in their original location and explain some facts about their origin, was build. Some Menhirs and Holed Stones got used in other ways. For example, some of them were integrated in some religious buildings. A good example is the holed stone in Fig. 8a. It is located besides a path and is used in the construction of a wayside shrine. Even the two holes are used for the fixation of a wooden cross. The farmers used them as boundary stones or stone gates as well. Especially the Holed Stones were for example used to fix fences. These usages can often be a hint, that they were not moved since their erection. Due to the changing landscape over the last thousands of years some can be found in other inaccessible places too. For example, some of them are located in a middle of a forest. There is no real coincidence between the distribution of the Menhirs and Holed Stones and the sea-level observable. The distribution of the sea-level varies between 369 m and 1109 m, whereas the majority is located between 600 m and 800 m (Fig. 7). But if you look at the location in the field and on the map, this sea-level distribution is just the result of the topography of Vorau and the vicinity. There are no signs of any attention paid to the sea-level during the erection of these potentially prehistoric monuments.

Fig. 8 shows their appearance is vary varied. The first big difference is the occurrence or the missing of human made holes. The Holed Stones mostly appear with just one hole, but the number can differ between one and four. Whereupon most of this holes are located on the top region of the holed stone and are placed, referred to the width, relatively central. Therefore,

the holes are very apparent and can be seen from a big distance. This fact strengthens the hypothesis that the orientation of the holes could have been important in the past. Due to the fact that many Holed Stones have been dislocated and it is impossible to get a clear correlation. The measurements do not show any signs of an intentional orientation. But this does not mean that there was no correlation in the past, when they have been erected. The shape of the holes is variable too. The majority has a more or less round shape (Fig. 8c). These round holes vary in the diameter between three and seven centimetres, at which most of them are in the range of four to five centimetres. Some however show a rectangular or quadratic shape (Fig. 8b and 8d). The size of the side lengths varies from 4 cm to 10 cm.

The Menhirs and Holed Stones show two different kinds of shapes. The first type of shape looks more or less natural. This means, that they were not formed in any special way (Fig. 8a and 8c).  The other ones look well processed. They can have a nearly rectangular shape as a whole (Fig. 8b and 8d). The weathered surface indicates that this happened long time ago. Some Menhirs and Holed Stones show signs of a later adaption. Due to the fresher not intensively weathered surface, a younger age of the modification can de indicated. The shape varies a lot referring to their dimensions as well. The height was measured beginning from the ground up to the top of the Menhir or Holed Stone. This means, that the buried parts of the Menhirs and Holed Stones are not included in my measurements. The visible height shows values between 20 cm and 231 cm. The majority of them lie in between 110 cm and 160 cm with constantly dropping numbers in both extremes (Fig. 9b). The few smaller examples can mostly be traced back to destroyed former bigger Menhirs and Holed Stones. But the really high ones are an exception too and occur seldom. The distribution of the widths shows a similar pattern (Fig. 9c). They vary between 18 cm and 91 cm, whereas the interval of 40 cm and 49 cm includes the highest number of Menhirs and Holed Stones (40/137). Besides this interval the numbers are constantly dropping in both directions. The majority values of the thickness vary between 10 cm and 29 cm. Just a few exceptions reach smaller values until 8 cm or higher values up to 34 cm (Fig. 9d). In summary, an average Menhir or Holed Stone is around 128 cm high, about 51 cm width and about 20 cm thick.
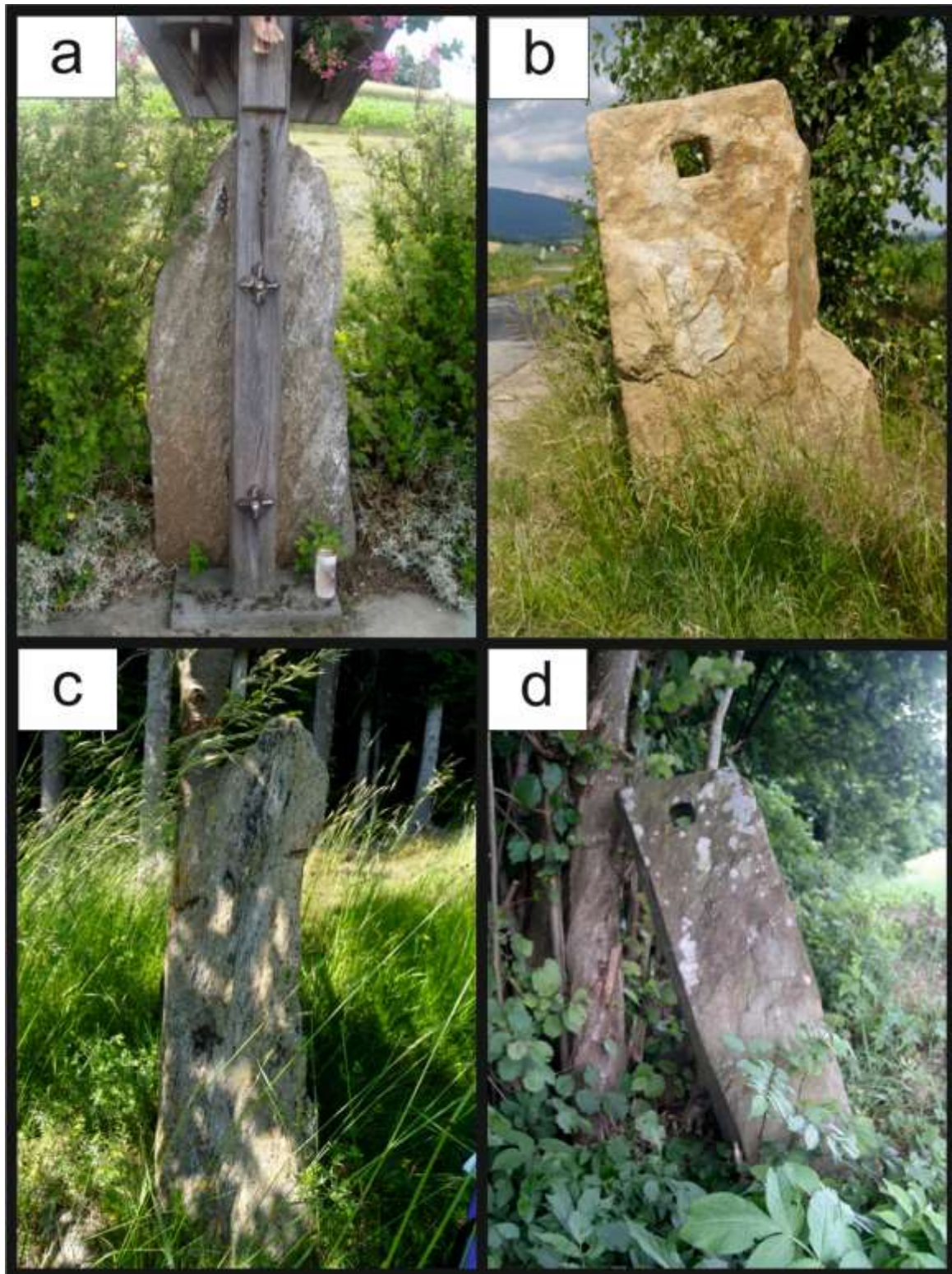
**Figure 8: Three examples of Holed Stones and one example of a Menhir. The photos are taken in vicinity of Vorau.**
**a) A Holed Stone integrated in a wayside shrine besides a path. The Holed Stone has two round holes with a diameter of 5 cm. Location: N47° 23.239', E 15° 52.587'; Sea-level: 738 m; dimension: 133 cm high, 60 cm wide and 16 cm thick. b) An almost rectangular formed Holed Stone with one quadratic hole with a side length of 7 cm. Location: N47° 24.603', E 15° 54.247'; Sea-level: 677 m; dimension: 125 cm high, 55 cm wide and 29 cm thick. c) A Menhir located beside a forest. Location: N47° 25.329', E 15° 49.944'; Sea-level: 870 m; dimension: 98 cm high, 46 cm wide and 16 cm thick. d) A Holed Stone with a well worked form and one quadratic hole with a side length of 7cm. Location: N47° 24.827', E 15° 54.244'; sea-level: 669 m; dimension: 114 cm high, 39 cm wide and 25 cm thick.**
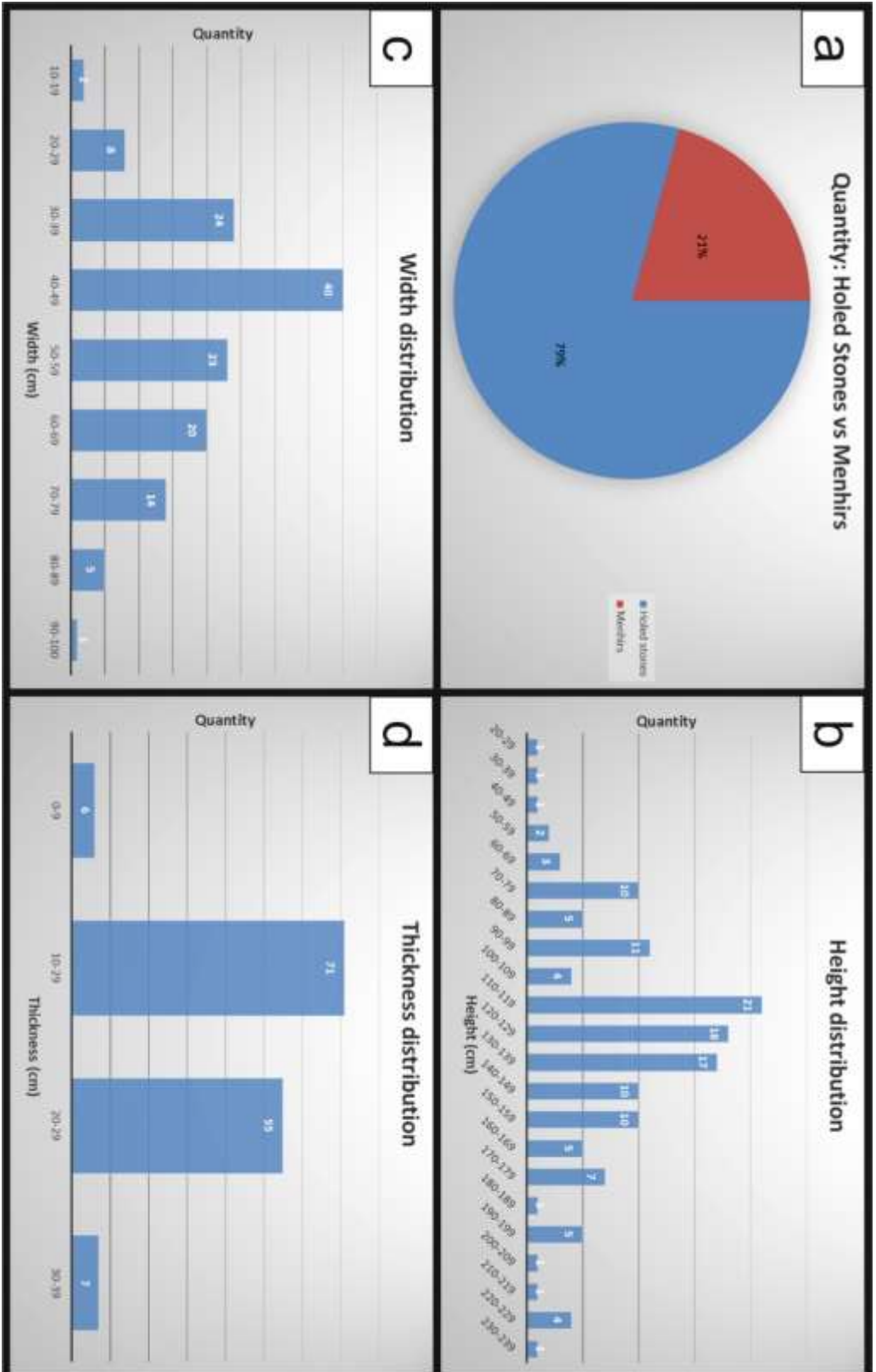
**Figure 9: This figure shows the different distributions of the Menhir*s and* Holed Stone*s,* from which the necessary information got registered.  Plot a shows a comparison of the quantity of Menhir*s* vs Holed Stone*s*. Plot b shows the Height distribution. Plot c shows the width distribution. Plot d shows the thickness distribution.**

# 5. Thin sections

Several thin sections from samples of the Menhirs and Holed Stones, local in-situ rocks and a near stone pit were made. The intention was to describe their mineralogy and structure. Besides that, some comparisons between them were made to get an idea of the origin of the Menhirs. The thin sections were analyzed with an Olympus polarization microscope. The pictures were taken with the digital camera SiS Colorview and the software AnalySIS. Most of the thin sections were taken from the Bachelor thesis, because it was very important to damage as few Menhirs as possible. This is the reason, why already existing information from samples was preferred to take new samples and analyze them.

## 5.1 Samples of the Menhirs

**Sample "L18": garnet-chlorite-schist**

Sample L18 (L18 in the complete list; see appendix) was taken from a Menhir close to a farmstead. It was selected, because of his striking quartz vein. This sample is mainly build up by quartz, garnet, chlorite, muscovite, plagioclase, hornblende and opaque phases (Fig. 10). The quartz builds a vein, which penetrates the whole sample. Besides the schistosity, the structure is dominated by highly deformed garnets with a poikiloblastic texture. Alteration is very present in this thin section.



Figure 10: Photo of a thin section from sample M1 .

## Sample "PS": paragneiss

The sample PS (SP30 in the complete list; see appendix) was chosen, because of his different type of rock. Paragneiss is a rare material among the Menhirs. This sample mainly consists out of quartz, feldspar and muscovite (Fig. 11). Other existing minerals are biotite and zoisite. The texture shows a schistosity, which can easily be seen on the muscovite grains. The quartz is recrystallized and has indications of bulging. The plagioclase has developed zonal structures and has fretting grain boundaries, which could be a sign of a dissolution or reorganization (Speil, 2014).
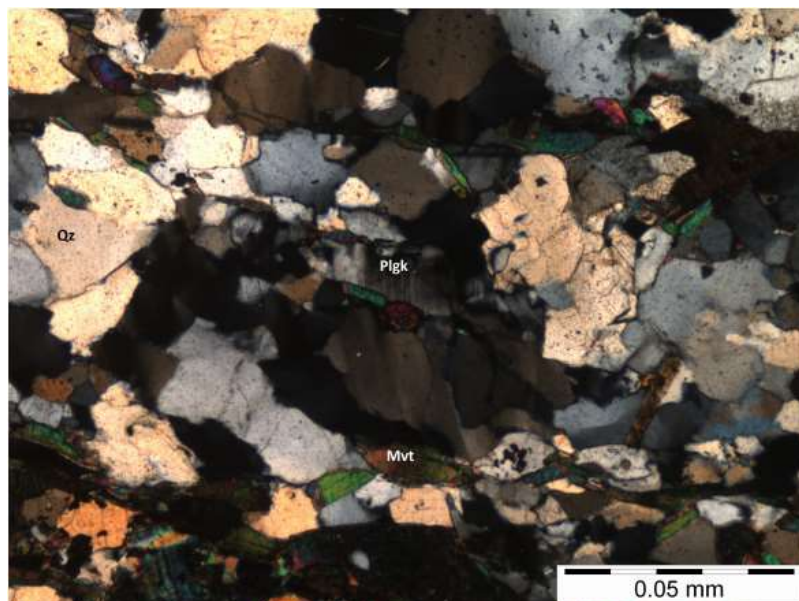


Figure 11: Photo of a thin section from sample PS; crossed-polarized illumination; taken by Speil Sasha.

## Sample "L13": garnet-mica-schist

Sample L13 (L13 in the complete list; see appendix) was selected, because his type of rock (garnet-mica-schist) is very common among the Menhirs. Therefore, this sample is representative. This sample mainly consists out of quartz, mica and garnets. The texture has a well formed schistosity (Fig. 12). These are the typical signs of a garnet-mica-schist (Landler, 2014).
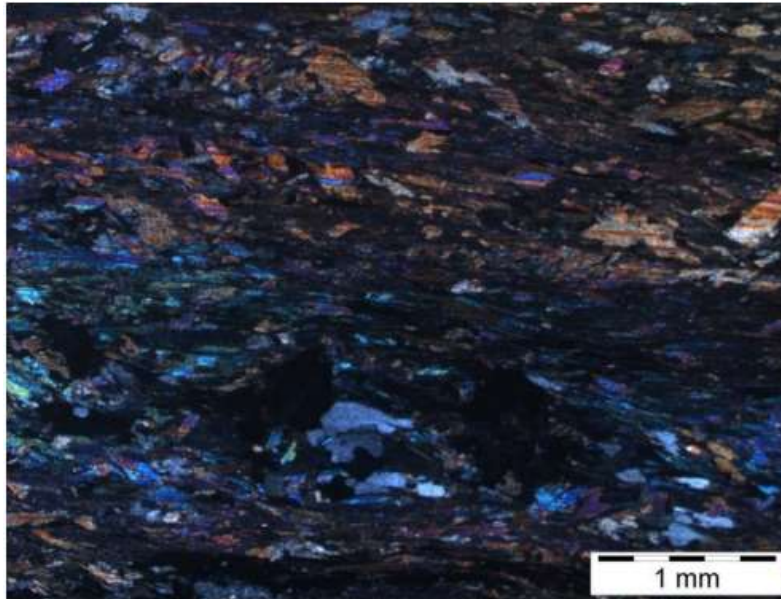
**Figure 12: Photo of a thin section from sample L13; crossed-polarized illumination; taken by Landler Andreas.**

## Sample "Menhir 8": garnet-chlorite-schist

The sample L11 (L11 in the complete list; see appendix) was taken, because like sample L13 it represents the majority of Menhirs. Therefore, it is one of five relatively similar samples to get a better overview about the possible origin rock type. The sample mainly consists out of quartz, chlorite, garnet, muscovite, plagioclase, hornblende and opaque phases. Besides its schistosity, the microstructure of this sample is dominated by highly deformed garnets with a poikiloblastic texture (Fig. 13). Furthermore, alteration processes in connection with the chlorite and garnet can be observed (Landler, 2014).
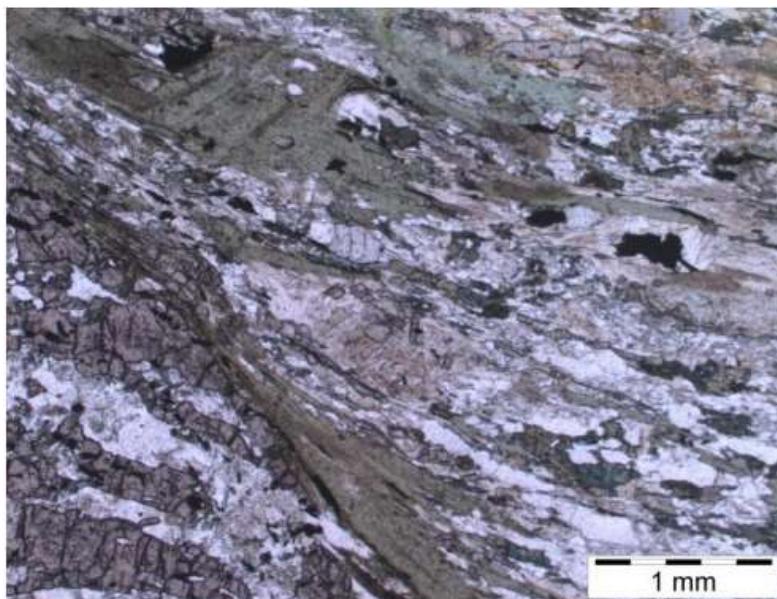


**Figure 13: Photo of a thin section from sample L11; taken by Landler Andreas.**

**Sample "L10": garnet-chlorite-biotite-schist**

The sample L10 (L10 in the complete list; see appendix) mainly consists out of quartz, garnet, chlorite and biotite (Fig. 14 and 15). The schistosity in this sample is good formed and the matrix is fine grained. Landler (2014)
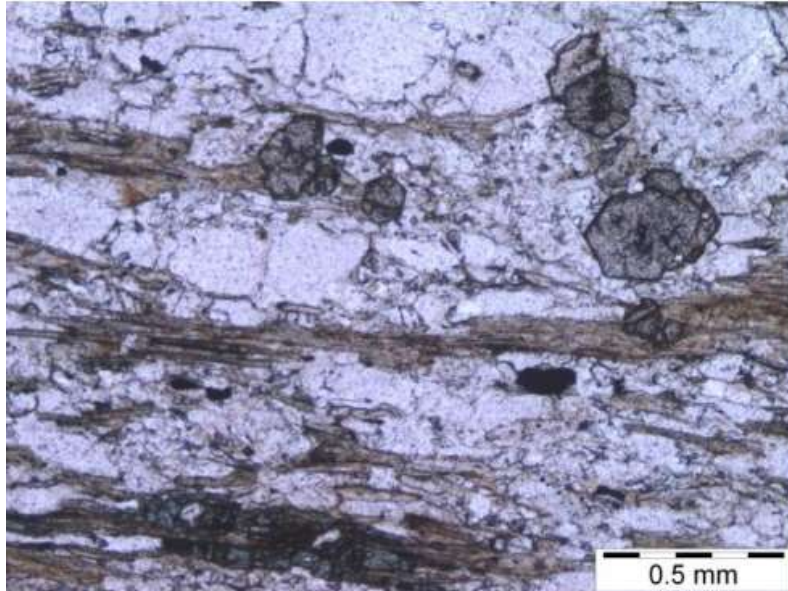


Figure 14: Photo of a thin section from sample L10; taken by Landler Andreas.
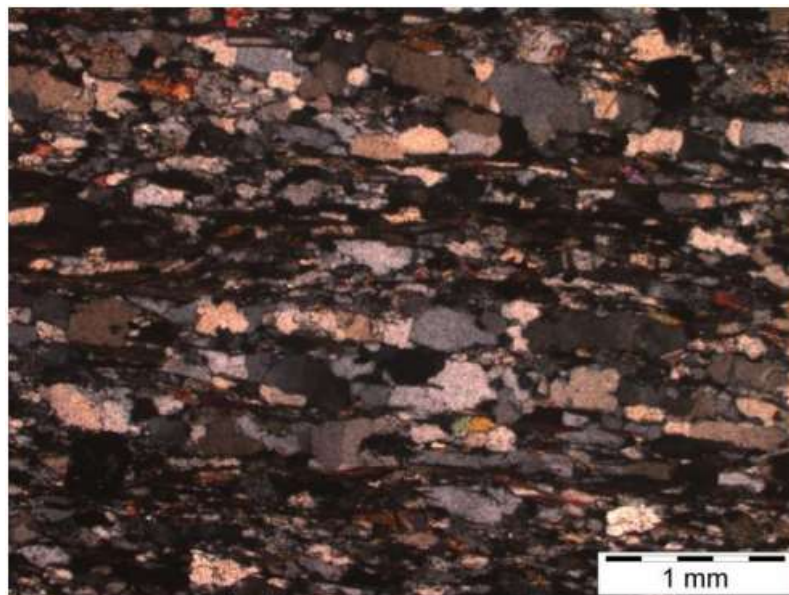


Figure 15: Photo of a thin section from sample L10; crossed-polarized illumination; taken by Landler Andreas.

**Sample "Menhir 10": garnet-mica-schist**

The sample mainly Menhir 10(L9 in the complete list; see appendix) consists out of quartz, muscovite, garnet, hornblende and chlorite. Besides the schistosity, the quartz vein and the alteration of the garnets are typical in the structure of this sample (Figs. 16 and 17) (Landler, 2014).
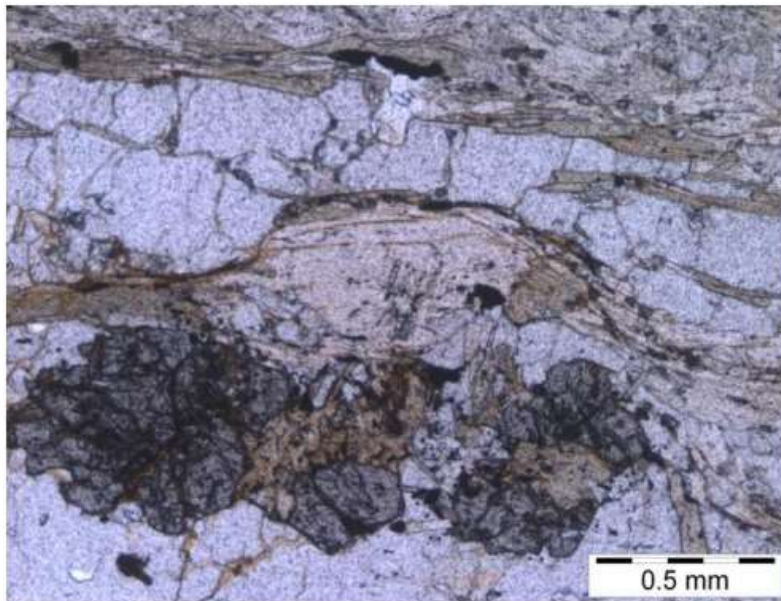


Figure 16: Photo of a thin section from sample Menhir 10; taken by Landler Andreas.
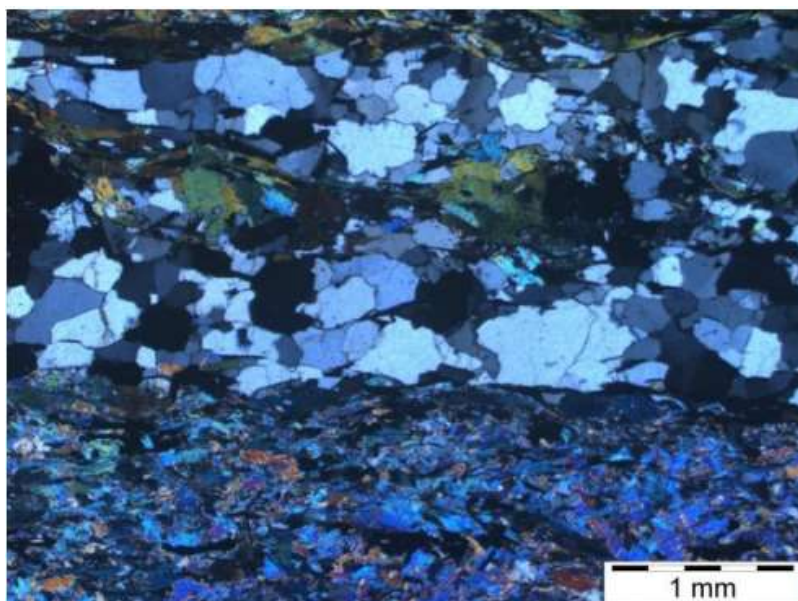


Figure 17: Photo of a thin section from sample Menhir 10; crossed-polarized illumination; taken by Landler Andreas.

## 5.2 Samples from outcrop and the stone pit

The samples in this sections were taken either from stone pits which may be a potential source for Menhir mining or from outcrops in the region. The sample locations are spread around Vorau and the vicinity and hence represent different geological units. The stone pits have good outcrops with different rock types. Therefore, more samples were taken from these places. In the following I use the abbreviation "STV" for all samples from the same stone-pit, and "B" for those from another one.

**Sample "STV1": amphibolite**

This sample is an amphibolite taken from the stone pit Steingraben in the south-east of Vorau. Therefore, it should be a good sample of the basement rock. The dominating geological unit in this area is the Waldbach Komplex. The sample has a lepidoblastic texture and contains mainly quartz and zoisite, plagioclase, amphibole and little garnet. The amphibole starts to transform to zoisite (Fig. 18). Although the minerals look like they have been grown irregularly, there is a visible primary schistosity in the amphibolite. Furthermore, the amphibole grains show two different growth phases, which can be identified via a color difference. In fact, the amphibole grains in the schistosity are dark green and the irregular ones light green (Speil, 2014).
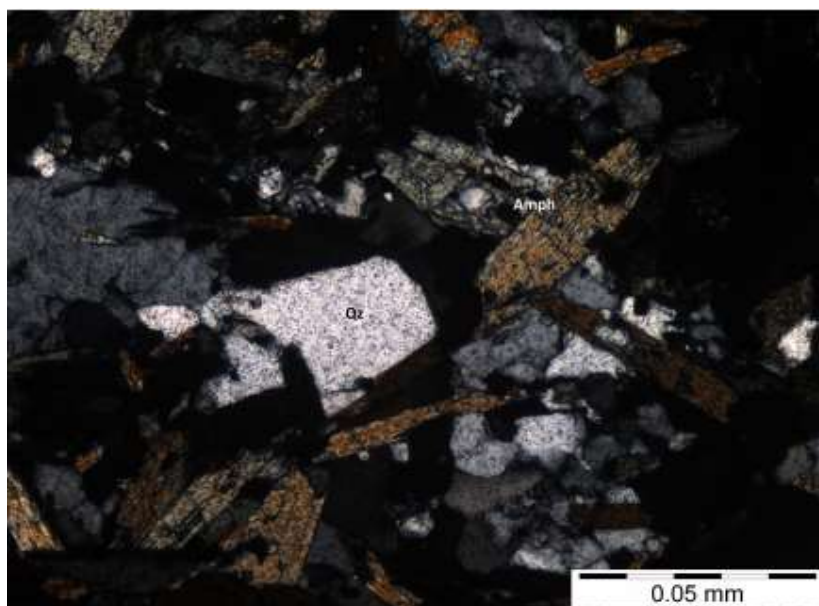


Figure 18: Photo of a thin section from sample STV1; crossed-polarized illumination; taken by Speil Sasha.

**Sample "STV2": garnet-micaschist**

This rock sample of a garnet micaschist from the same quarry looks a lot like the majority of the Menhir samples. Therefore, it was taken to get a better comparison. The dominating geological unit in this area is the Waldbach Komplex. This sample is mainly build up by quartz, muscovite, garnet and amphibole (Fig. 19). Omphacite, plagioclase, and titanite occur in minor amounts. The texture shows a fine mica matrix with quartz, garnet and altered amphibole grains. The quartz and mica grains are crushed and broken into subgrains (Speil, 2014).
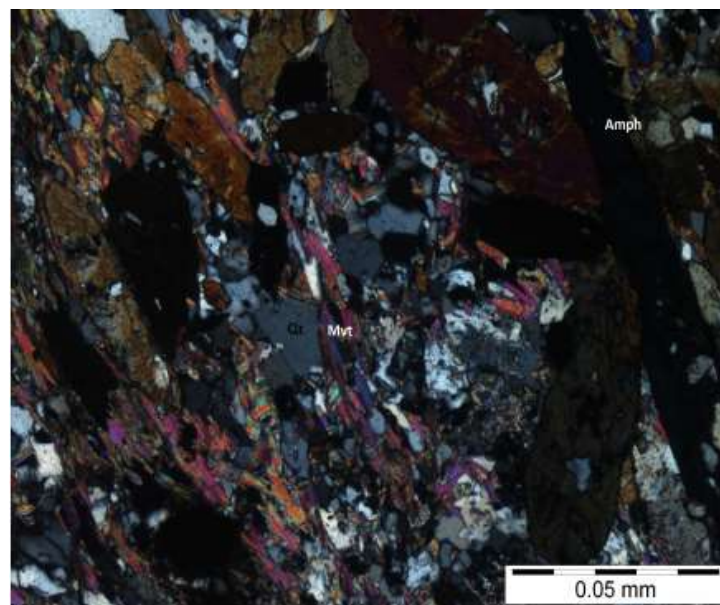


Figure 19: Photo of a thin section from sample STV2; crossed-polarized illumination; taken by Speil Sasha.

**Sample "STV3": paragneiss**

This outcrop sample from the same quarry was chosen because it looked similar to the Menhir sample PS. The dominating geological unit in this area is the Waldbach Komplex. The sample mainly consists out of quartz, muscovite, plagioclase and garnet. In addition, accessories like opaque phases, chlorite, zoisite and titanite are present. The plagioclase exhibits twinning and the quartz shows signs of recrystallization (Fig. 20). Furthermore, the chlorite is partly oriented and was grown as the last mineral (Speil, 2014).

## Sample "STV5": amphibolite

Besides different mica-schists and gneisses amphibolites occur as primary material for the Menhirs. Therefore, some samples like this one were taken. As for all other STV-samples from this quarry the dominating geological unit in this area is the Waldbach Komplex. It contains mainly amphibole, muscovite and quartz and little amounts of plagioclase, garnet, titanite and opaque phases. The quartz shows signs of a recrystallization. An exception is the quartz vein, which shows grains without the in this thin section typical deformation and alteration (Fig. 21). This shows that the vein was formed secondarily. The thin section shows a good schistosity (Speil, 2014).
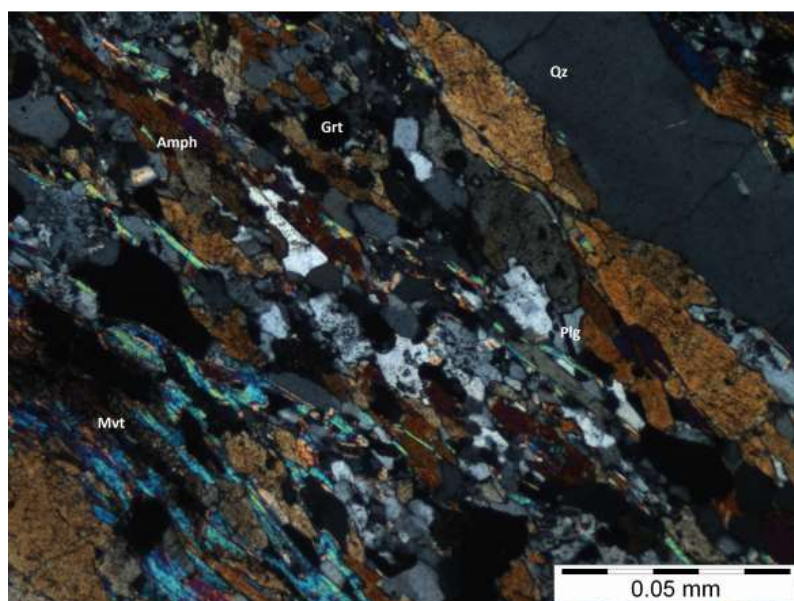


**Figure 21: Photo of a thin section from sample** STV5; crossed-polarized illumination; taken by Speil Sasha.

## Sample "A": garnet-mica-schist

Sample A was taken from an outcrop rock. In the field it looks like the main rock type of the Menhirs and can hence be compared well. The dominating geological unit in this area is the Strallegg Komplex. This sample is mainly build up by mica, quartz and garnet. This sample is highly deformed and the minerals in it have a parallel orientation (Fig. 22 and 23). In addition, the texture is schistose (Landler, 2014).
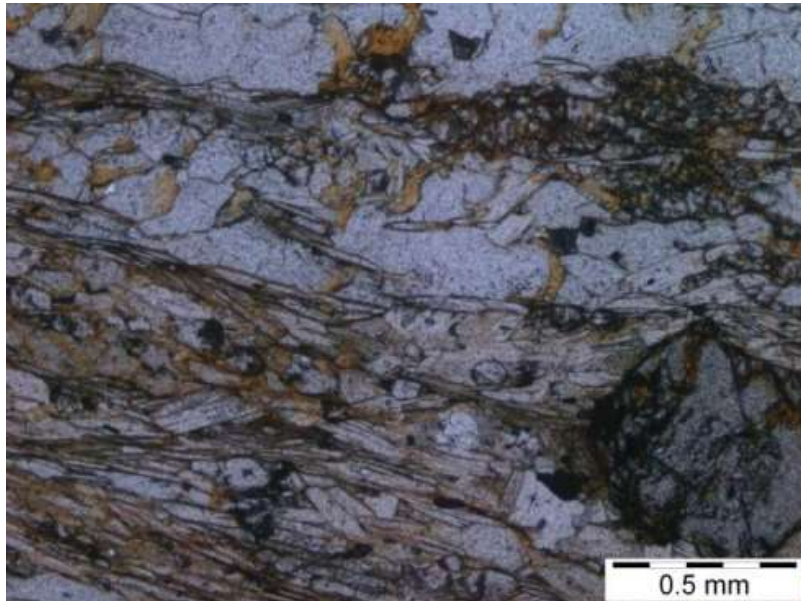


Figure 22: Photo of a thin section from sample A; taken by Speil Sasha.
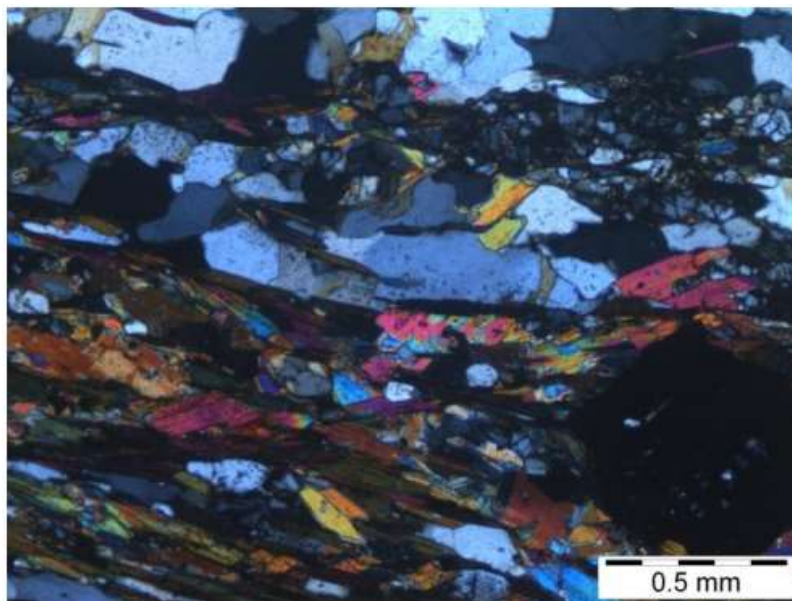


Figure 23: Photo of a thin section from sample A; crossed-polarized illumination; taken by Speil Sasha.

## Sample "B1": garnet- chlorite-muscovite-schist

This sample of an outcrop rock was chosen, because like sample A, his type of rock has a lot of similarities to most of the seen Menhirs. The dominating geological unit in this area is the Semmering Komplex. The main mineral assemblage is composed of quartz, chlorite, garnet, hornblende and plagioclase (Fig. 24). The poikiloblastic garnets show signs of alteration. Furthermore, they contain quartz, muscovite and opaque phases as inclusions. In addition, the schistose texture contains quartz veins (Landler, 2014).



Figure 24: Photo of a thin section from sample B1; taken by Landler Andreas.

## Sample "B2": garnet-chlorite-muscovite-schist

This sample was chosen, because it looked like sample B3 and hence like a lot of Menhirs. The dominating geological unit in this area is the Semmering Komplex. The thin section has an identical mineralogy and texture as the sample B1 (Fig. 25) (Landler, 2014).
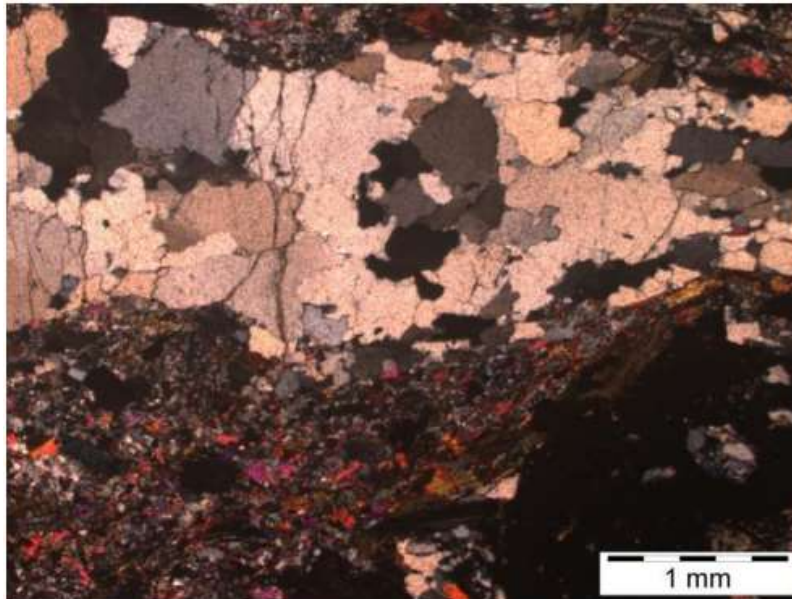
## Sample "B3": amphibole-schist

This sample taken from an outcrop was picked, because it represents a different rock type (amphibolite-schist), which occurs in context with some Menhirs. Like in context with all other STV-samples, the dominating geological unit in this area is the Semmering Komplex. This sample mainly consists out of hornblende, quartz, garnet and chlorite. The garnets are poikiloblastic and the hornblendes represent more than 80 % of the mineral content (Fig. 26). Furthermore, the texture is schistose (Landler, 2014).
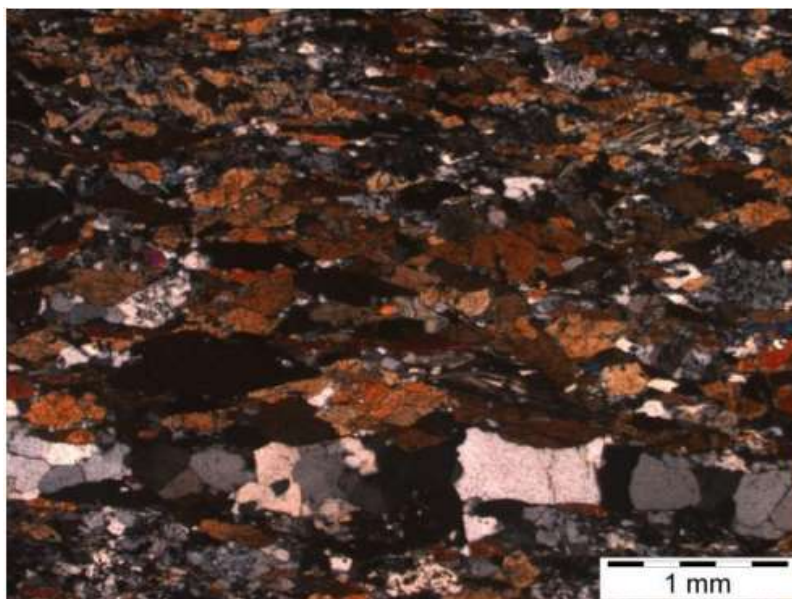
40

**Sample "B4": gneiss**

This sample of an outcrop was picked, because of his similarities to the Menhir sample PS. The dominating geological unit in this area is the Semmering Komplex. The main components in this sample are plagioclase, quartz, garnet, chlorite and biotite (Fig. 27). The biotite starts to transform to chlorite (Landler, 2014).
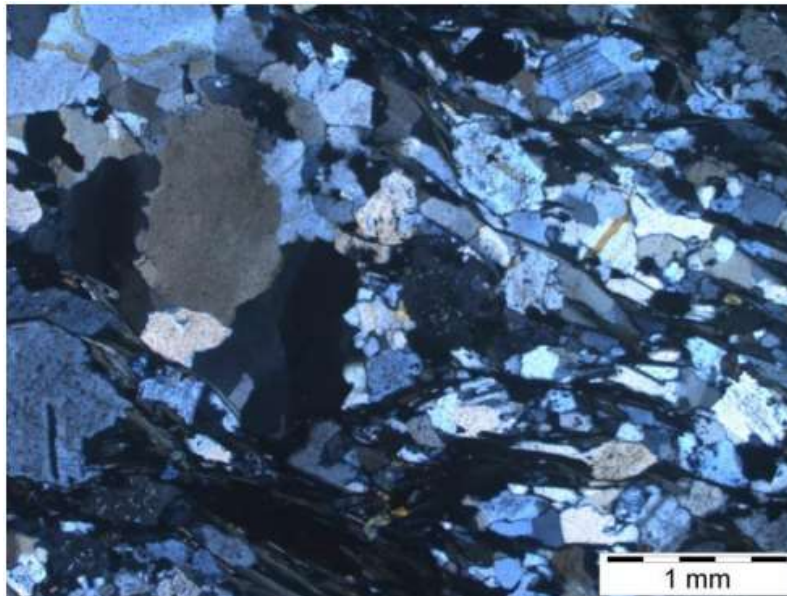


Figure 27: Photo of a thin section from sample B4; crossed-polarized illumination; taken by Landler Andreas.

## 5.3 Summary

The analysis of the mineral assemblage and texture of several outcrops and Menhir samples confirms the results from the field work. Three main types of rocks can be identified: Gneiss, different kinds of schists and amphibolite. Most of the samples have a metamorphic schistose texture. The gneiss mainly consists out of plagioclase, quartz, garnet, chlorite and biotite. The schists are mainly built up of quartz, garnet, plagioclase and muscovite. Depending on the sample other minerals like chlorite, hornblende and opaque phases can occur. All of the thin sections show a good schistosity and an advanced alteration. The amphibolites are mainly composed of amphibole, plagioclase, zoisite and garnet. Other minerals which occur in certain samples are: titanite, muscovite and chlorite. Like the schists, the amphibolites have a good schistosity. The mineral assemblage and texture do not vary a lot between the samples of a

certain rock type. In matters of the rock type, their mineral assemblage and their structure, there are no differences between the samples taken from the Menhirs and Holed Stones and the samples taken from outcrop. Four samples of the in-situ rocks are taken from areas within the Semmering Komplex. These are two amphibolites, one garnet-muscovite-schist and a paragneiss. Four more samples were taken in the area of the Waldbach Komplex. In particular, two garnet-chlorite-muscovite-schists and one gneiss. The last one was collected in the area of the Strallegg Komplex. In fact, a garnet-muscovite-schist. The studied samples all fit well into the respective petrological description of Schuster et al. (2001).

# 6. Scanning electron microprobe analysis

The section above has shown that the Menhirs and Holed Stones are made up of several rock types that are common basement rocks in the Eastern Alps. Therefore, to get better evidence about on the origin of the Menhirs and Holed Stones, more specifying analyses were done with the aid of the scanning electron microscope. Firstly, some garnet zoning profiles were prepared and secondly some geothermobarometry calculations were done, so this data can then be compared to published data for different geological units from the literature.

## 6.1 Garnet zoning profiles

Some significant garnets of four samples were analyzed with respect to their zoning profiles. The aim was to identify possible second garnet growths. The reason are the polymetamorphic units in the vicinity of Vorau. Just monomorphic garnet profiles could lead to the assumption of an origin from further away. Second growths could be a sign of a nearby origin.

**Sample 1(L10)**
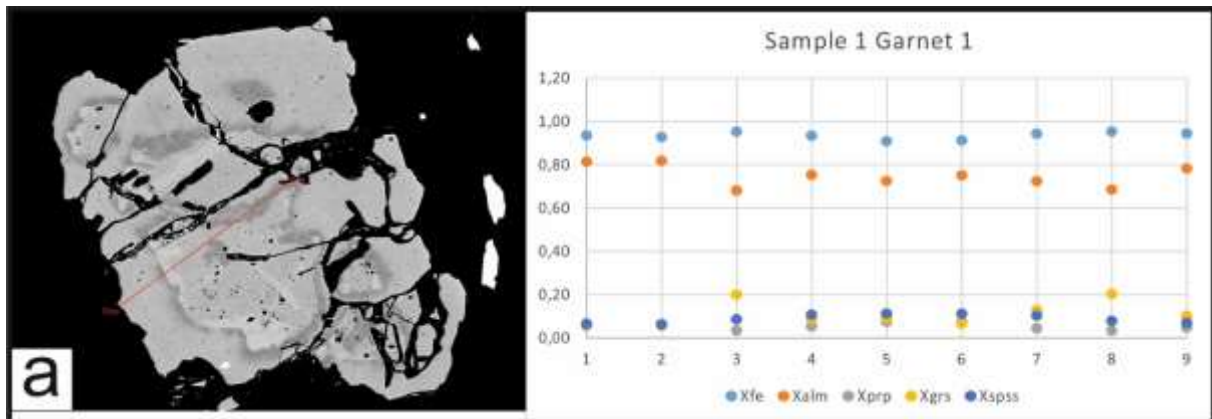


Figure 28: The figure shows BSE image of the sample 1. The analysed garnet is located in the middle of the image. The red profile line marks the different points of the analyses. The analysis with the weight percentage of the different garnets and the XFe is added. In which the Xalm symbolizes the almandine component, the Xprp symbolizes the pyrope component, the Xgrs symbolizes the grossular component and the Xspss symbolizes the spessartine component.

This garnet from the sample L10 shows some small chemical differences, but generally speaking there is no real second growth rim observable. Almandine is the predominating endmember. Pyrope, grossular and spessartine just reach small concentrations. Furthermore, the garnet grain looks altered with a lot of cracks (Fig. 28). These cracks combined with diffusion processes could be responsible for the small chemical changes along the profile line.

**Sample 2(L11)**
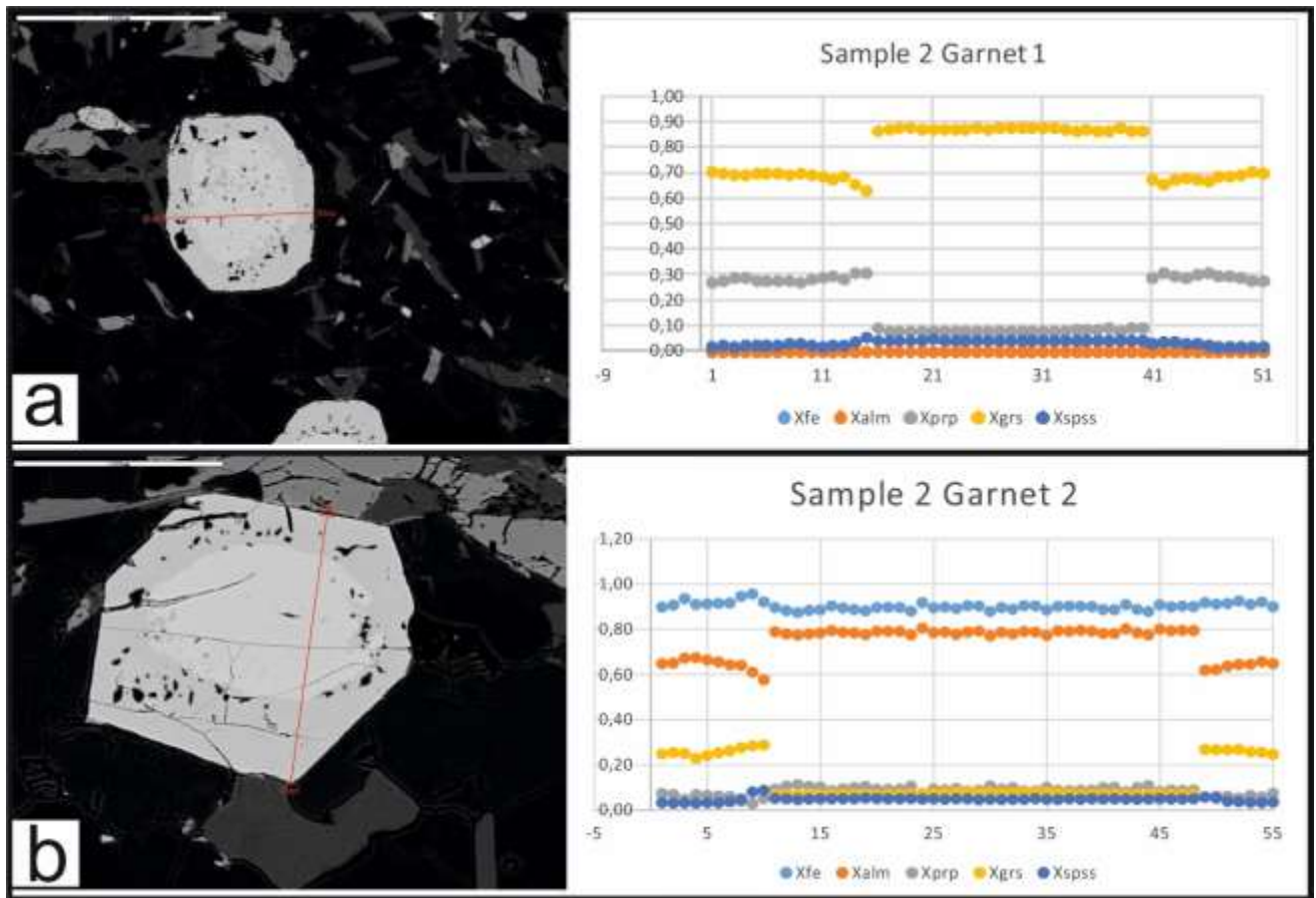


**Figure 29: The figure shows two different BSE images of sample 2. The analysed garnets are located in the middle of the image. The red profile line marks the different points of the analyses. The analysis with the weight percentage of the different garnets and the XFe is added. In which the Xalm symbolizes the almandine component, the Xprp symbolizes the pyrope component, the Xgrs symbolizes the grossular component and the Xspss symbolizes the spessartine component.**

These garnets from the sample L11 show some chemical zoning. There is an obvious gap between the core and the rim. This could be seen in the BSE images as well as in the measured garnet zoning profiles (Fig. 29). An increased grossular component and a decreased almandine component at the rim are responsible for this discontinuity in the zoning profile. Furthermore, especially the garnet in Fig. 29b shows an almost perfect idiomorphic grain boundary.

**Sample 3(L13)**
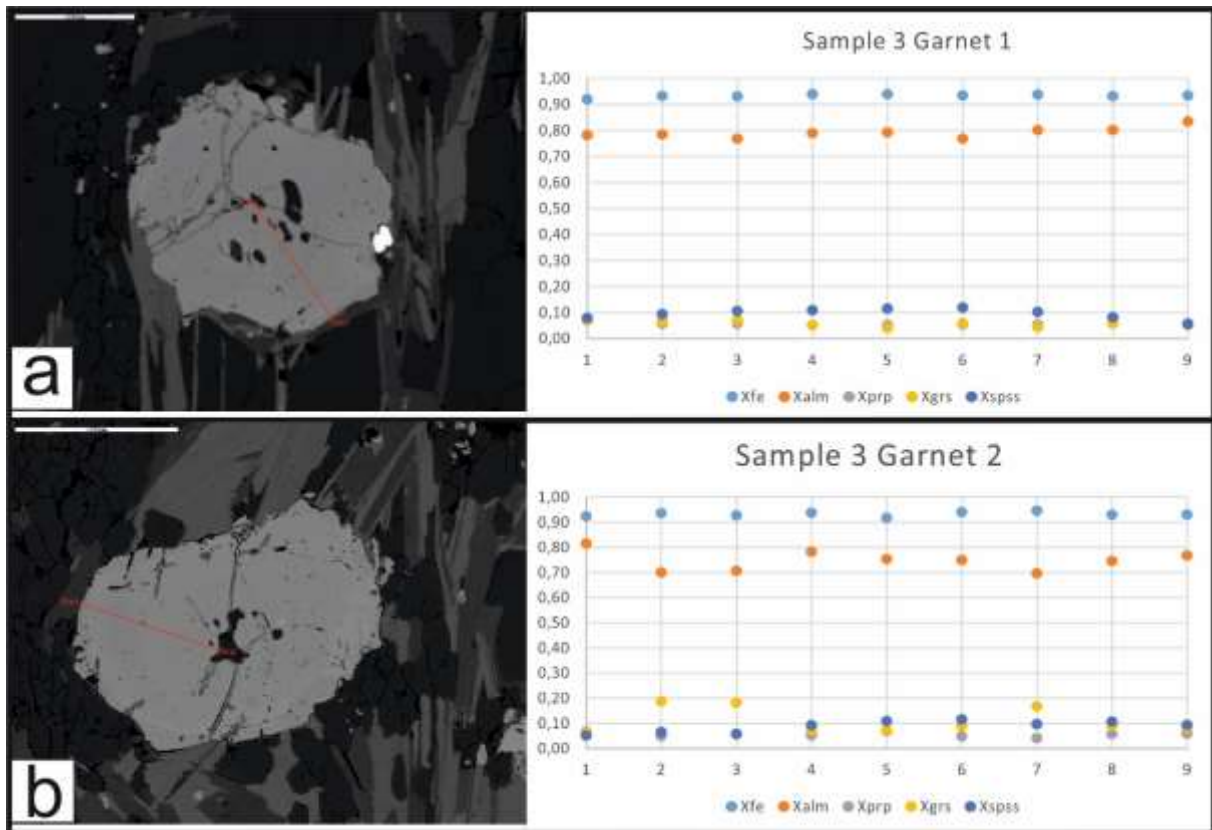


**Figure 30: The figure shows two different BSE images of the sample L13. The analysed garnets are located in the middle of the image. The red profile line marks the different points of the analyses. The analysis with the weight percentage of the different garnets and the XFe is added. In which the Xalm symbolizes the almandine component, the Xprp symbolizes the pyrope component, the Xgrs symbolizes the grossular component and the Xspss symbolizes the spessartine component.**

This garnet from L13 shows almost no chemical differences. The profiles end in the middle of the garnet grains. That is the reason for the just one-sided marks of a diffusion process at the beginning of the profile line (Fig. 30b). Almandine is the predominating endmember again. Furthermore, the garnet grain looks altered especially at the grain boundaries.

# Sample 4(L18)
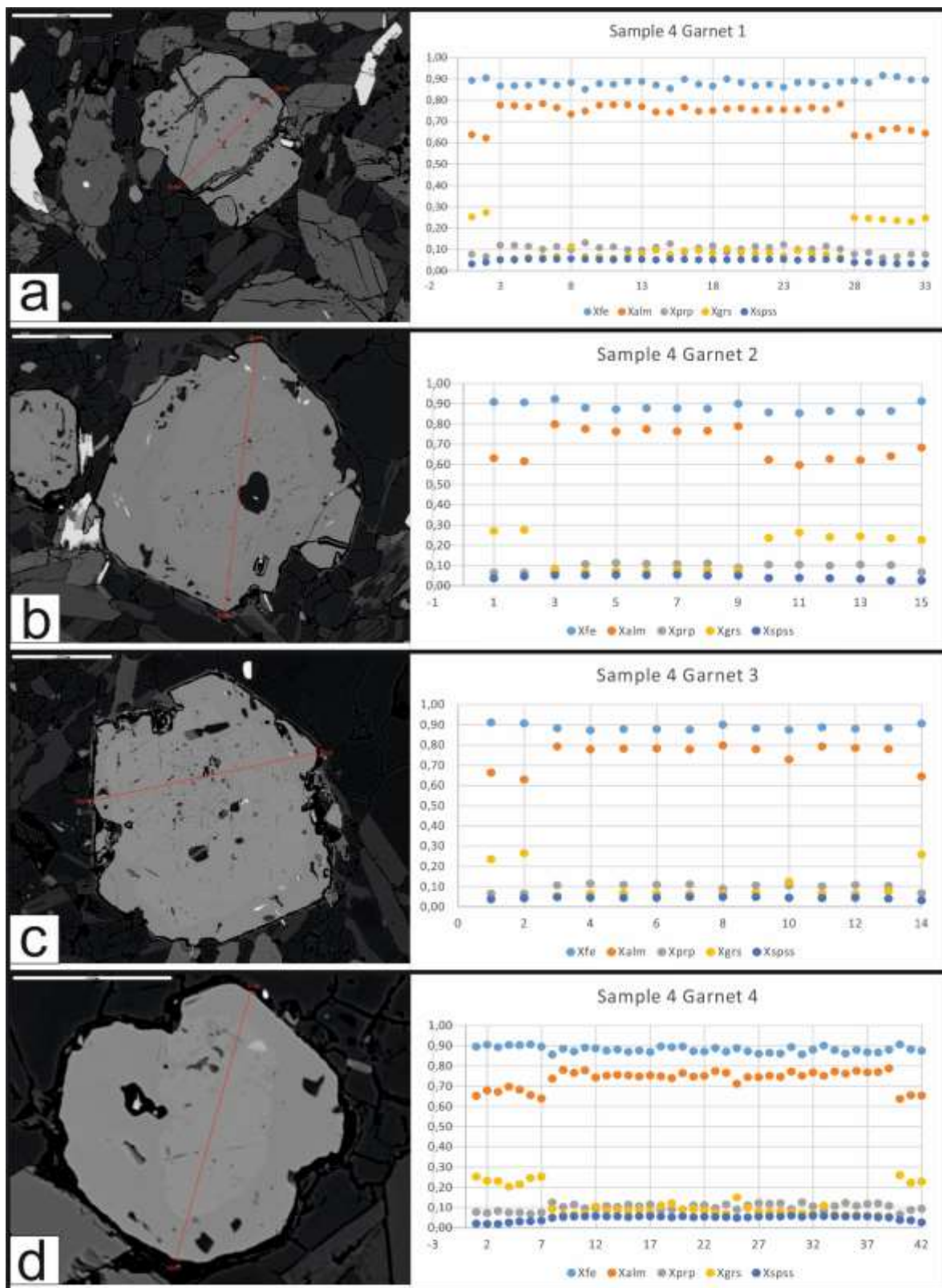


Figure 31: The figure shows four different BSE images of the sample L18. The analysed garnets are located in the middle of the image. The red profile line marks the different points of the analyses. The analysis with the weight percentage of the different garnets and the XFe is added. In which the Xalm symbolizes the almandine component, the Xprp symbolizes the pyrope component, the Xgrs symbolizes the grossular component and the Xspss symbolizes the spessartine component.

These garnets from sample L18 show relatively similar chemical zoning compared to the garnets of sample L11. There is an obvious gap between the core and the rim again. This could be seen in the BSE images as well as in the garnet profiles (Fig. 31). Once again an increased grossular component and a decreased almandine component are responsible for this discontinuity in the zoning profile. Furthermore, the garnets have more or less idiomorphic grain boundaries.

## 6.2 Conclusion

The samples can be divided in two subgroups. Sample L10 and L13 show no signs of a second growth on their rim (Fig. 28 and 30). The profile lines are relatively constant in their garnet endmember weight percentages. Just on their rims small changes can be detected. These small changes are likely to be caused by diffusion processes with interacting minerals. In these samples almandine is the predominating endmember. In contrast, samples number L11 and L18 show changes from the rim to the core (Fig. 29 and 31). These differences can easily be seen in the BSE images, due to the different gray shades. This kind of change in the endmember concentration can identified even more explicitly in the garnet profiles. In these, the rim shows a higher grossular component and lower almandine component than the core. The clear cut compositional change between core and rim are an evidence of a second growth. A diffusion process would cause more gently slopes. The almandine component is predominating in theses samples too. Especially in the core it has the highest weight percentage by far. But on the rims the grossular component increases. This increasing grossular and therefore calcium component could be the sign of a second from higher pressures pressure influenced growth (Spear, 1993). It is worth mentioning, that the samples without a second growth on the rim were both taken from garnet-mica-schists and the two samples with the second growth were taken from amphibole-bearing schists.

## 6.3 Geothermobarometry analyses

To get a better comparison between Menhirs and outcrop in the region three samples were used to get information about their formation *PT* conditions. These samples were chosen because they had enough phases and they seemed to be in equilibrium and can therefore be

used for this kind of calculations. For a geothermometer I chose the iron - magnesium exchange between garnet and biotite or between garnet and amphibole. The pressure was calculated in two ways. Firstly, the assemblage of the minerals garnet-plagioclase-biotite and secondly the assemblage of the minerals garnet-amphibole-plagioclase were taken. The analyses of each mineral used for the calculations are illustrated in tables in the appendix in chapter 11.3 (see appendix). The labels of the plots always give notice of the exact method used. The symbol "_" divides three groups of acronyms. In the first group Pr2 represents sample L11, Pr3 represents sample L13 and Pr4 represents sample L18. The second group of acronyms represents the mineral assemblages used for barometry calculations. In which the abbreviation gt is used for garnet, pl for plagioclase, am for amphibole and bt for biotite. The ending "2" following the mineral abbreviation indicates the magnesium endmember reactions. The gtplbt-geobarometer after Hoisch, (1990) is based on the equation

$$1/3 \text{ pyrope} + 2/3 \text{ grossular} + 2 \text{ quartz} \leftrightarrow 2 \text{ anorthite} + \text{annite}$$

and the gtampl-geobarometer after Dale et al., (2000) follows the reaction

$$\text{tschermakite} + 4/3 \text{ grossular} + 2/3 \text{ pyrope} + \text{quartz} = \text{tremolite} + 4 \text{ anorthite}$$
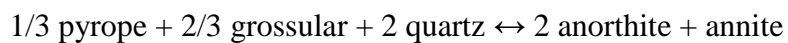
The missing of the number "2" indicates iron endmembers reactions. The gtplbt-geobarometer after Hoisch, (1990) is based on the equation

$$1/3 \text{ almandine} + 2/3 \text{ grossular} + \text{syderophyllite} + 2 \text{ quartz} \leftrightarrow 2 \text{ anorthite} + \text{annite}$$

and the gtampl-geobarometer after Dale et al., (2000) follows the reaction

$$\text{pargasite} + 2/3 \text{ grossular} + 1/3 \text{ pyrope} + 6 \text{ quartz} = \text{tremolite} + 2 \text{ anorthite} + \text{albite}$$
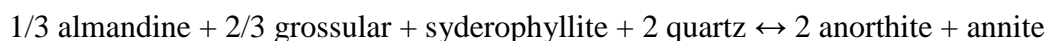
The third group of acronyms indicates the mineral assemblage used for thermometry calculations. The mineral abbreviations have similar meaning as described in connection with the barometry.

**Sample 2(L11)**
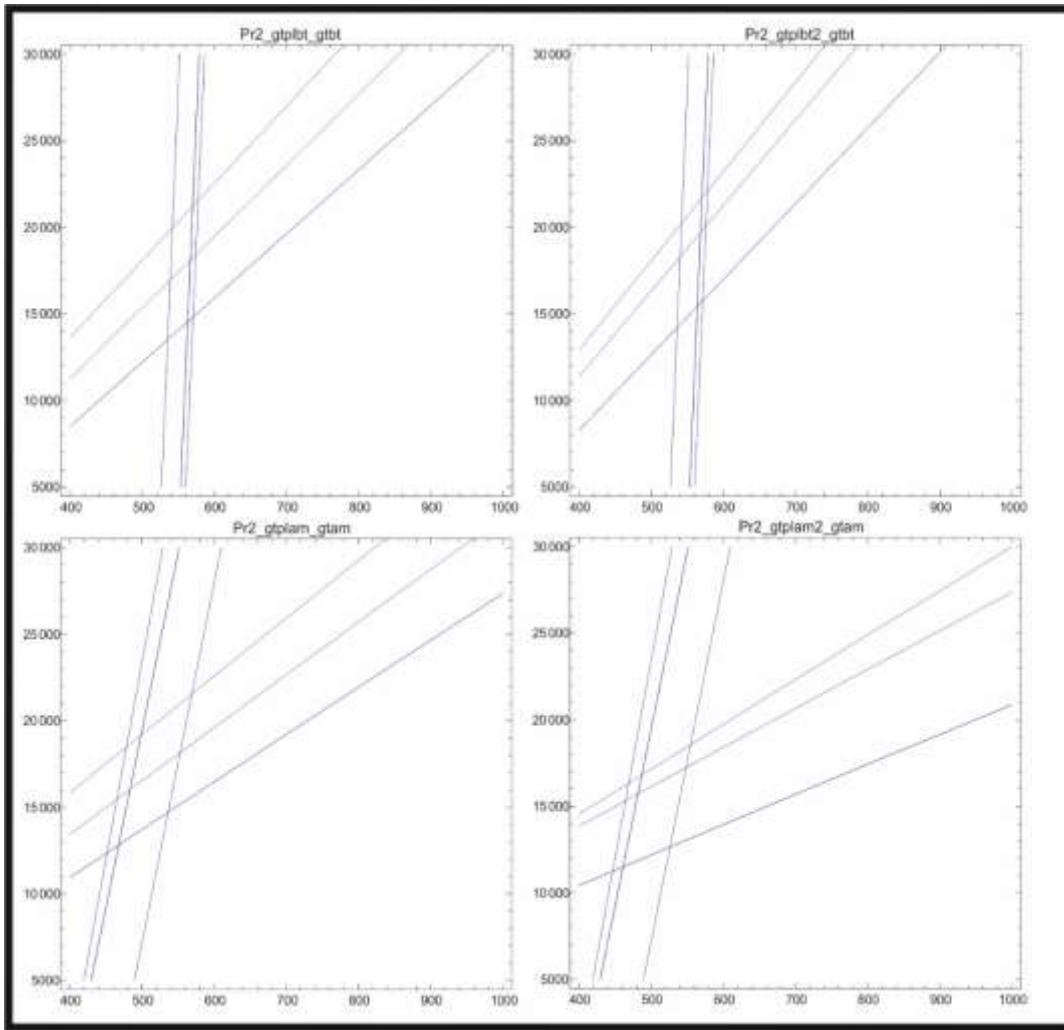


Figure 32: The result of the geothermobarometry of sample L11. This image shows four differently calculated possible *PT* conditions. In which, Pr2_gtplbt_gtbt was calculated based on the interaction of the magnesium endmembers within the mineral assemblage of garnet-plagioclase-biotite, Pr2_gtplbt2_gtbt based on the interaction the iron endmembers within the mineral assemblage of garnet-plagioclase-biotite, Pr2_gtplam_gtam based on the interaction of the magnesium endmembers within the mineral assemblage of garnet-amphibole-plagioclase and Pr2_gtplam2_gtam based on the interaction the iron endmembers within the mineral assemblage of garnet-amphibole-plagioclase.

These four geothermobarometers show relatively similar results. The first two, which are based on garnet-plagioclase-biotite reactions, would indicate a temperature of 520 °C to 560 °C and a pressure of 13 kbar to 22 kbar. The differences between the magnesium endmember reaction and the iron endmember reaction are very small. The garnet-amphibole-plagioclase reaction shows a bigger discrepancy. Furthermore, it provides a little bit lower temperatures of 420 °C to 540 °C but relatively similar pressure values (Fig. 32).

**Sample 3(L13)**
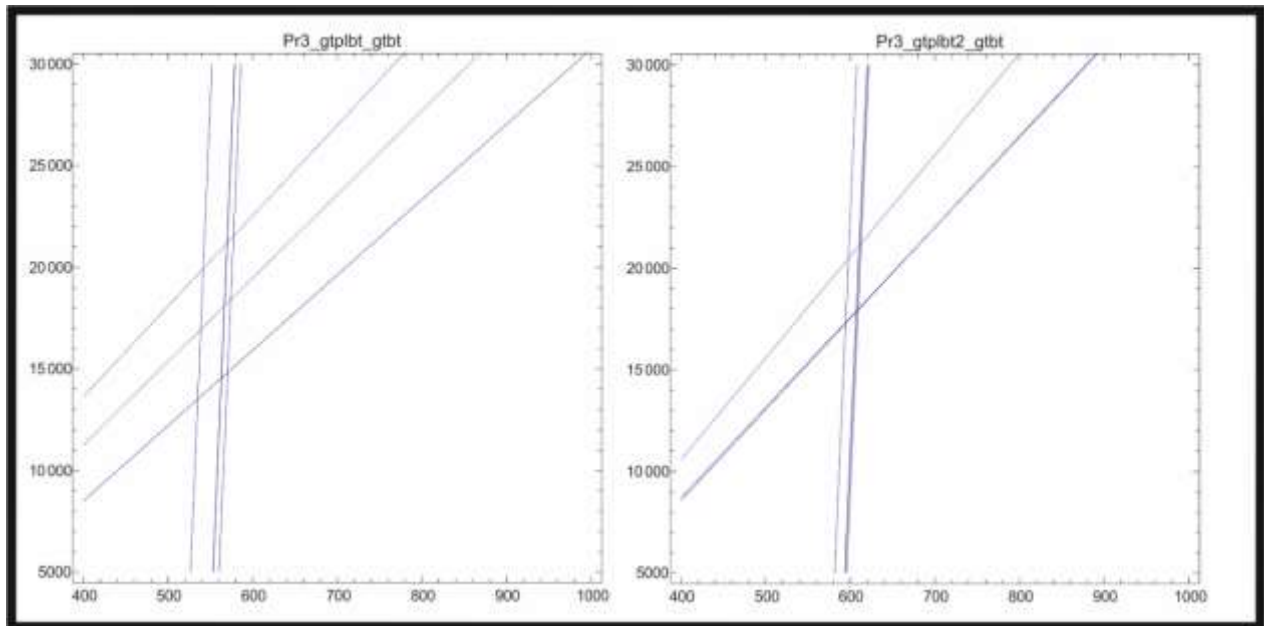


Figure 33: The result of the geothermobarometry of sample L13. This image shows two differently calculated possible *PT* conditions. In which, Pr3_gtplbt_gtbt was calculated based on the interaction of the magnesium endmembers within the mineral assemblage of garnet-plagioclase-biotite and Pr3_gtplbt2_gtbt based on the interaction the iron endmembers within the mineral assemblage of garnet-plagioclase-biotite.

These two geothermobarometers show relatively similar results. They are based on garnet-plagioclase-biotite reactions. The result would indicate a temperature of 520 °C to 600 °C and a pressure of 13 kbar to 22 kbar. There are some differences between the magnesium endmember reaction and the iron endmember reaction. The iron related calculation "Pr3_gtplbt2_gtbt" show a smaller variation in terms of the possible *PT* conditions (Fig. 33).

**Sample 4(L18)**
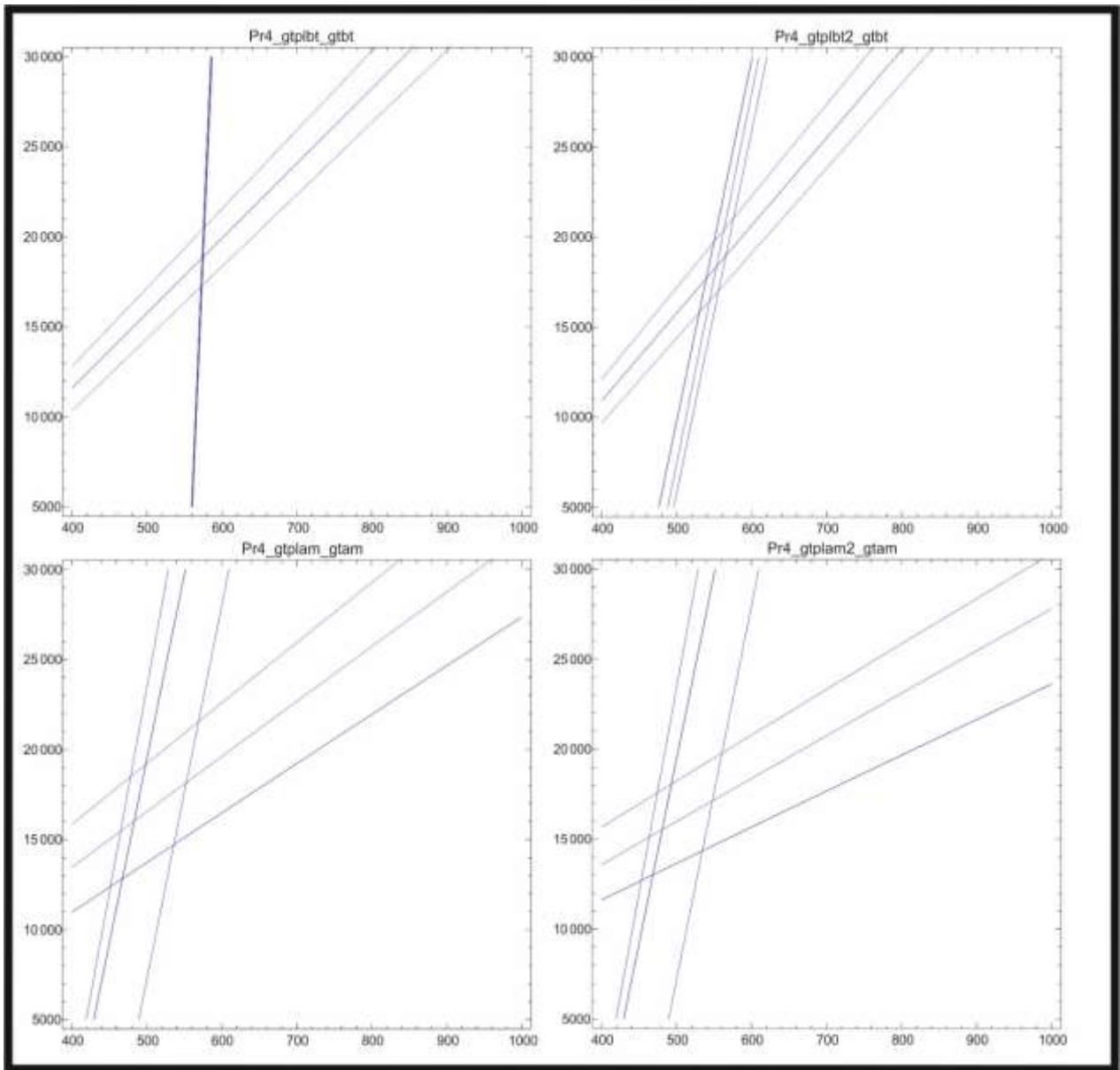
**Figure 344: The result of the geothermobarometry of sample number L18. This image shows four differently calculated possible *PT* conditions. In which, Pr4_gtplbt_gtbt was calculated based on the interaction of the magnesium endmembers within the mineral assemblage of garnet-plagioclase-biotite, Pr4_gtplbt2_gtbt based on the interaction of the iron endmembers within the mineral assemblage of garnet-plagioclase-biotite, Pr4_gtplam_gtam based on the interaction of the magnesium endmembers within the mineral assemblage of garnet-amphibole-plagioclase and Pr4_gtplam2_gtam based on the interaction of the iron endmembers within the mineral assemblage of garnet-amphibole-plagioclase.**

These four geothermobarometers show relatively similar results. The first two geothermobarometers, which are based on garnet-plagioclase-biotite reactions, would indicate a temperature of 520 °C to 560 °C and a pressure of 16 kbar to 21 kbar. The differences between the magnesium endmember reaction and the iron endmember reaction are relatively small, especially in relation to the pressure. The garnet-amphibole-plagioclase reaction shows

a small discrepancy as well. Furthermore, it provides a little bit lower temperatures of 440 °C to 540 °C and a little bit lower pressures of 14 kbar to 21 kbar (Fig. 34).

## 6.3.1 Summary

All the calculated geothermobarometers show relatively similar pressure and temperature conditions (Figs. 32, 33 and 34). In fact, the temperature varies between 440 °C and 600 °C. The garnet-amphibole thermometer indicates lower temperatures of about 440 °C to 500 °C and the garnet-biotite thermometer a little bit higher temperatures of 450 °C to 600 °C. The formation pressures range from about 10 kbar until even 22 kbar. This thesis gets strengthened by the lnK numbers of the barometers. According to Hoisch (1990), the lnK number of the garnet-plagioclase-biotite barometer should be between 3.61 and 6.62 for the magnesium reaction and between 1.85 and 4.89 for the iron reaction. But the sample L11 shows calculated values of lnK = -6.21317, lnK = -7.70965 and lnK = -9.25935 for the magnesium endmember reaction and calculated values of lnK = -10.8083, lnK = -9.95181 and lnK = -11.6878 for the iron endmember reaction. Sample L13 shows calculated values of lnK = -6.70356, lnK = -7.20381 and lnK = -7.83255 for the magnesium endmember reaction and calculated values of lnK = -8.65736, lnK = -9.12639 and lnK = -10.0146 for the iron endmember reaction. Sample L18 shows calculated values of lnK = -8.19074, lnK = -7.35577 and lnK = -9.06581 for the magnesium reaction and calculated values of lnK = -10.8083, lnK = -9.95181 and lnK = -11.6878 for the iron endmember reaction. None of them fits into the proposed range. Additionally, the calcium content of the garnets is much higher than the calcium content of the garnets used to get this calibration. According to Hoisch (1990), really low lnK values could lead to higher pressure results, which imply that my pressure estimates may be overestimated.

## 6.4 Comparison to the geology of the vicinity

The rock types and their mineral parageneses of the Menhirs and Holed Stones are largely consistent with all geological units described in chapter 3 and in fact with many basement rocks from the Austroalpine nappe complex across the eastern Alps. The majority of the Menhirs are made out of different types of schists containing especially mica, garnet, chlorite and biotite, as they are the basement rocks in the region. Additionally, some Menhirs are made up of amphibolite and gneiss. The same three rock types are described in the Wechsel-, the Waldbach Komplex, the Semmering Komplex and the Strallegg Komplex (Schuster et al., 2001). Therefore, a location of the origin of the Menhirs and Holed Stones cannot uniquely be identified on the basis their mineralogy alone. To get a further constraint on the possible origin    nonetheless, the calculated *PT* conditions were used. The geothermometry shows formation temperatures of 440 °C to 600 °C. The geobarometry shows formation pressures of 10 kbar to 22 kbar, albeit the majority of the barometers plot between 18 kbar to 20 kbar. The lnK values show that these results are possibly falsified to a little bit higher pressures and the actual formation pressures may be somewhat lower than this. The comparison with the geological units allows neglecting some of them.

The Eoalpidic overprint of the Wechsel Komplex reaches conditions of the lower greenschist facies. Therefore, much lower temperature and pressure conditions as calculated for Menhirs and Holed Stones. According to the literature the area around the Wiesmather Fenster show a little bit higher *PT* conditions. But especially the calculated pressure is still too low. Therefore, the Wechsel Komplex cannot be considered as a high potential source for the Menhirs.  The Pre-Alpidic metamorphism of the Waldbach Komplex reached conditions of upper amphibolite facies and the Eopaldic overprint conditions of the greenschist facies (Schuster et al., 2001). These conditions would fit well in context with the temperature. However, the pressure is much too low. Consequently, I infer that this complex is also not a source for the Menhirs. However, the Semmering Komplex shows relatively similar formation characteristics to the Menhirs. The calculated temperature conditions of up to about 570 °C (Schuster et al., 2001) fit relatively well compared with the calculated temperature conditions of the Menhirs and Holed Stones. But again the calculated pressure in Birkfeld (within the Semmering Komplex) of 9 kbar to 11 kbar (Schuster et al., 2001) is far too low. As a consequence, this unit is also an unlikely origin of the Menhirs and Holed Stones. The most convenient crystalline unit in the vicinity is the Strallegg Komplex. Like in context with the

other units the Permian HT/LP conditions of the Strallegg Komplex (Schuster et al., 2001) are not suitable with the *PT* conditions calculated for the Menhirs and Holed Stones. But the rocks with an Eoalpidic metamorphic overprint show better fitting results. This event was pressure dominated and thus reaches calculated pressure conditions of up to 12 kbar to 15 kbar (Schuster et al., 2001). The calculated pressures of the Menhirs and Holed Stones start with 12 kbar and going up to 22 kbar. Moreover, like mentioned in chapter 6.3.1 the calculated pressures are a little bit overestimated. Considering this, the Strallegg Komplex is a high potential origin unit. The calculated temperatures of 530 °C to 600 °C match very well too compared to the temperature conditions calculated for the Menhirs and Holed Stones. All this makes the Strallegg Komplex the most suitable origin of all compared units. As discussed in chapter 3, the Strallegg complex crops out directly in Vorau and in several spots west and south of it, so a local origin of the Menhirs is likely.

# 7. Age dating

Because of the lack of historical documents and archaeological records, the erection age of the Menhirs is completely unknown. No organic artefacts for carbon dating were found. One possibility to constrain the age of these Menhirs is therefore the dating of the exposure of their surface with cosmogenically generated nuclides like $^{10}$Be or $^{26}$Al (TCN method). While this method has a range of limitations for archaeological purposes (Akcar et al., 2008), expertise at the university of Graz made it possible to try this attempt. This is the reason why in 2012 five samples were analyzed via cosmogenic nuclides. Four more samples were analyzed in 2014. In the following section I present a summary of all nine analyses and recalculate them for exposure age and erosion rate. The calculation of the ages was done with CRONUS-Earth online calculator. This program is available online and it is hosted by the Cosmogenic Nuclide Lab, University of Washington.

## 7.1 The Method

The method of using cosmogenic nuclides has become a very important way to date and characterize landscapes and surface. When rocks reach the last few meters to the surface during their geological history, their exposure to cosmic rays causes the build-up of cosmogenic nuclides in certain minerals (Kubik et al., 1998). One important advantage of this method is the number of nuclides available, for example: $^{10}$Be, $^{14}$C, $^{26}$Al, $^{36}$Cl, $^{2}$He, or $^{21}$Ne. As a result, a variety of minerals and lithologies can be used. Some of these isotopes have a high production rate and short half-life, so that they can be used to date time spans of thousands of years. For example, radiocarbon dating that makes use of the cosmogenic isotope $^{14}$C, can be used to date time spans of 50 ka and is therefore a great method for archaeological purposes. Others, like $^{10}$Be or $^{26}$Al, can be used to date time spans of tens of millions of years (Ivy-Ochs and Kober, 2008).

The creation of these cosmogenic isotopes is due to cosmic radiation. Cosmic radiation and neutrons coming from α-decay and spontaneous fission of uranium and thorium. Three other nuclear processes are caused by cosmic-rays. These are: spallation, nuclear emission and the muon induction. In most cases the exposure dating is done with $^{10}$Be and $^{26}$Al in quartz (Heisinger and Nolte, 2000). The process of building-up the radionuclides in the concerned

minerals continues until saturation is reached and there is a balance between radioactive decay and production rate. This secular equilibrium means that the number of decays and the production of nuclides per unit time is equivalent (Ivy-Ochs and Kober, 2008). The final concentration of the cosmogenically generated isotopes can be interpreted in terms of two different end member scenarios: Firstly, to determine exposure ages and secondly to get erosion rates (Brown et al., 1992) (Fig. 35).
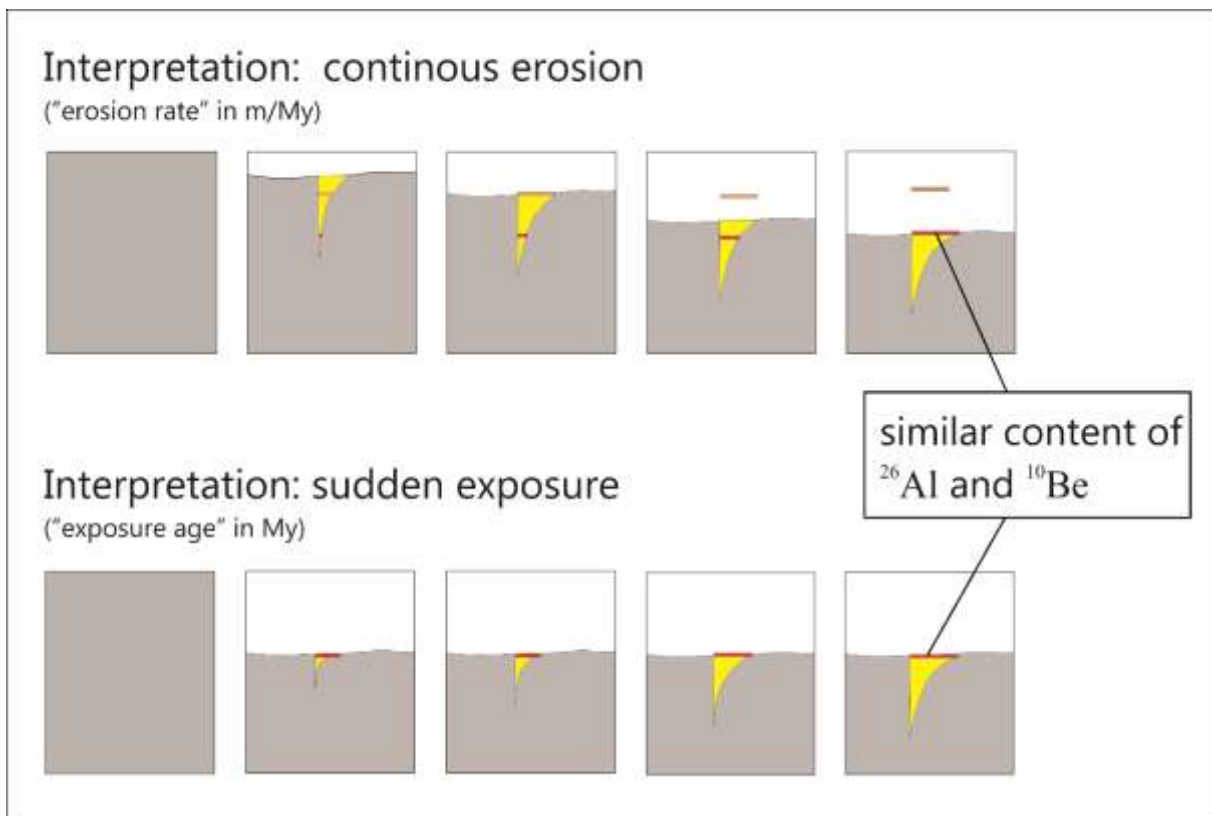


**Figure 35: Interpretation of the $^{10}$Be and $^{26}$Al content; continuous erosion vs sudden exposure. The continuous erosion shows a lithology, which is continuously eroded. The upper and brighter red marker represents the theoretical $^{10}$Be and $^{26}$Al content without erosion. The lower and darker red marker represents the actual $^{10}$Be and $^{26}$Al content after erosion has taken place over a certain time period. The red marker of the sudden exposure is always at the same position on the surface. So an exposure age can be analyzed. But if you look at the markers of the same time period (last step in the figure) they have a similar $^{10}$Be and $^{26}$Al content. This fact is responsible for the difficulties in deciding if the result can be taken as an exposure age or an erosion rate.**

## 7.2 Exposure age vs erosion rate

Continuous erosion of the last 5 - 10 meters to the surface or sudden exposure of the very surface are two end member processes that can potentially result in similar concentrations of cosmogenic isotopes in surface rocks, for example if the exposure age is short and the erosion rate slow and long lived. In order to discern between these two end member processes, careful

depth profiling needs to be done so that the drop off in production rate with depth can be interpreted. Nevertheless, a brief overview over the two end member interpretations is given below.

**Exposure age**

Radionuclides build up in surface-near minerals when they are exposed to cosmic rays. The production rate of these isotopes decreases exponentially with distance from the surface, but complete shielding is only achieved when rocks are about 10 m removed from the surface. If a rock reaches the surface instantaneously, for example by fluvial erosion of a strath terrace, by deglaciation of a glacially carved surface, by exposure of a new surface through landslides or by excavating a Menhir from a quarry, then the concentration of cosmogenic isotopes is directly proportional to the exposure of this surface to cosmic radiation. As a result, it is possible to figure out how long this exposure of the rock or soil has been and thus get the exposure age. The method is best calibrated for the isotopes $^{10}$Be or $^{26}$Al in quartz. However, it must be noted that after 4 - 5 million years, the radioactive decay begins to balance the production rate so that the method for the isotopes $^{10}$Be or $^{26}$Al in quartz is limited to this time scale.

When using this method certain corrections have to be considered to get representative results. These corrections include the altitude/latitude correction, the shielding by mountains and sample geometry, shielding by soil and rock, the erosion, and the prior exposure (Kubik et al., 1998). Although cosmogenic isotopes are still generated in several meters depth, a clear interpretation of exposure age should generally be done with samples from the top 10 cm of an exposure (Fig. 35).

**Erosion rate**

Alternatively, the concentration of cosmogenic isotopes measured in rocks may be caused by successive accumulation of these isotopes during the exhumation of rocks through the last few meters near the surface by continuous erosion that exposed the rock only recently to the very surface (Fig. 35). Thus, the concentration can be re-calculated in terms of an erosion rate. Von

Blanckenburg (2008) pioneered a new interpretation of erosion rate measurements using cosmogenic isotopes by sampling not surface exposure of outcrop, but by sampling river sediments. This method can be used to obtain catchment integrated erosion rates on the time scale of several ka.

## 7.3 Samples

In an attempt to constrain the erection age of the Menhirs, a total of nine samples were collected in two different sampling runs. The first five samples were taken by Heinrich und Ingrid Kusch on September 29th 2012. They were convoyed by director Peter Behringer and a filming team from Servus TV. They were analysed for their $^{10}$Be content by Prof. D. Granger in the TCN lab in California-Berkeley, USA. The second sampling run was done two years later and the four samples collected then were analysed for the $^{10}$Be content by Professor D. Fabel in the TCN lab of NERC, Glasgow, Scotland. All samples were crushed, ground and sieved for two fractions: 250 - 500 micron and 125 - 250 micron, before they were sent to the respective laboratories for further wet chemical processing and ultimately $^{10}$Be measurements.

**Sample LS1-9/2012 (1. location, first sampling run)**

This sample was taken in Sommersgut near Wenigzell some km away from Vorau. The taken sample refers to a Holed Stone, which is made out of garnet-mica-schist and have a height of 1.80 m (Fig. 36a). In the appendix the Menhir is listed as sample K136. It is located next to a Christian wayside shrine. The exposure to the sun is nearly 180° and the mountains are in all direction at maximum 5° over the horizon. The sample was taken mainly from NW side of the Holed Stones, which is SW-NE orientated.  The location of the sample is: 47° 27' 57.6'' N; 15° 49' 12'' E and the elevation is 816 m.a.s.l..

**Sample FHM1-9/2012 (2. location, first sampling run)**

The second sample, which has about 2 kg, is not a Menhir, but a cover plate of a subsurface chamber. It was taken from the "Franzosenhöhle" in the forest near Miesenbach (Fig. 36b). The sampling point is situated near the forest floor on the capstone of the entrance chamber. This rock is 1 m long and seems not to be treated. The rock material is quartzite. The entrance is oriented almost exactly in direction south. The entrance of the chamber with a diameter of ca 3 m is located on 15° steep and south directed hillside. The location of the sample is: 47° 24' 25.2''N; 15° 49' 40.8'' E and the elevation is:  1100 m.a.s.l..

**Sample MZ2-9/2012 (3. location, first sampling run)**

This sample was taken from the so called "Schiff" near the Almer Menhir Zeilerviertel (Fig. 36c).  The so called "Schiff" is a rounded block of about 10 x 5 x 2 m dimension lying around in the forest. According to Heinrich Kusch its surface is somewhat processed by human beings. The sample was taken from the upper flat side.  The location of the sample is: 47° 21' 25.2'' N; 15° 54' 25.2'' E and the elevation is: 900 m.a.s.l..

**Sample SBPK1-9/2012 (4. location, first sampling run)**

The next sample was taken from the upper side of a spectacular rock in the prehistoric stonepit Pongratzer Kogel near Stammbach (Fig. 36d). This rock has several man-made holes along a line which look like they were used to insert wedges to cleave off further plates from it. The location of the sample is: 47° 20' 27.6'' N; 15° 54' 18'' E and the elevation is: 823 m.a.s.l.. The sample was taken from the top five centimeters of the rock surface.

**Sample SGP1-9/2012 (5. location, first sampling run)**

This sample was taken from a subsurface tunnel called "Grubergang", located near Pongrazen (Fig. 36e). The entrance of this tunnel is located in the cellar of farmhouse. The origin of the

taken sample is the cover plate of the entrance. The location of the sample is: 47° 20' 16.8''
N; 15° 54' 3.6'' and the sampling elevation is: 588 m.a.s.l..



**Figure 36: Photos of the sample location of the first sample run; photos taken by Ingrid Kusch; a) A Holed Stone in Sommersgut near Wenigzell Location: N47° 27' 57.6''; E15° 49' 12''; Sea-level: 816 m. b) The" Franzosenhöhle" in the forest near Miesenbach; Location: N47° 24' 25.2''; E15° 49' 40.8''; Sea-level: 1100 m. c) The so called „Schiff"; Location: N47° 21' 25.2''; E15° 54' 25.2''; Sea-level: 900 m. d) A spectacular rock in the prehistoric stonepit Pongrazer Kogel; Location: N47° 20' 27.6''; E15° 54' 18''; Sea-level: 823 m. e) A subsurface tunnel called "Grubergang"; Location: N47° 20' 16.8''; E15° 54' 3.6 ''; Sea-level: 588 m.**

**Sample SBPK22014 (1. location, second sampling run)**

This sample was taken from the prehistoric stone pit near Humertal nearby St. Pankrazen on October 5$^{th}$ 2014 by Heinrich and Ingrid Kusch (Fig. 37). The sampling point is located in a forest and is exposed to the sun from the early morning until late afternoon. The border of the taken sample is orientated in direction east. The location of the sample is: 47° 20' 30.0'' N; 15° 54' 20.5'' E and the elevation is: 825 m.a.s.l.



Figure 37: SBPK22014; The sample location the prehistoric stone pit near Humertal nearby St. Pankrazen.

**Sample STKH22013 (2. location, second sampling run)**

The origin of this sample is the subsurface tunnel on the southwest hillside of the mountain Hintereck in Prätis. It was taken on November 28th 2012 by Heinrich and Ingrid Kusch. The sample is originated directly under the cover plates of a subsurface tunnel. At that, there is an overlap with soil from about 0.5 m (Fig. 38). The subsurface tunnel is located in the forest and is oriented in direction SW. Furthermore, the spot is exposed to the sun from the morning until the evening. In which the light incidence is angular in the morning. The location of the sample is: 47° 22' 19.3'' N; 15° 49' 21.8'' E and the elevation is: 1009 m.a.s.l..



Figure 38: STKH22013. The sample location is a subsurface tunnel on the southwest hillside of the mountain Hintereck in Prätis.

**Sample KEPU12013 (3. location, second sampling run)**

This sample was taken from a human worked cover plate from the Kandelhofer Erdstall near by the Erzherzog Johann Höhe in Puchegg by Dr. Heinrich and Ingrid Kusch on October 20th 2013 (Fig. 39). The Kandelhofer Erdstall is a more than 26 m long subterranean construction with an 8 m long corridor made out of rubble masonry. This construction is covered with about one m of sediments and is exposed to the sun from the morning until the evening and is oriented in direction E-W. The location of the sample is: 47° 23' 22.2'' N; 15° 53' 29.46'' E and the elevation is: 794 m.a.s.l..



Figure 39: Location of sample KEPU12013. The sample location is the Kandelhofer Erdstall near by the Erzherzog Johann Höhe in Puchegg.

**Sample SGPU12012 (4. location, second sampling run)**

The origin of this sample is the Strebl-Felsgang in Puchegg. It was taken on September 20<sup>th</sup> 2012 by Kurt Stüwe. The Strebl-Felsgang is an 89 m long, subterranean and walkable construction with an entrance made out of rubble masonry. The sample was taken from the cap stone, which is not covered by soil. It is exposed to the sun from the morning until the evening and is oriented in direction W (Fig. 40). The location of the sample is: 47° 23.017' N; 15° 52.652' E and the elevation is 755 m.a.s.l..



Figure 40: Location of sample SGPU12012. The sample location is the Strebl-Felsgang in Puchegg.

## 7.4 Analysis and results

The [10]Be measurements performed by the two laboratories for the two sampling runs form a consistent picture. In order to use them as a potential time constraint for building the sampled monuments, the data were re-calculated using the CRONUS-Earth online calculator with the newest production rates. For this, a series of input data had to be prepared (Fig. 41, 42). In particular, these include a series of corrections for shielding, production rates, sample thickness and more (see Figs 43 and 44). With this input data and the both the hypothetical exposure age and the hypothetical erosion rate were calculated (Figs. 45 and 46).

| Sample name | Latitude (Decimal degrees) | Longitude (Decimal degrees) | Elevation (meters) | Elevation flag | Sample thickness (cm) | Sample density (g cm-3) | Shielding correction |
|---|---|---|---|---|---|---|---|
| SGP192012 | 47.338 | 15.901 | 588 | std | 1 | 2.8 | 1 |
| FHM192012 | 47.407 | 15.828 | 1100 | std | 2 | 2.8 | 1 |
| LS192012 | 47.466 | 15.820 | 816 | std | 2 | 2.8 | 1 |
| SBPK92012 | 47.341 | 15.905 | 823 | std | 3 | 2.8 | 1 |
| MZ292012 | 47.357 | 15.907 | 900 | std | 3 | 2.8 | 1 |
| Sample name | Erosion rate (cm yr-1) | 10Be concentration (Atoms g-1) | Uncertainty in 10Be concentration (Atoms g-1) | Name of Be-10 standardization | 26Al concentration (Atoms g-1) | Uncertainty in 26Al concentration (Atoms g-1) | Name of Al-26 standardization |
| SGP192012 | 0 | 78959 | 2182 | 07KNSTD | 0 | 0 | KNSTD |
| FHM192012 | 0 | 125836 | 4524 | 07KNSTD | 0 | 0 | KNSTD |
| LS192012 | 0 | 127710 | 3041 | 07KNSTD | 0 | 0 | KNSTD |
| SBPK92012 | 0 | 375302 | 5723 | 07KNSTD | 0 | 0 | KNSTD |
| MZ292012 | 0 | 534334 | 7709 | 07KNSTD | 0 | 0 | KNSTD |

Figure 41: The input data of the first analyses run. The five samples SGP192012, FHM192012, LS192012, SBPK192012 and MZ292012 were analysed.

| Sample name | Latitude (Decimal degrees) | Longitude (Decimal degrees) | Elevation (meters) | Elevation flag | Sample thickness (cm) | Sample density (g cm-3) | Shielding correction |
|---|---|---|---|---|---|---|---|
| SSP12012 | 47.333 | 15.877 | 755 | std | 2 | 2.65 | 0.9989 |
| STKH22013 | 47.369 | 15.820 | 1009 | std | 2 | 2.65 | 0.9956 |
| KEPU12013 | 47.389 | 15.891 | 794 | std | 2 | 2.65 | 1 |
| SBPK22014 | 47.338 | 15.903 | 825 | std | 3 | 2.65 | 0.9786 |
| Sample name | Erosion rate (cm yr-1) | 10Be concentration (Atoms g-1) | Uncertainty in 10Be concentration (Atoms g-1) | Name of Be-10 standardization | 26Al concentration (Atoms g-1) | Uncertainty in 26Al concentration (Atoms g-1) | Name of Al-26 standardization |
| SGP192012 | 0 | 177209 | 4619 | NIST_27900 | 0 | 0 | KNSTD |
| FHM192012 | 0 | 111904 | 5104 | NIST_27900 | 0 | 0 | KNSTD |
| LS192012 | 0 | 216659 | 6234 | NIST_27900 | 0 | 0 | KNSTD |
| SBPK92012 | 0 | 451033 | 10114 | NIST_27900 | 0 | 0 | KNSTD |

Figure 42: The input data of the second analyses run. The four samples SSP12012, STKH22013, KEPU12013 and SBPK22014 were analysed.

## CRONUS-Earth $^{10}$Be - $^{26}$Al exposure age calculator -- results

| Version information -- | Component | Version |
|---|---|---|
| | Wrapper script: | 2.2 |
| | Main calculator: | 2.1 |
| | Constants: | 2.2.1 |
| | Muons: | 1.1 |

Comments:

| Production rate calibration information: | Using default calibration data set |
|---|---|

### $^{10}$Be results:

Results not dependent on spallogenic production rate model:     Exposure ages -- constant production rate model:

Scaling scheme for spallation: Lal(1991) / Stone(2000)

| Sample name | Thickness scaling factor | Shielding factor | Production rate (muons) (atoms/g/yr) | Internal uncertainty (yr) | Exposure age (yr) | External uncertainty (yr) | Production rate (spallation) (atoms/g/yr) |
|---|---|---|---|---|---|---|---|
| SGP192012 | 0.9913 | 1.0000 | 0.220 | 285 | 10293 | 941 | 7.47 |
| FHM192012 | 0.9827 | 1.0000 | 0.261 | 389 | 10801 | 1018 | 11.42 |
| LS192012 | 0.9827 | 1.0000 | 0.237 | 331 | 13835 | 1250 | 9.03 |
| SBPK92012 | 0.9742 | 1.0000 | 0.237 | 633 | 41104 | 3662 | 8.99 |
| MZ292012 | 0.9742 | 1.0000 | 0.243 | 806 | 55084 | 4917 | 9.59 |

**Figure 43: Calculated exposure age of the first analyses run. The calculation was done by the CHRONUS-Earth calculator. The five samples SGP192012, FHM192012, LS192012, SBPK192012 and MZ292012 were analysed.**

## CRONUS-Earth $^{10}$Be - $^{26}$Al exposure age calculator -- results

| Version information -- | Component | Version |
|---|---|---|
| | Wrapper script: | 2.2 |
| | Main calculator: | 2.1 |
| | Constants: | 2.2.1 |
| | Muons: | 1.1 |

Comments:

| Production rate calibration information: | Using default calibration data set |
|---|---|

### $^{10}$Be results:

Results not dependent on spallogenic production rate model:     Exposure ages -- constant production rate model:

Scaling scheme for spallation: Lal(1991) / Stone(2000)

| Sample name | Thickness scaling factor | Shielding factor | Production rate (muons) (atoms/g/yr) | Internal uncertainty (yr) | Exposure age (yr) | External uncertainty (yr) | Production rate (spallation) (atoms/g/yr) |
|---|---|---|---|---|---|---|---|
| SSP12012 | 0.9836 | 0.9989 | 0.232 | 531 | 20258 | 1846 | 8.56 |
| STKH22013 | 0.9836 | 0.9956 | 0.253 | 475 | 10379 | 1021 | 10.58 |
| KEPU12013 | 0.9836 | 1.0000 | 0.235 | 694 | 23965 | 2206 | 8.86 |
| SBPK22014 | 0.9756 | 0.9786 | 0.237 | 1145 | 50416 | 4680 | 8.82 |

**Figure 44: Calculated exposure age of the second analyses run. The calculation was done by the CHRONUS-Earth calculator. The four samples SSP12012, STKH22013, KEPU12013 and SBPK22014 were analysed.**

## CRONUS-Earth $^{10}$Be - $^{26}$Al erosion rate calculator -- results

| Version information -- | Component | Version |
|---|---|---|
| | Wrapper script: | 2.2 |
| | Main calculator: | 2.1 |
| | Objective function: | 2.0 |
| | Constants: | 2.2.1 |
| | Muons: | 1.1 |

Comments:

| Production rate calibration information: | Using default calibration data set |
|---|---|

### $^{10}$Be results:

| | Results not dependent on spallogenic production rate model: | | | Erosion rates -- constant production rate model: | | | |
|---|---|---|---|---|---|---|---|
| | | | | Scaling scheme for spallation: Lal(1991) / Stone(2000) | | | |
| Sample name | Shielding factor | Production rate (muons) (atoms/g/yr) | Internal uncertainty (m/Myr) | Erosion rate (g/cm2/yr) | Erosion rate (m/Myr) | External uncertainty (m/Myr) | Production rate (spallation) (atoms/g/yr) |
| SGP192012 | 1.0000 | 0.220 | 2.11 | 0.02102 | 75.08 | 5.44 | 7.54 |
| FHM192012 | 1.0000 | 0.261 | 2.40 | 0.01837 | 65.62 | 5.24 | 11.62 |
| LS192012 | 1.0000 | 0.237 | 1.29 | 0.01486 | 53.07 | 3.90 | 9.19 |
| SBPK92012 | 1.0000 | 0.237 | 0.27 | 0.00474 | 16.94 | 1.28 | 9.23 |
| MZ292012 | 1.0000 | 0.243 | 0.19 | 0.00344 | 12.28 | 0.96 | 9.85 |

**Figure 45: Calculated erosion rate of the first analyses run. The calculation was done by the CHRONUS-Earth calculator. The five samples SGP192012, FHM192012, LS192012, SBPK192012 and MZ292012 were analysed.**

## CRONUS-Earth $^{10}$Be - $^{26}$Al erosion rate calculator -- results

| Version information -- | Component | Version |
|---|---|---|
| | Wrapper script: | 2.2 |
| | Main calculator: | 2.1 |
| | Objective function: | 2.0 |
| | Constants: | 2.2.1 |
| | Muons: | 1.1 |

Comments:

| Production rate calibration information: | Using default calibration data set |
|---|---|

### $^{10}$Be results:

| | Results not dependent on spallogenic production rate model: | | | Erosion rates -- constant production rate model: | | | |
|---|---|---|---|---|---|---|---|
| | | | | Scaling scheme for spallation: Lal(1991) / Stone(2000) | | | |
| Sample name | Shielding factor | Production rate (muons) (atoms/g/yr) | Internal uncertainty (m/Myr) | Erosion rate (g/cm2/yr) | Erosion rate (m/Myr) | External uncertainty (m/Myr) | Production rate (spallation) (atoms/g/yr) |
| SSP12012 | 0.9989 | 0.232 | 1.02 | 0.01009 | 38.08 | 2.86 | 8.70 |
| STKH22013 | 0.9956 | 0.253 | 3.40 | 0.01941 | 73.25 | 6.16 | 10.73 |
| KEPU12013 | 1.0000 | 0.235 | 0.94 | 0.00840 | 31.71 | 2.45 | 9.01 |
| SBPK22014 | 0.9786 | 0.237 | 0.34 | 0.00383 | 14.46 | 1.14 | 9.04 |

**Figure 46: Calculated erosion rate of the second analyses run. The calculation was done by the CHRONUS-Earth calculator. The four samples SSP12012, STKH22013, KEPU12013 and SBPK22014 were analysed.**

## Results

The results show different age-groups. The two cover plates of the subsurface tunnels show an exposure age of 10801 ± 389 y and 10293 ± 285 y and 10379 ± 1021 y. The analyzed cap stones of the Kandelhofer Erdstall and the Strebl-Felsgang show relatively similar ages of 23965 ± 694 y and 20258 ± 531 y. The analyzed Holed Stone shows an exposure age 13835 ± 331. On the other hand, the big block, called "Schiff" shows an age of 55084 ± 806 y, which is almost twice the age of the cap stones and Menhir described above. The samples from the stone pit also show older ages than those from cap stones and the Menhir. The ages of the two stone pit samples are: 41104 ± 633 y and 50416 ± 1145 y. Thus these both represent much higher ages than the cover plates of the subsurface tunnels.

The erosion age can be divided in two subgroups too. On the one hand there are the samples of the stone pit and the big block with inferred erosion rates of 12.28 ± 0.19 m/Myr, 14.46 ± 0.34 m/Myr and 16.94 ± 0.27 m/Myr. On the other hand, there are the two cap stones of the Kandelhofer Erdstall and the Strebl-Felsgang with erosion rates of about 31.71 ± 0.94 and 38.08 ± 1.02. The three cover plates with erosion rates of 65.62 ± 2.40, 73.07 ± 3.4 m/Myr and 75.08 ± 2.11 are significant higher. In addition, the Holed Stone shows a quite similar erosion rate of 53.07 ± 1.29.

## 8. Discussion

The area around Vorau in Eastern Styria/Austria has a high density of Menhirs and Holed Stones, which is uncommon in this part of Europe (Fig. 4). If these Menhirs are in fact of prehistoric age, then they are proof of megalithic cultures east of the line shown in Fig. 2. Because it is impossible to identify all the displaced and removed Menhirs and Holed Stones (and this number is obviously high), it was impossible to get any significant spatial relationship between the way they were placed. Neither a correlation with the sea-level nor a comparison between monoliths with and without a hole gave any significant result. The only outstanding pattern was that the number of Menhirs and Holed Stones increased near homesteads and along some field yards. This is an indication that many Menhirs were displaced or removed. However, it is also possible that this observation implies that the Menhirs are not a prehistoric feature, but were built in the time scale since the farm existed - usually this is about 500 years in the region. The orientation of the holes shows in random directions and thus cannot be interpreted in any meaningful way. On average, more than one Menhir and/or Holed Stone can be found every km$^2$ in an area of about 400 km near Vorau. This is just the number of remaining Monoliths. Findings of buried Menhir and/or Holed Stone and stories of the population show that the number was even higher in the past.

A possible function of the Holed Stones is mentioned in the book "Versiegelte Unterwelt" (Kusch and Kusch, 2014). These authors interpret the Menhirs and Holed Stones to be of prehistoric age and place substantial cultural and mythological significance on their position. They observe that some of the Holed Stones are located at the entrances of prehistoric subsurface tunnels and therefore suggest that there is the possibility that the placement of the Holed Stones was used as a prehistoric guide or carrier for information about these subsurface tunnels. But because my work did not deal with the functionality of the subsurface tunnels, but just with the building age, I can neither prove it nor negate this thesis.

As there are widely different interpretations on the erection age of the Menhirs and Holed Stones an attempt was made to document this time of exposure of their surface via measurements of cosmogenically generated nuclides (TCN method). Archaeology tries to use this method to get exposure ages and hence the erection ages or building ages of different historically important constructions (Akcar et al., 2008).

To get an idea about the connections between the different prehistoric remnants and the surrounding several different sample points were used for the age dating. The results indicate some groups of samples with an almost same exposure age. Rocks from the subsurface constructions show exposure ages of around 10000 y (The Grubergang with 10293 ± 285 y, the Franzosenhöhle with 10801 ± 389 y and the subsurface tunnel of Prätis with 10379 ± 475 y). These ages are all from walls made by humans. If the rocks were mined from many meters underground before using them as building stones for these constructions, then this would indicate a postglacial construction age for the walls. This is in fact the interpretation of Kusch (2016). According to Kusch (2016) these constructions, from which one is an adapted Erdstall, were used as shelters in the mountain settlement. However, the rocks from the other two subsurface constructions show even much older exposure ages. This result does not mean that the subsurface tunnels themselves are much older. In fact, Kusch (2016) even proposes a Paleolithic period as possible construction age for the Kandelhofer Erdstall itself.

In matters of the Menhir, the book "Versiegelte Unterwelt" (Kusch and Kusch, 2014) provides an interpretation how the calculated age of the Menhir fits into the other ages. To obtain the age of the rocks lying on the surface, the age of the 7.6 m long and 60 ton Menhir called "Schiff" was used. The origin of this special Menhir could be a landslide from the Masenberg. The results of the terrestrial cosmogenic nuclides show an age about 55560 ± 813 y. To get the possible age of the placement of this Menhirs, the exposure age of a holed stone was measured. This sample shows an exposure age of about 13953 ± 333 years. Because of the comparison with the age of the "Schiff", the possibility, that this age just shows the age of an erratic block and not the age of the treatment, was excluded by Kusch and Kusch (2014). Furthermore, the last ice age between 26000 - 15000 y and the following cold phase between 13000 - 12000 y did not build an ice cover in this region. Consequently, this influence was excluded by these authors too. As a result, the age of around 14000 years was allocated by these authors to the actual age of the erection. The implication of this interpretation is that a megalithic cultural development in Vorau took place in the Upper Paleolithic. This would be the oldest known megalithic culture in Europe and would cause a significant rethinking about the age classification of the megalithic cultures in Europe.

However, the interpretation of the obtained ages is not trivial. It is possible that the raw material lies on the surface exposed to cosmic radiation for thousands of years before it gets used. The exposure age would hence be much older than the erection age. In case of the

sampled Menhir, the age of about 14000 years could point to a glacially weathered bolder as an origin. Some connected archaeological findings like stone age tools, or organic matter that can be dated with Carbon dating would be very helpful to support any interpretation about the erection age. In the Vorau region such evidence has not been found. However, in view of the fact that all measured ages are consistent with geological periods for which it is known that climate was harsh and weathering processes rapid a natural formation of the rocks from which the megalith were built is throughout plausible.

The second interpretation of the measured $^{10}$Be concentration can be interpreted somewhat easier. It is used to calculate erosion rates. In the Eastern Alps this method was previously used to study erosion rates (Norton et al., 2011; Wittmann et al., 2016) to study aspects of the landscape evolution (Legrain et al., 2014) and in order to compare erosion rates between catchments that were glaciated and that were not glaciated in the glaciation periods (Dixon et al., 2016). Although most of these erosion rate measurements document only time averaged erosion over the last 5000 years or so, the results of these authors are generally in good agreement with other methods that document longer time scales like apatite (U – Th)/He thermochronology (Legrain et al., 2014) and therefore help to get an idea about the landscape evolution on geological time scales. These studies show that erosion rates in glaciated catchments of the Alps vary between 100 m/Myr and 1000 m/Myr, while they are only 10 m/Myr to 100 m/Myr at the eastern end of the Alps were catchments were never glaciated (Fig. 47) Legrain et al. (2015) and Dixon et al. (2016) dealt with some unglaciated catchments in the Koralpe. The origins of their samples were categorized into three different locations: "relict," "incised," and "mixed". The result of this analysis is consistent with the long-term exhumation rate of ca. 100 m/my. In fact, the erosion rate of the relict landscape ranges from 36 ± 3 mm/k.y. to 59 ± 4 mm/k.y, of the two entirely incised catchments from 111 ± 9 mm/k.y. to 149 ± 14 mm/k.y and the mixed catchments, including both incised and relict landscape range from 56 ± 3 mm/k.y. to 123 ± 9 mm/k.y.. This makes an average of 81 ± 24 mm/k.y.. Furthermore, the erosion rates from the Styrian Basin range from 33 ± 2 mm/k.y. to 123 ± 9 mm/k.y.. Compared to erosion rate from previous non glaciated regions of Alps at similar sea-levels this erosion rates from the Koralpe are approximately one order of magnitude lower (Legrain et al., 2015). The rocks dated for this thesis suggest erosion rates between 12.28 ± 0.19 m/Myr and 75.08 ± 2.11. They fit very well with the results of the Koralpe as reported by Legrain et al. (2014) and Dixon et al. (2016) (Fig. 47). But calculations of transported rocks like the Menhirs are very difficult to be connected to a

certain event. But the gained erosion rates could give an idea about his origin.
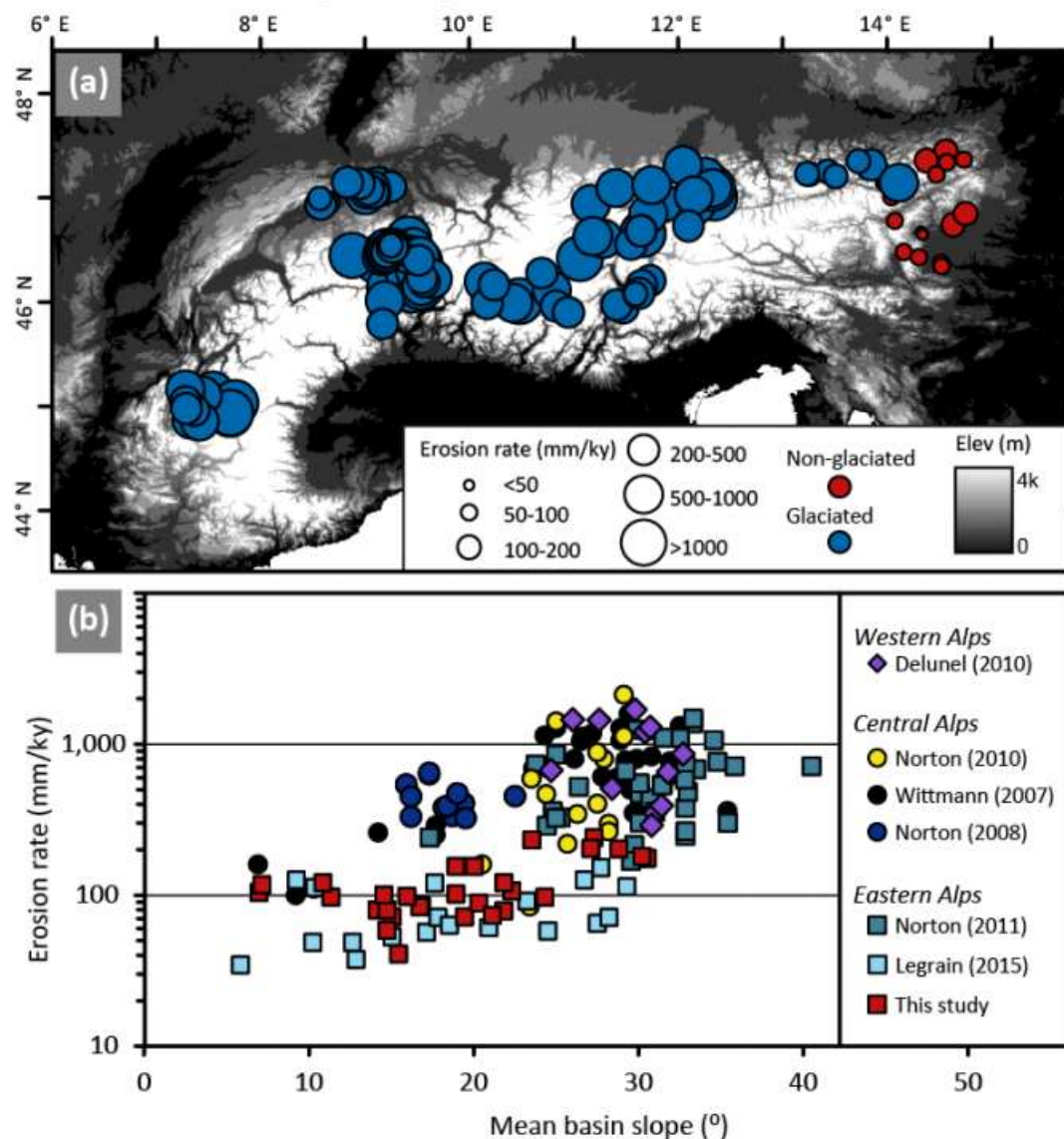


Figure 47: Calculated erosion rates of the Alps (from over 100 cosmogenic analyses), a) the size of the circles symbolises the erosion rate and the colour the occurrence or missing of a glaciation; b) comparison of the erosion rates with the mean basin slope. Figure taken from Dixon et al. (2016).

Summarizing, the TCN analyses discussed above are not very useful. The extremely old ages make them not very plausible to be related to prehistoric cultures. Indeed, the good correspondence of the ages and inferred erosion rates with other studies makes it much more likely that the ages obtained here are related to weathering processes during the glaciation periods. If, however, an archaeological interpretation is to be favored on the basis of other arguments, such an interpretation would of course require substantial further support. In order to provide this support by TCN analyses, careful depth profiling on a single selected Menhir would be required. As an alternative, it would be possible to date the surface of the Menhirs using Optically Stimulated Luminescence (OSL dating). This method also has a range of

limitations, but has successfully been used to answer a range of archaeological questions in the past (Akcar et al. 2008). Using the OSL method to date vertical profiles along the Menhir surface every 10 cm or so is likely to give good evidence for the erection age.

The petrological investigations presented above give some support to the interpretation of a natural origin of the rocks from which the Menhirs were built.  This showed that the origin of the Menhirs and Holed Stones should be the nearer surrounding. There are some facts, which support this idea. As mentioned in chapter 5 the taken samples from the Menhirs and Holed Stones are similar to the samples taken from outcrop. Firstly, there are no real differences in the mineral assemblage, metamorphic phase and texture between the analyzed Menhir and Holed Stone samples and the samples taken from outcrops in the region. Furthermore, the rock types fit into the geological units mentioned in chapter 3. To get a better comparison the *PT* conditions of four Menhirs and Holed Stones were calculated. The temperatures of 520 °C to 600 °C and the pressure of 12 kbar to 22 kbar were compared to the geological units of the vicinity. The good correspondence of these estimates to the Strallegg Komplex makes this unit the most suitable source rock of the megalithic monuments. The other units do not fit very well. The mineral assemblages and rock types fit very well too.

# 9. Conclusion

In summary from this thesis, I conclude the following points:

- A database of the Menhirs in the Vorau region was made. The data base shows that there is more than one Menhir or Holed Stone per square kilometer in an area of some 400 km$^2$ around Vorau. Various attempts to derive spatial correlations between the megaliths and between megaliths and other features were made, but no clear correlation could be made, expect for the fact that megalithic monuments occur in higher concentrations near farmsteads. This could either be interpreted in terms of them being removed in historic times, or it could mean that they were only built in the last few hundreds of years in the vicinity of local medieval homesteads.

- In order to constrain the building age of these monuments, an attempt was made to date them via cosmogenically generated $^{10}$Be measurements. The calculated exposure ages range between about 10000 and 55000 years and calculated erosion rates are between 12 m/Myr and 75 m/Myr. If these ages would correspond to the erection age of these monuments, they would lead to an historical sensation. However, there is no other proof of a megalithic culture in Europe in the Neolithic so far. Furthermore, the good correlation of the calculated erosion rates with other measurements of Holocene erosion rates from the literature suggests an interpretation of a natural origin instead of erection age. A better interpretation would demand the careful depth profiling TCN analysis of more samples or alternative dating methods, for example OSL.

- In view of the badly constrained age of the Menhirs, their origin was constrained by comparing the formation conditions of the metamorphic rocks that they are built from, with published formation conditions of the rocks from the region. The petrological analyses as well as the geothermobaromteric analyses induce to the exclusion of most of the units in the vicinity. The geothermometry shows formation temperatures around 440 °C to 600 °C. The geobarometry shows formation pressures of 10 kbar to 22 kbar. Only the Strallegg Komplex has a lot of similarities and hence is a high potential resource. These similarities reinforce the basic assumption of a nearby origin.

# 10. Bibliography

Akcar N., Ivy-Ochs I. and Schlüchterer C., (2008); Application of in-situ produced terrestrial cosmogenic nuclides to archaeology; Eiszeitalter und Gegenwart Quaternary Science Journal, v. 57/1–2, p. 226–238, Hannover.

Dale, J., Holland, T. and Powell R., (2000): Hornblende-garnet-plagioclase thermobarometry: a natural assemblage calibration of the thermodynamics of hornblende; Contributions to Mineralogy and Petrology, v. 140, p. 353-362.

Berka, R., (2000): Die Stellung der Traibachschiefer im Semmering-Wechsel System; unveröff. Dipl. Arb. Formalnatwiss. Fak. Univ. Wien, 133 p., Wien.

Berka, R., Schmidt, K., Schuster, R. and Frank, W., (1998): Hercynian and Permian metamorphism in the eastern part of the Austroalpine basement units (Eastern Alps); Mitteilungen der Österreichischen Geologischen Gesellschaft, v. 143, p. 242-245.

Biedermann, H., (1963): Das Europäische Megalithikum; p. 7-13; Illustrierte Welt Kunstgeschichte 4004, Verlag Ullstein Gmbh, Frankfurt Berlin

Brown, E.T., Brook, E.J., Raisbeck, G.M., Yiou, F. and Kurz, M.D., (1992): Effective attenuation lengths of cosmic rays producing 10Be and 26A1 in quartz: Implications for exposure age dating; Geophysical Research Letters, v. 19, p. 369-372.

Dallmeyer, R.D., Handler, R., Neubauer, F. and Fritz, H., (1998): Sequence of thrusting within a thick skinned tectonic wedge: Evidence from 40Ar/39Ar and Rb-Sr Ages from the Austroalpine Nappe Complex of the Estern Alps; Journal of Geology, v. 106, p. 71-86.

Dixon, J.L., von Blanckenburg, F., Stüwe, K. and Christl, M., (2016): Glaciation's topographic control on Holocene erosion at the eastern edge of the Alps; Earth Surface Dynamics doi:10.5194/esurf-2016-29.

Faupl, P., (1970a): Zur Geologie des NW-Abschnittes des Wechselgebietes zwischen Trattenbach (NÖ.) und Fröschnitz (Stmk.) – Österreich; Mitteilungen der Gesellschaft der Geologie und Bergbaustudenten, v. 19, p. 27-70.

Faupl, P., (1970b): Zur Geologie und Petrographie des südlichen Wechselgebietes; Mitt. Geol. Ges. Wien, v. 63, p. 22-51, Wien.

Flügel, H.W. and Neubauer, F. (1984): Erläuterungen zur geologischen Karte der Steiermark; Geologische Bundesanstalt, 127 p., Wien.

Frank, W., Lelkes-Felvari, G. and Dunkl, I., (1996): Thermal history of Austroalpine rocks of the borehole Fertöràkos-1004, Western Hungary. In: Dudich, E. and Lobitzer, H. (eds.): Advances in Austrian Hungarian Joint Geological Research. Occas. Papers Geol. Inst. Hung. (Budapest), v. 189, p. 177-195.

Habel, J., (1987): Von Megalithenkulturen über die Kelten zu König Arthus; Hagenberg Verlag, p. 12-25.

Heisinger, B. and Nolte, E., (2000): Cosmogenic in situ production of radionuclides: Exposure ages and erosion ages; Nuclear Instruments and Methods in Physics Research, v. 172, p. 790-795.

Hoffmann, E., (2012): Lexikon der Steinzeit; Books on Demand, 486 p. p. 47-87

Hoisch, T., (1990): Empirical calibration of six geobarometers for the mineral assemblage quartz + muscovite + biotite + plagioclase + garnet; Contributions to Mineralogy and Petrology v. 104, p. 225-234.

Huber, M., (1994): Bildung und geotektonische Bedeutung von Scherzonen (Leukophylliten) am Alpenostrand; unveröff. Diss. Inst. für Geowissenschaften, Leoben, 136 p., Leoben.

Ivy-Ochs, S. and Kober, F., (2008): Surface exposure dating with cosmogenic nuclides; Eiszeitalter und Gegenwart; Quaternary Science Journal, v. 57, p. 179–209.

Kirchner, H., (1955): Die Menhire in Mittel Europa und der Menhirgedanke; Verlag der Akademie der Wissenschaften und der Literatur in Mainz in Kommission bei Franz Steiner Verlag GMBH, Wiesbaden, 208 p.

Koller, F. and Wieseneder, H., (1981): Gesteinsserien und Metamorphosen der Rechnitzer Serie im Burgenland und des Unterostalpins in der Oststeiermark; Exk.-Führer ÖMG-DMG-Tagung 1981, Fortschr. Miner. 59, Beih. 2, p. 167-178.

Koller, F., Pumhösl, H., Thöni, M., Faryad, S.W., Seifert-Falkner, C., Frank, W., Miller, C., and Satir, M. (2002). Permian garbbroic intrusion within the Lower Austroalpine Grobogneiss Unit (Eastern Alps, Austria): Origin, evolution and tectonic setting. DMG-Tagung 2002, Beiheft zum European Journal of Mineralalogy, v. 14, p. 86.

Korikovsky, S.P., Putis, M., Kotov, A.B., Salnikova, E.B. and Kovach, V.P., (1998): High pressure metamorphism of the phengite gneisses of the Lower Austroalpine nappe complex in the Eastern Alps: mineral equilibria, P-T parameters, age. Journal of Petrology, v. 6/4, p. 603-619.

Korn, W., (2005): Megalithenkulturen. Rätselhafte Monumente; 106 p., Theiss Verlag Stuttgart.

Kovach, A. and Svingor, E., (1981): On the age of metamorphism in the Fertörákos Metamorphic Complex; NW Hungary, Verhandlungen der Geologischen Bundesanstalt., v. 2, p. 73-81, Wien.

Kretz, R., (1983): Symbols for rock-forming minerals. American Mineralogist, v. 68, p. 277-279.

Kubik, P.W., Ivy-Ochs, S., Masarik, J., Frank, M., Schlüchter, C., (1998): 10Be and 26Al production rates deduced from an instantaneous event within the dendro-calibration curve, the landslide of Köfels, Ötz Valley, Austria. Earth and Planetary Science Letters, v. 161, p. 231–241.

Kusch H., (2016): Zur archäologischen Untersuchung des Kandelhofer-/Kandlhofer-Erdstalles bei Puchegg, Steiermark, Österreich; Der Erdstall 42, p. 12-35.

Kusch H. und Kusch I., (2009): Tore zur Unterwelt; V. F.Sammler, Graz, 208 p.

Kusch H. und Kusch I., (2014): Versiegelte Unterwelt; V.F.Sammler, Graz, 208 p.

Landler A., (2014): Menhire in Vorau; Bakkalaureatsarbeit; Karl-Franzens-Universität Graz, Institut für Erdwissenschaften, 39 p.

Legrain, N., Stüwe, K. and Wölfler, A., (2014): Incised relict landscapes in the eastern Alps; Geomorphology, v. 221, p. 124–138.

Legrain, N., Dixon, J., Stüwe, K., von Blanckenburg, F. and Kubik, P., (2015): Post-Miocene landscape rejuvenation at the eastern end of the Alps; Lithosphere 7, 1, p. 3—13.

Maier, B., (2005): Stonehenge: Archäologie, Geschichte, Mythos; Verlag C. H. Beck OHG, München, 108 p.

Mohen, J., (1989): Megalithkultur in Europa: Geheimnis der frühen Zivilisation. Übers. von Ina Brümann. Belser Verlag, Stuttgart, Zürich, 317 p.

Müller, W., (1994): Neue geochronologische und strukturgeologische Daten zur geodynamischen Entwicklung des nördlichen Semmering- und Wechselgebietes (Niederösterreich); Unveröff. Diplomarbeit Formal u. Naturwiss. Fak. Univ. Wien, 267 p.

Müller, W., Dallmeyer, R. D., Neubauer, F. and Thöni, M., (1999): Deformation-induced resetting of Rb/Sr and 40Ar/39Ar mineral systems in a low-grade, polymetamorphic terrane (Eastern Alps, Austria). Journal of the Geological Society, v. 156/3, p. 261-278.

Norton, K.P., von Blanckenburg, F., DiBiase, R., Schlunegger, F. and Kubik, P.W., (2011): Cosmogenic [10]Be-derived denudation rates of the Eastern and Southern European Alps; International Journal of Earth Sciences, v. 100, p. 1163–1179.

Pahr, A., (1977): Ein neuer Beitrag zur Geologie des Nordostsporns der Zentralalpen; Verhandlungen der Geologischen Bundesanstalt., v. 2, p. 23-33.

Schuster, K. Berka, R., Dragantis, E., Frank, W. and Schuster, R., (2001): Lithologien, Metamorphosegeschichte und tektonischer Bau der kristallinen Einheiten am Alpenostrand; Geologische Bundesanstalt Arbeitstagung, Neuberg an der Mürz, p. 29-56.

Spear, F., (1993): Metamorphic Phase Equilibria and Pressure-Temperature-Time Paths; Mineralogical Society of America, Washington, D.C, p. 575-639, 799 p.

Speil, S.J.E., (2014): Menhire um Schachen bei Vorau. Kartierung und erdwissenschaftliche Untersuchungen; Bachelorarbeit der Studienrichtung Erdwissenschaften, Karl-Franzens-Universität Graz, Institut für Erdwissenschaften, 38 p.

Teichmann, F., (1983): Der Mensch und seine Tempel: Megalithkultur in Irland, England und der Bretagne; Verlag Urachhaus Johannes M. Mayer GmbH Stuttgart, 249 p.

Tollmann, A., (1964): Das Permoskyth in den Ostalpen sowie Alter und Stellung des "Haselgebirges"; Neues Jahrbuch für Geologie und Paläontologie Monatshefte, p. 270-299.

Tollmann, A., (1977): Geologie von Österreich. Band 1. Die Zentralalpen; Deuticke, Wien, 766 p.

Vacek, M., (1892): Über die krystallinischen Inseln am Ostende der alpinen Centralzone; Verh. geolog. R.-A., v. 15, p. 367-377.

Von Blanckenburg, F., (2008): Kosmogene Nuklide in den Geo- und Umweltwissenschaften; Geowissenschaftliche Mitteilungen, v. 33, p. 6-18.

Wieseneder, H., (1961): Die Korund-Spinellfelse der Oststeiermark als Restite einer Anatexis; Miner. Mittbl. Joanneum, 1961/1, p. 1-30.

Wieseneder, H., (1971): Gesteinsserien und Metamorphose im Ostabschnitt der Österreichischen Zentralalpen; Verh. Geol. Bundesanstalt, v. 2, p. 344-357.

Wittmann, H. and von Blanckenburg, F., (2016): The geological significance of cosmogenic nuclides in large lowland river basins. Earth Science Reviews, v. 159, p. 118-141.


Wittmann, H., Malusà, M. G., Resentini, A., Garzanti, E., Niedermann, S., (2016): The cosmogenic record of mountain erosion transmitted across a foreland basin: Source-to-sink analysis of in situ 10Be, 26Al and 21Ne in sediment of the Po river catchment. Earth and Planetary Science Letters, in print.

Zylmann, D., (2008): Das Rätsel der Menhire; GRIN Verlag, 132 p., München

# 11. Appendix

## 11.1 Chart of Menhirs and Holed Stones

The following table shows the complete database of all Menhirs and Holed Stones that were mapped in this thesis. The table includes the location, sea-level, the number of Menhirs and/or Holed Stones at one location and partly the dimensions.

| ID | X | Y | Z | *Holed* Stone (HS) or Menhir (M) | Number | Dimension (width*height*thickness) (cm*cm*cm) |
|---|---|---|---|---|---|---|
| K1 | 47° 21.209'' N | 15° 51.717'' E | 1110 m | M | | |
| K2 | 47° 25.203'' N | 15° 54.239'' E | 695 m | M | 4 Menhirs | |
| K3 | 47° 25.145'' N | 15° 54.155'' E | 682 m | HS | | |
| K4 | 47° 25.013'' N | 15° 54.374'' E | 665 m | HS | | |
| K5 | 47° 25.755'' N | 15° 52.995'' E | 846 m | HS | | |
| K6 | 47° 25.992'' N | 15° 53.274'' E | 815 m | HS | | |
| K7 | 47° 23.453'' N | 15° 53.237'' E | 753 m | HS | | |
| K8 | 47° 23.380'' N | 15° 53.478'' E | 796 m | HS | | |
| K9 | 47° 23.419'' N | 15° 53.496'' E | 774 m | HS | 2 Holed Stones | |
| K10 | 47° 23.407'' N | 15° 53.524'' E | 774 m | HS | | |
| K11 | 47° 23.394'' N | 15° 53.522'' E | 772 m | HS | 3 Holed Stones | |
| K12 | 47° 23.398'' N | 15° 53.517'' E | 776 m | HS | | |
| K13 | 47° 23.319'' N | 15° 53.444'' E | 792 m | HS | | |
| K14 | 47° 23.333'' N | 15° 53.506'' E | 799 m | HS | | |
| K15 | 47° 23.194'' N | 15° 54.100'' E | 77 9 m | HS | | |
| K16 | 47° 22.940'' N | 15° 53.733'' E | 839 m | HS | | |
| K17 | 47° 22.958'' N | 15° 53.747'' E | 843 m | HS | | |
| K18 | 47° 22.828'' N | 15° 53.584'' E | 853 m | HS | | |
| K19 | 47° 28.632'' N | 15° 57.873'' E | 1304 m | M | | |
| K20 | 47° 35.361'' N | 15° 55.055'' E | 696 m | HS | | |
| K21 | 47° 21.863'' N | 15° 55.111'' E | 878 m | M | | |
| K22 | 47° 25.454'' N | 15° 56.962'' E | 512 m | HS | | |
| K23 | 47° 25.644'' N | 15° 55.232'' E | 699 m | HS | | |
| K24 | 47° 26.162'' N | 15° 52.720'' E | 884 m | HS | | |
| K25 | 47° 24.604'' N | 15° 46.163'' E | 1077 m | M | | |
| K26 | 47° 26.167'' N | 15° 53.201'' E | 834 m | M | | |
| K27 | 47° 21.923'' N | 15° 50.694'' E | 840 m | HS | | |
| K28 | 47° 19.559'' N | 15° 49.259'' E | 496 m | M | 3 | |
| K29 | 47° 23.078'' N | 15° 52.907'' E | 821 m | HS | | |
| K30 | 47° 24.862'' N | 15° 54.032'' E | 724 m | HS | | |
| K31 | 47° 23.864'' N | 15° 57.595'' E | 621 m | HS | | |
| K32 | 47° 23.635'' N | 15° 55.875'' E | 713 m | HS | | |

| | | | | | | |
|---|---|---|---|---|---|---|
| K33 | 47° 25.714' N | 15° 55.446' E | 710 m | HS | | |
| K34 | 47° 25.125' N | 15° 53.927' E | 723 m | M | 3 | |
| K35 | 47° 25.009' N | 15° 53.895' E | 711 m | HS+ M | 2 Holed Stones and 1 Menhir | |
| K36 | 47° 24.739' N | 15° 53.651' E | 708 m | M | 8 | |
| K37 | 47° 24.769' N | 15° 54.128' E | 684 m | HS | 2 Holed Stones | |
| K38 | 47° 24.741' N | 15° 54.250' E | 674 m | HS + M | 1 Holed Stone and 1 Menhir | |
| K39 | 47° 24.608' N | 15° 54.221' E | 675 m | HS | | |
| K40 | 47° 24.627' N | 15° 54.386' E | 669 m | HS | | |
| K41 | 47° 22.646' N | 15° 50.586' E | 815 m | HS | | |
| K42 | 47° 22.078' N | 15° 51.185' E | 722 m | HS | | |
| K43 | 47° 24.673' N | 15° 51.931' E | 809 m | HS | | |
| K44 | 47° 25.516' N | 15° 51.315' E | 1010 m | HS | | |
| K45 | 47° 25.265' N | 15° 51.120' E | 971 m | HS | | |
| K46 | 47° 25.083' N | 15° 53.007' E | 766 m | HS | | |
| K47 | 47° 25.027' N | 15° 53.417' E | 711 m | HS | | |
| K48 | 47° 24.972' N | 15° 53.556' E | 714 m | HS | | |
| K49 | 47° 24.943' N | 15° 53.891' E | 719 m | HS | | |
| K50 | 47° 22.204' N | 15° 53.378' E | 987 m | HS | | |
| K51 | 47° 24.571' N | 15° 53.923' E | 660 m | HS | | |
| K52 | 47° 24.535' N | 15° 53.975' E | 662 m | HS | | |
| K53 | 47° 24.520' N | 15° 53.989' E | 662 m | HS | | |
| K54 | 47° 25.975' N | 15° 53.749' E | 784 m | HS | | |
| K55 | 47° 25.944' N | 15° 53.899' E | 755 m | HS | | |
| K56 | 47° 22.093' N | 15° 50.953' E | 797 m | HS | | |
| K57 | 47° 23.623' N | 15° 56.582' E | 640 m | HS | | |
| K58 | 47° 23.591' N | 15° 56.500' E | 654 m | HS | 2 Holed Stones | |
| K59 | 47° 23.551' N | 15° 56.253' E | 666 m | HS | | |
| K60 | 47° 23.605' N | 15° 56.419' E | 655 m | HS | | |
| K61 | 47° 23.697' N | 15° 56.312' E | 652 m | HS | | |
| K62 | 47" 25.755' N | 15° 54.364' E | 699 m | HS | | |
| K63 | 47° 24.362' N | 15° 53.774' E | 676 m | HS | | |
| K64 | 47° 24.285' N | 15° 53.943' E | 673 m | HS | 2 Holed Stones | |
| K65 | 47° 24.081' N | 15° 54.507' E | 679 m | HS | | |
| K66 | 47° 16.078' N | 15° 46.316' E | 649 m | HS | | |
| K67 | 47° 14.906' N | 15° 47.646' E | 469 m | M | | |
| K68 | 47° 20.063' N | 15° 57.729' E | 440 m | HS | | |
| K69 | 47° 20.246' N | 15° 54.305' E | 549 m | HS | | |
| K70 | 47° 20.308' N | 15° 54.116' E | 588 m | HS | | |
| K71 | 47° 20.603' N | 15° 55.739' E | 652 m | HS | | |
| K72 | 47° 20.620' N | 15° 55.988' E | 617 m | HS | 2 Holed Stones | |
| K73 | 47° 21.435' N | 15° 58.080' E | 583 m | HS | 2 Holed Stones | |
| K74 | 47° 25.549' N | 15° 47.212' E | 830 m | HS | | |
| K75 | 47° 25.530' N | 15° 47.215' E | 829 m | HS | | |
| K76 | 47° 22.114' N | 15° 52.642' E | 819 m | HS | | |
| K77 | 47° 22.743' N | 15° 51.691' E | 705 m | HS | | |

| K78 | 47° 22.774' N | 15° 52.074' E | 733 m | HS | | |
|------|----------------|----------------|--------|--------|----------------------------|--|
| K79 | 47° 22.690' N | 15° 52.241' E | 748 m | HS | | |
| K80 | 47° 22.680' N | 15° 52.378' E | 757 m | HS | | |
| K81 | 47° 23.021' N | 15° 48.937' E | 902 m | M | | |
| K82 | 47° 20.292' N | 15° 56.058' E | 586 m | M | | |
| K83 | 47° 20.552' N | 15° 56.040' E | 627 m | HS | | |
| K84 | 47° 25.314' N | 15° 51.841' E | 911 m | HS | | |
| K85 | 47° 25.178' N | 15° 51.930' E | 893 m | HS | | |
| K86 | 47° 19.439' N | 15° 52.805' E | 756 m | HS + M | 1 Holed Stone and 2 Menhirs | |
| K87 | 47° 18.385' N | 15° 51.289' E | 531 m | M | | |
| K88 | 47° 18.581' N | 15° 51.185' E | 580 m | HS | | |
| K89 | 47° 22.418' N | 15° 52.785' E | 852 m | HS | 2 Holed Stones | |
| K90 | 47° 22.103' N | 15° 52.420' E | 840 m | HS | 5 Holed Stones | |
| K91 | 47° 25.124' N | 15° 51.459' E | 905 m | HS | | |
| K92 | 47° 23.324' N | 15° 57.246' E | 630 m | HS | | |
| K93 | 47° 23.320' N | 15° 57.114' E | 624 m | HS | | |
| K94 | 47° 22.785' N | 15° 52.449' E | 743 m | HS | 2 Holed Stones | |
| K95 | 47° 19.580' N | 15° 46.026' E | 643 m | M | | |
| K96 | 47° 22.453' N | 15° 43.163' E | 773 m | HS | | |
| K97 | 47° 22.957' N | 15° 44.401' E | 889 m | HS | | |
| K98 | 47° 24.660' N | 15° 53.669' E | 695 m | M | 2 Menhirs | |
| K99 | 47° 20.351' N | 15° 55.324' E | 697 m | HS | | |
| K100 | 47° 20.532' N | 15° 54.620' E | 796 m | HS | | |
| K101 | 47° 19.961' N | 15° 57.404' E | 481 m | HS | | |
| K102 | 47° 20.520' N | 15° 54.678' E | 793 m | M | | |
| K103 | 47° 20.506' N | 15° 54.749' E | 795 m | HS | 3 Holed Stones | |
| K104 | 47° 20.540' N | 15° 54.615' E | 789 m | HS | 4 Holed Stones | |
| K105 | 47° 20.170' N | 15° 54.892' E | 755 m | HS | | |
| K106 | 47° 27.562' N | 16° 00.950' E | 983 m | HS | | |
| K107 | 47° 27.566' N | 16° 00.975' E | 973 m | M | | |
| K108 | 47° 27.532' N | 16° 00.954' E | 957 m | HS | | |
| K109 | 47° 27.329' N | 16° 00.531' E | 970 m | HS | | |
| K110 | 47° 27.368' N | 16° 00.571' E | 965 m | HS | | |
| K111 | 47° 26.863' N | 15° 59.779' E | 842 m | HS | | |
| K112 | 47° 26.747' N | 15° 59.981' E | 773 m | HS | | |
| K113 | 47° 26.592' N | 16° 00.004' E | 785 m | HS | | |
| K114 | 47° 26.670' N | 16° 00.075' E | 742 m | HS | | |
| K115 | 47° 26.505' N | 16° 00.138' E | 729 m | HS | | |
| K116 | 47° 26.503' N | 16° 00.146' E | 719 m | M | | |
| K117 | 47° 26.588' N | 16° 00.030' E | 757 m | HS | | |
| K118 | 47° 25.652' N | 16° 00.432' E | 581 m | M | | |
| K119 | 47° 20.234' N | 15° 56.299' E | 561 m | HS | 2 Holed Stones | |
| K120 | 47° 20.694' N | 15° 54.516' E | 887 m | HS | | |
| K121 | 47° 29.574' N | 15° 54.373' E | 853 m | HS | 2 Holed Stones | |
| K122 | 47° 23.798' N | 15° 51.373' E | 746 m | HS | | |

| K123 | 47° 24.011' N | 15° 51.231' E | 757 m | HS | | |
|---|---|---|---|---|---|---|
| K124 | 47° 24.697' N | 15° 50.384' E | 918 m | M | 2 Menhirs | |
| K125 | 47° 24.634' N | 15° 50.630' E | 892 m | M | | |
| K126 | 47° 28.883' N | 16° 02.150' E | 826 m | HS | | |
| K127 | 47° 28.931' N | 16° 02.175' E | 828 m | M | | |
| K128 | 47° 23.281' N | 15° 46.066' E | 1090 m | M | 2 Holed Stones and 1 Menhir | |
| K129 | 47° 24.357' N | 15° 52.317' E | 729 m | HS | | |
| K130 | 47° 23.292' N | 15° 46.126' E | 1090 m | HS | | |
| K131 | 47° 26.671' N | 16° 00.382' E | 755 m | HS | | |
| K132 | 47° 26.697' N | 16° 00.620' E | 776 m | HS | | |
| K133 | 47° 26.635' N | 16° 00.774' E | 753 m | HS | | |
| K134 | 47° 26.464' N | 16° 00.674' E | 727 m | HS | | |
| K135 | 47° 26.022' N | 16° 01.105' E | 648 m | HS | | |
| K136 | 47° 26.350' N | 15° 48.395' E | 816 m | HS | | |
| K137 | 47° 26.330' N | 15° 48.205' E | 819 m | HS | | |
| K138 | 47° 26.426' N | 15° 47.858' E | 829 m | HS | | |
| K139 | 47° 25.929' N | 15° 47.863' E | 791 m | HS | | |
| K140 | 47° 26.977' N | 15° 47.607' E | 878 m | M | | |
| K141 | 47° 26.418' N | 15° 47.190' E | 854 m | HS | | |
| K142 | 47° 25.923' N | 15° 47.781' E | 795 m | HS | | |
| K143 | 47° 18.683' N | 15° 42.351' E | 826 m | HS | | |
| K144 | 47° 24.776' N | 15° 53.965' E | 687 m | HS | | |
| K145 | 47° 23.242' N | 15° 52.579' E | 740 m | M | | |
| K146 | 47° 23.258' N | 15° 52.907' E | 747 m | HS | | |
| K147 | 47° 23.284' N | 15° 52.904' E | 743 m | HS | | |
| K148 | 47° 23.274' N | 15° 52.946' E | 740 m | HS | | |
| K149 | 47° 23.235' N | 15° 52.953' E | 760 m | HS | | |
| K150 | 47° 23.180' N | 15° 52.963' E | 784 m | HS | | |
| K151 | 47° 22.380' N | 15° 53.796' E | 910 m | M | | |
| K152 | 47° 22.719' N | 15° 49.761' E | 949 m | HS | | |
| K153 | 47° 22.889' N | 15° 49.635' E | 947 m | HS | | |
| K154 | 47° 22.885' N | 15° 49.552' E | 962 m | HS | | |
| K155 | 47° 26.476' N | 16° 01.106' E | 740 m | HS | | |
| K156 | 47° 26.376' N | 16° 01.186' E | 725 m | HS | | |
| K157 | 47° 23.309' N | 15° 45.486' E | 1077 m | HS | | |
| K158 | 47° 23.354' N | 15° 45.485' E | 1078 m | HS | | |
| K159 | 47° 22.927' N | 15° 45.595' E | 1009 m | HS | 4 Holed Stones | |
| K160 | 47° 25.922' N | 15° 46.629' E | 863 m | HS | | |
| K161 | 47° 26.560' N | 15° 46.208' E | 931 m | HS | | |
| K162 | 47° 26.536' N | 15° 46.156' E | 942 m | HS | | |
| K163 | 47° 26.738' N | 15° 47.057' E | 880 m | HS | | |
| K164 | 47° 26.552' N | 15° 47.262' E | 859 m | HS | | |
| K165 | 47° 26.102' N | 15° 47.606' E | 831 m | HS | | |
| K166 | 47° 24.511' N | 15° 47.707' E | 855 m | HS | | |
| K167 | 47° 24.060' N | 15° 56.708' E | 676 m | HS | | |

| K168 | 47° 21.473' N | 15° 54.454' E | 900 m | M | | |
|---|---|---|---|---|---|---|
| K169 | 47° 23.222' N | 15° 53.252' E | 819 m | HS | 2 Holed Stones | |
| K170 | 47° 24.849' N | 15° 51.142' E | 904 m | HS | | |
| K171 | 47° 23.299' N | 15° 45.458' E | 1078 m | M | 2 Menhirs | |
| K172 | 47° 20.676' N | 15° 56.452' E | 625 m | HS | 2 Holed Stones | |
| K173 | 47° 24.720' N | 15° 55.796' E | 626 m | HS | | |
| K174 | 47° 24.796' N | 15° 55.082' E | 621 m | M | | |
| K175 | 47° 25.093' N | 15° 55.531' E | 613 m | HS | | |
| K176 | 47° 25.070' N | 15° 55.594' E | 614 m | HS | | |
| K177 | 47° 25.013' N | 15° 55.709' E | 608 m | HS | | |
| K178 | 47° 25.235' N | 15° 55.605' E | 636 m | HS | | |
| K179 | 47° 25.274' N | 15° 55.574' E | 623 m | HS | | |
| K180 | 47° 25.311' N | 15° 55.523' E | 658 m | HS | | |
| K181 | 47° 24.860' N | 15° 55.475' E | 630 m | HS | | |
| K182 | 47° 25.001' N | 15° 55.178' E | 651 m | HS | | |
| K183 | 47° 22.958' N | 15° 51.953' E | 723 m | HS | | |
| K184 | 47° 23.064' N | 15° 51.923' E | 682 m | HS | | |
| K185 | 47° 23.016' N | 15° 45.860' E | 1000 m | HS | | |
| K186 | 47° 22.993' N | 15° 45.794' E | 996 m | HS | | |
| K187 | 47° 24.048' N | 15° 44.336' E | 898 m | HS | | |
| K188 | 47° 22.646' N | 15° 45.216' E | 885 m | HS | | |
| K189 | 47° 16.422' N | 15° 57.298' E | 369 m | HS | 2 Holed Stones | |
| K190 | 47° 17.094' N | 15° 57.289' E | 525 m | HS | | |
| K191 | 47° 22.174' N | 15° 53.940' E | 867 m | HS | | |
| K192 | 47° 19.438' N | 15° 52.775' E | 724 m | M | | |
| K193 | 47° 19.000' N | 15° 45.009' E | 799 m | HS | 3 Holed Stones | |
| K194 | 47° 26.913' N | 16° 01.717' E | 7 98 m | HS | | |
| K195 | 47° 26.912' N | 16° 01.676' E | 789 m | HS | 2 Holed Stones | |
| K196 | 47° 22.155' N | 15° 56.607' E | 685 m | HS | several Holed Stones | |
| K197 | 47° 21.147' N | 15° 57.230' E | 619 m | HS | | |
| K198 | 47° 21.159' N | 15° 57.155' E | 619 m | M | | |
| K199 | 47° 21.171' N | 15° 57.108' E | 628 m | M | | |
| K200 | 47° 27.182' N | 15° 50.067' E | 759 m | HS | | |
| K201 | 47° 21.507' N | 15° 54.491' E | 881 m | M | | |
| K202 | 47° 25.181' N | 15° 53.010' E | 777 m | HS | | |
| K203 | 47° 25.101' N | 15° 53.511' E | 736 m | HS | | |
| K204 | 47° 23.524' N | 15° 44.997' E | 1052 m | HS | | |
| K205 | 47° 23.613' N | 15° 44.925' E | 978 m | HS | | |
| K206 | 47° 24.514' N | 15° 55.065' E | 669 m | HS | | |
| K207 | 47° 24.158' N | 15° 51.498' E | 730 m | HS | | |
| K208 | 47° 24.163' N | 15° 51.440' E | 754 m | HS | | |
| K209 | 47° 26.872' N | 15° 51.519' E | 615 m | HS | | |
| K210 | 47° 22.211' N | 15° 52.491' E | 795 m | HS | | |
| K211 | 47° 21.592' N | 15° 54.069' E | 967 m | HS | | |
| K212 | 47° 18.719' N | 15° 44.087' E | 1109 m | M | | |

| | | | | | | |
|------|----------------|----------------|--------|----|----------------|------------|
| K213 | 47° 28.505' N | 15° 47.456' E | 924 m | HS | | |
| K214 | 47° 19.278' N | 15° 50.326' E | 542 m | HS | | |
| K215 | 47° 19.741' N | 15° 51.236' E | 668 m | HS | | |
| K216 | 47° 21.090' N | 15° 51.536' E | 1015 m | HS | | |
| K217 | 47° 26.328' N | 15° 48.206' E | 810 m | HS | | |
| K218 | 47° 21.485' N | 15° 49.890' E | 775 m | HS | | |
| K219 | 47° 23.138' N | 15° 51.146' E | 729 m | HS | | |
| K220 | 47° 26.315' N | 15° 57.765' E | 730 m | HS | | |
| K221 | 47° 24.061' N | 15° 54.245' E | 678 m | HS | | |
| K222 | 47° 24.040' N | 15° 54.210' E | 676 m | HS | | |
| K223 | 47° 24.030' N | 15° 54.210' E | 675 m | HS | | |
| K224 | 47° 24.050' N | 15° 54.168' E | 679 m | HS | | |
| K225 | 47° 24.035' N | 15° 54.138' E | 677 m | HS | | |
| K226 | 47° 24.770' N | 15° 54.118' E | 690 m | HS | | |
| K227 | 47° 22.995' N | 15° 50.838' E | 764 m | M | | |
| K228 | 47° 25.306' N | 15° 44.723' E | 1024 m | HS | | |
| K229 | 47° 25.620' N | 15° 44.630' E | 1050 m | M | | |
| K230 | 47° 24.836' N | 15° 52.345' E | 770 m | HS | | |
| K231 | 47° 23.326' N | 15° 48.765' E | 802 m | M | | |
| K232 | 47° 23.231' N | 15° 48.811' E | 795 m | HS | 2 Holed Stones | |
| K233 | 47° 23.888' N | 15° 49.131' E | 757 m | HS | | |
| K234 | 47° 24.528' N | 15° 54.356' E | 669 m | HS | | |
| K235 | 47° 24.420' N | 15° 47.096' E | 953 m | HS | | |
| K236 | 47° 22.636' N | 15° 46.795' E | 957 m | M | | |
| K237 | 47° 22.535' N | 15° 54.710' E | 747 m | HS | | |
| K238 | 47° 22.966' N | 15° 46.043' E | 949 m | HS | | |
| K239 | 47° 22.911' N | 15° 46.043' E | 958 m | HS | | |
| K240 | 47° 22.911' N | 15° 46.043' E | 958 m | HS | | |
| K241 | 47° 20.468' N | 15° 53.865' E | 938 m | M | | |
| K242 | 47° 24.736' N | 15° 54.023' E | 675 m | HS | | |
| K243 | 47° 18.006' N | 15° 42.948' E | 824 m | HS | | |
| K244 | 47° 15.486' N | 15° 44.481' E | 614 m | HS | | |
| K245 | 47° 16.838' N | 15° 45.765' E | 980 m | HS | | |
| K246 | 47° 22.908' N | 15° 52.971' E | 742 m | HS | | |
| K247 | 47° 22.358' N | 15° 54.656' E | 748 m | M | | |
| K248 | 47° 22.420' N | 15° 54.265' E | 819 m | HS | | |
| K249 | 47° 24.976' N | 15° 58.435' E | 599 m | HS | | |
| K250 | 47° 23.820' N | 15° 53.398' E | 621 m | HS | 6 Holed Stones | |
| K251 | 47° 26.802' N | 15° 58.435' E | 794 m | HS | | |
| L1 | 47° 25.352' N | 15° 51.279' E | 959 m | M | | 50*73*8 |
| L2 | 47° 24.386' N | 15° 52.288' E | 744 m | HS | | 60*110*17 |
| L3 | 47° 24.357' N | 15° 52.320' E | 736 m | HS | | 69*140*23 |
| L4 | 47° 26.321' N | 15° 52.483' E | 851 m | HS | | 47*157*23 |
| L5 | 47° 26.161' N | 15° 52.731' E | 874 m | HS | | 66*140*23 |
| L6 | 47° 25.752' N | 15° 52.996' E | 848 m | HS | | 80*157*17 |

| | | | | | | |
|------|-----------------|------------------|--------|----|--|----------------|
| L7 | 47° 25.771' N | 15° 52.955' E | 855 m | HS | | 26*152*28 |
| L8 | 47° 25.180' N | 15° 53.013' E | 776 m | HS | | 41*130*27 |
| L9 | 47° 25.087' N | 15° 52.995' E | 764 m | HS | | 51*145*10 |
| L10 | 47° 25.221' N | 15° 53.980' E | 722 m | M | | 40*88*16 |
| L11 | 47° 26.926' N | 15° 51.546' E | 601 m | HS | | 60*153*30 |
| L12 | 47° 24.695' N | 15° 50.384' E | 919 m | M | | 42*66*22 |
| L13 | 47° 24.874' N | 15° 50.820' E | 950 m | M | | 71*73*11 |
| L14 | 47° 24.410' N | 15° 50.837' E | 835 m | M | | |
| L15 | 47° 24.416' N | 15° 50.849' E | 840 m | HS | | 71*223*14 |
| L16 | 47° 24.008' N | 15° 51.240' E | 770 m | HS | | 48*124*25 |
| L17 | 47° 24.634' N | 15° 50.632' E | 895 m | M | | 48*94*28 |
| L18 | 47° 23.809' N | 15° 50.297' E | 872 m | M | | 56*57*16 |
| St1 | 47° 24.725' N | 15° 55.794' E | 623 m | HS | | 35.5*220*26.5 |
| St2 | 47° 24.700' N | 15° 55.451' E | 642 m | HS | | 69*158*17 |
| St3 | 47° 24.990' N | 15° 55.369' E | 631 m | M | | 42*92*13 |
| St4 | 47° 24.793' N | 15° 55.083' E | | M | | 82*154*19 |
| St5 | 47° 25.134' N | 15° 55.775' E | 635 m | HS | | 46*140*13.5 |
| St6 | 47° 25.172' N | 15° 55.723' E | 636 m | M | | 41*96*21.5 |
| St7 | 47° 25.075' N | 15° 55.611' E | 620 m | HS | | 60*227.5*15 |
| St8 | 47° 25.068' N | 15° 55.595' E | 618 m | HS | | 76*147*28 |
| St9 | 47° 25.099' N | 15° 55.533' E | 624 m | HS | | 50*120.5*21 |
| St10 | 47° 25.164' N | 15° 55.569' E | 632 m | M | | 42*118*16.5 |
| St11 | 47° 25.232' N | 15° 55.612' E | 640 m | HS | | 55.5*157*23 |
| St12 | 47° 25.274' N | 15° 55.570' E | | HS | | 37*75.5*17 |
| St13 | 47° 24.830' N | 15° 55.674' E | 624 m | HS | | 53*139*23.5 |
| St14 | 47° 24.784' N | 15° 55.633' E | 640 m | HS | | 22*176*21 |
| St15 | 47° 24.786' N | 15° 55.632' E | 637 m | M | | |
| St16 | 47° 25.414' N | 15° 56.269' E | 662 m | HS | | 69*140*19 |
| St17 | 47° 25.442' N | 15° 56.207' E | 660 m | HS | | 64*138*15 |
| St18 | 47° 25.537' N | 15° 55.693' E | 682 m | HS | | 45*231*15 |
| St19 | 47° 25.524' N | 15° 55.713' E | 680 m | HS | | 32*114*23 |
| St20 | 47° 25.528' N | 15° 55.692' E | 682 m | HS | | 55*98*17.5 |
| St21 | 47° 25.503' N | 15° 55.665' E | 682 m | HS | | 33*123*21.5 |
| St22 | 47° 25.521' N | 15° 55.628' E | 682 m | HS | | 50*175*16.5 |
| St23 | 47° 25.540' N | 15° 55.636' E | 684 m | HS | | 42*111*27 |
| St24 | 47° 25.714' N | 15° 55.450' E | 713 m | HS | | 61*122*21.5 |
| St25 | 47° 25.643' N | 15° 55.234' E | 706 m | HS | | 70*169*19.5 |
| St26 | 47° 25.352' N | 15° 55.337' E | 682 m | HS | | 30*143*26 |
| St27 | 47° 25.319' N | 15° 55.525' E | 662 m | HS | | 65*195*12 |
| St28 | 47° 25.362' N | 15° 55.058' E | 694 m | HS | | 52*196*28.5 |
| St29 | 47° 25.655' N | 15° 54.682' E | 702 m | HS | | 75.5*88*20 |
| St30 | 47° 25.630' N | 15° 54.599' E | 697 m | M | | |
| St31 | 47° 25.760' N | 15° 54.368' E | 696 m | HS | | 29*77*16 |
| St32 | 47° 25.746' N | 15° 54.216' E | 705 m | HS | | 55*91*21.5 |
| St33 | 47° 25.729' N | 15° 54.218' E | 705 m | HS | | 62*160*20 |

| St34 | 47° 25.271' N | 15° 54.223' E | 701 m | HS | | 76*143*17 |
| St35 | 47° 24.970' N | 15° 54.671' E | 653 m | HS | | 57*207*21 |
| St36 | 47° 24.862' N | 15° 54.031' E | 693 m | HS | | 86*172*17 |
| St37 | 47° 24.770' N | 15° 53.968' E | 685 m | HS | | 43*113*15 |
| St38 | 47° 24.770' N | 15° 54.129' E | 686 m | HS | | 50*123*34 |
| St39 | 47° 24.770' N | 15° 54.124' E | 686 m | HS | | 60*141*28 |
| St40 | 47° 24.772' N | 15° 54.121' E | 686 m | HS | | 19*115*23 |
| St41 | 47° 24.765' N | 15° 54.123' E | 693 m | M | | |
| St42 | 47° 24.759' N | 15° 54.099' E | 697 m | M | | 30*47*13 |
| St43 | 47° 24.828' N | 15° 54.244' E | 678 m | HS | | 61*133*24 |
| St44 | 47° 24.749' N | 15° 54.249' E | 676 m | HS | | 47*123.5*34 |
| St45 | 47° 24.748' N | 15° 54.246' E | 677 m | HS | | 44*110*30.5 |
| St46 | 47° 24.705' N | 15° 54.073' E | 685 m | HS | | 71*116.5*18.5 |
| St47 | 47° 24.607' N | 15° 54.229' E | 677 m | M | | |
| St48 | 47° 24.607' N | 15° 54.225' E | 677 m | HS | | 42*223*19 |
| St49 | 47° 24.605' N | 15° 54.248' E | 679 m | HS | | 55.5*166*19 |
| St50 | 47° 24.589' N | 15° 54.054' E | 683 m | HS | | 52.5*173*12 |
| St51 | 47° 24.527' N | 15° 54.986' E | 657 m | M | | |
| St52 | 47° 24.512' N | 15° 55.052' E | 657 m | HS | | 71*223*18 |
| St53 | 47° 24.627' N | 15° 54.384' E | 677 m | HS | | 48.5*146*16 |
| St54 | 47° 24.572' N | 15° 53.923' E | 669 m | HS | | 66*160.5*21 |
| St55 | 47° 24.534' N | 15° 53.974' E | 666 m | HS | | 56*168.5*28.5 |
| St56 | 47° 24.518' N | 15° 53.992' E | 666 m | HS | | 66.5*180*21.5 |
| St57 | 47° 24.366' N | 15° 53.776' E | 675 m | HS | | 36.5*129.5*26.5 |
| St58 | 47° 24.322' N | 15° 53.874' E | 677  m | M | | 24.5*78.5*18.5 |
| St59 | 47° 24.287' N | 15° 53.939' E | 677 m | HS | | 39.5*100*19 |
| St60 | 47° 24.130' N | 15° 54.261' E | 683 m | M | | 40*75*20.5 |
| St61 | 47° 24.062' N | 15° 54.245' E | 680 m | HS | | 37.5*126*20.5 |
| St62 | 47° 24.040' N | 15° 54.208' E | 679 m | HS | | 56*73.5*8 |
| St63 | 47° 24.031' N | 15° 54.210' E | 677 m | M | | |
| St64 | 47° 24.051' N | 15° 54.158' E | | HS | | 42*139.5*13 |
| St65 | 47° 24.034' N | 15° 54.140' E | | HS | | 36*157*13.5 |
| St66 | 47° 24.080' N | 15° 54.505' E | 681 m | HS | | 46.5*131*21 |
| St67 | 47° 24.070' N | 15° 54.506' E | 681 m | M | | 25.5*124 |
| St68 | 47° 23.984' N | 15° 54.535' E | 671 m | HS | | 78*139*23 |
| St69 | 47° 24.943' N | 15° 54.679' E | 663 m | HS | | 52*101*11 |
| St70 | 47° 24.934' N | 15° 53.886' E | 700 m | HS | | 69*123*26 |
| St71 | 47° 24.982' N | 15° 53.900' E | 708 m | HS | | 61.5*197*26.5 |
| St72 | 47° 25.973' N | 15° 53.709' E | 777 m | M | | 60*96*10 |
| St73 | 47° 25.985' N | 15° 53.265' E | 817 m | HS | | 72*132*12.5 |
| St74 | 47° 26.164' N | 15° 53.201' E | 830m | M | | 87*180*14 |
| Sp1 | 47° 21.921' N | 15° 50.701' E | 840 m | HS | | 81*113*18.5 |
| Sp2 | 47° 22.648' N | 15° 50.572' E | 784 m | HS | | 91*136*20.5 |
| Sp3 | 47° 24.011' N | 15° 51.232' E | 759 m | HS | | 46.5*129*16 |
| Sp4 | 47° 23.702' N | 15° 51.351' E | 734 m | M | | 45.5*84.5*34 |

| | | | | | | |
|------|----------------|----------------|-------|------|---|----------------|
| Sp5  | 47° 23.210' N  | 15° 48.956' E  | 865 m | M    |   |                |
| Sp6  | 47° 23.212' N  | 15° 48.941' E  | 865 m | M    |   | 47.5*109*34    |
| Sp7  | 47° 22.884' N  | 15° 49.552' E  | 960 m | HS   |   | 61.5*119*14.5  |
| Sp8  | 47° 22.891' N  | 15° 49.642' E  | 950 m | HS   |   | 48*134*17.5    |
| Sp9  | 47° 22.646' N  | 15° 49.764' E  | 937 m | HS   |   | 46*145*14      |
| Sp10 | 47° 24.085' N  | 15° 53.137' E  |       | M    |   |                |
| Sp11 | 47° 24.163' N  | 15° 51.442' E  | 746 m | HS   |   | 36*146*26      |
| Sp12 | 47° 24.152' N  | 15° 51.484' E  | 729 m | HS   |   |                |
| Sp13 | 47° 23.889' N  | 15° 51.111' E  | 777 m | M    |   |                |
| Sp14 | 47° 23.864' N  | 15° 50.815' E  | 814 m | M    |   |                |
| Sp15 | 47° 23.798' N  | 15° 51.372' E  | 749 m | HS   |   | 73*78*11       |
| Sp16 | 47° 23.776' N  | 15° 51.368' E  | 749 m | M    |   | 66*70*11       |
| Sp17 | 47° 23.019' N  | 15° 48.943' E  | 894 m | M    |   | 46.5*91*27.5   |
| Sp18 | 47° 22.779' N  | 15° 52.075' E  | 728 m | HS   |   | 74*146*17      |
| Sp19 | 47° 22.996' N  | 15° 50.839' E  | 748 m | HS   |   | 23*96*22       |
| Sp20 | 47° 23.451' N  | 15° 53.239' E  | 780 m | HS   |   | 80*123.5*20.5  |
| Sp21 | 47° 23.379' N  | 15° 53.479' E  | 799m  | HS   |   | 32*129*24.5    |
| Sp22 | 47° 23.402' N  | 15° 53.529' E  | 764 m | HS   |   | 43*114*24.5    |
| Sp23 | 47° 23.401' N  | 15° 53.531' E  | 769 m | HS   |   | 49*111*19      |
| Sp24 | 47° 23.396' N  | 15° 53.533' E  | 769 m | HS   |   | 40*60*11.5     |
| Sp25 | 47° 23.395' N  | 15° 53.532' E  | 769 m | HS   |   | 45*74*13       |
| Sp26 | 47° 23.390' N  | 15° 53.524' E  | 773 m | HS   |   | 48*130*12      |
| Sp27 | 47° 23.391' N  | 15° 53.526' E  | 771 m | HS   |   | 46*86*20       |
| Sp28 | 47° 23.396' N  | 15° 53.515' E  | 785 m | HS   |   | 49*133*18.5    |
| Sp29 | 47° 23.401' N  | 15° 53.513' E  | 779 m | HS   |   | 61*125*11.5    |
| Sp30 | 47° 23.404' N  | 15° 53.510' E  | 779 m | HS   |   | 37.5*97*12.5   |
| Sp31 | 47° 23.403' N  | 15° 53.510' E  | 779 m | HS   |   | 47*115*17      |
| Sp32 | 47° 23.403' N  | 15° 53.510' E  | 783 m | HS   |   | 55*86.5*14     |
| Sp33 | 47° 23.416' N  | 15° 53.496' E  | 784 m | M    |   | 46*117.5*10    |
| Sp34 | 47° 23.417' N  | 15° 53.495' E  | 784 m | HS   |   | 41*161*29      |
| Sp35 | 47° 23.369' N  | 15° 53.522' E  | 794 m | HS   |   | 76*134*19.5    |
| Sp36 | 47° 23.335' N  | 15° 53.515' E  | 793 m | HS   |   | 86*190*17.5    |
| Sp37 | 47° 23.350' N  | 15° 53.491' E  | 794 m | HS   |   | 60*151*35      |
| Sp38 | 47° 22.090' N  | 15° 52.464' E  | 837 m | HS   |   | 52*112*20      |
| W1   | 47° 22.906' N  | 15° 52.984' E  | 790 m | HS   |   |                |
| W2   | 47° 22.422' N  | 15° 54.265' E  | 819 m | HS   |   |                |
| W3   | 47° 22.359' N  | 15° 54.655' E  | 749 m | HS   |   |                |
| W4   | 47° 24.842' N  | 15° 49.097' E  | 805 m | HS   |   | 123*63*15      |
| W5   | 47° 24.830' N  | 15° 49.162' E  | 803 m | HS   |   | 198*64*21      |
| W6   | 47° 24.040' N  | 15° 49.513' E  | 795 m | HS   |   | 197*66*24      |
| W7   | 47° 24.055' N  | 15° 50.001' E  | 818 m | HS   |   | 67*35*17       |
| W8   | 47° 25.204' N  | 15° 50.754' E  | 979 m | HS   |   | 30*40*17       |
| W9   | 47° 25.329' N  | 15° 49.944' E  | 870 m | HS   |   | 98*49*16       |
| W10  | 47° 23.239' N  | 15° 52.587' E  | 738 m | HS   |   | 133*60*16      |
| W11  | 47° 23.271' N  | 15° 52.901' E  | 730 m | HS   |   | 120*40*15      |

| | | | | | | |
|---|---|---|---|---|---|---|
| W12 | 47° 23.261' N | 15° 52.908' E | 734 m | HS | | 150*40*28 |
| W13 | 47° 23.303' N | 15° 52.892' E | 734 m | M | | 40*34*7 |
| W14 | 47° 23.155' N | 15° 52.459' E | 720 m | M | | 20*18*11 |
| W15 | 47° 24.977' N | 15° 55.587' E | 597 m | HS | | 112*31*22 |
| W16 | 47° 24.958' N | 15° 54.147' E | 685 m | HS | | 118*63*33 |
| W17 | 47° 25.018' N | 15° 54.377' E | 670 m | HS | | 114*39*25 |
| W18 | 47° 24.919' N | 15° 54.423' E | 638 m | HS | | 137*55*18 |
| W19 | 47° 24.860' N | 15° 54.302' E | 660 m | HS | | 120*35*23 |
| W20 | 47° 24.827' N | 15° 54.244' E | 669 m | HS | | 120*43*26 |
| W21 | 47° 24.751' N | 15° 54.253' E | 677 m | HS | | 120*33*26 |
| W22 | 47° 24.749' N | 15° 54.249' E | 677 m | HS | | 113*33*26 |
| W23 | 47° 24.714' N | 15° 54.140' E | 686 m | HS | | 125*55*29 |
| W24 | 47° 24.603' N | 15° 54.247' E | 677 m | HS | | 180*50*17 |
| W25 | 47° 25.066' N | 15° 55.079' E | 649 m | HS | | 80*50*12 |
| B1 | 47° 27.444' N | 15° 67.916' E | | M | | |
| B2 | 47° 24.027' N | 15° 71.527' E | | M | | |
| B3 | 47° 30.361' N | 15° 72.250' E | | M | | |
| B4 | 47° 28.888' N | 15° 73.944' E | | M | | |
| B5 | 47° 25.805' N | 15° 74.138' E | | M | | |
| B6 | 47° 27.194' N | 15° 76.083' E | | M | | |
| B7 | 47° 28.111' N | 15° 76.250' E | | M | | |
| B8 | 47° 25.555' N | 15° 75.138' E | | M | | |

**Figure 48: Chart of Menhirs and Holed Stones**.

## 11.2 The "Schwarzer Stein" of Klosterneuburg

### 11.2.1 Origin of the stone

This "Schwarzer Stein" is one of three special stones, which were found during excavation works at the 12 Apostel Zeche in Klosterneuburg. This stones were packed in wooden crates and buried among many tons of rock in a side corridor. They are even mentioned in a transcript from the year 1580. The feature of this stones is their change of color if they get in contact with sun light and/or heat or if they get touched with the hand (KUSCH and KUSCH 2014)

### 11.2.2 Analyses

To get an idea of the mineral and element composition some analysis like thin section and RFA were made.

### 11.2.3 Thin section

This sample has a microgranulitic texture. It consists of a fine grained siliciclastic matrix with larger grains and ledges. These larger minerals are mainly plagioclase, pyroxene, biotite and some opaque phases. The plagioclase shows typical twinnings and chemical zonal structures (Fig. 49). Especially the pyroxenes and the biotite show signs of an alteration. Some mineral grains even have fretting grain boundaries.
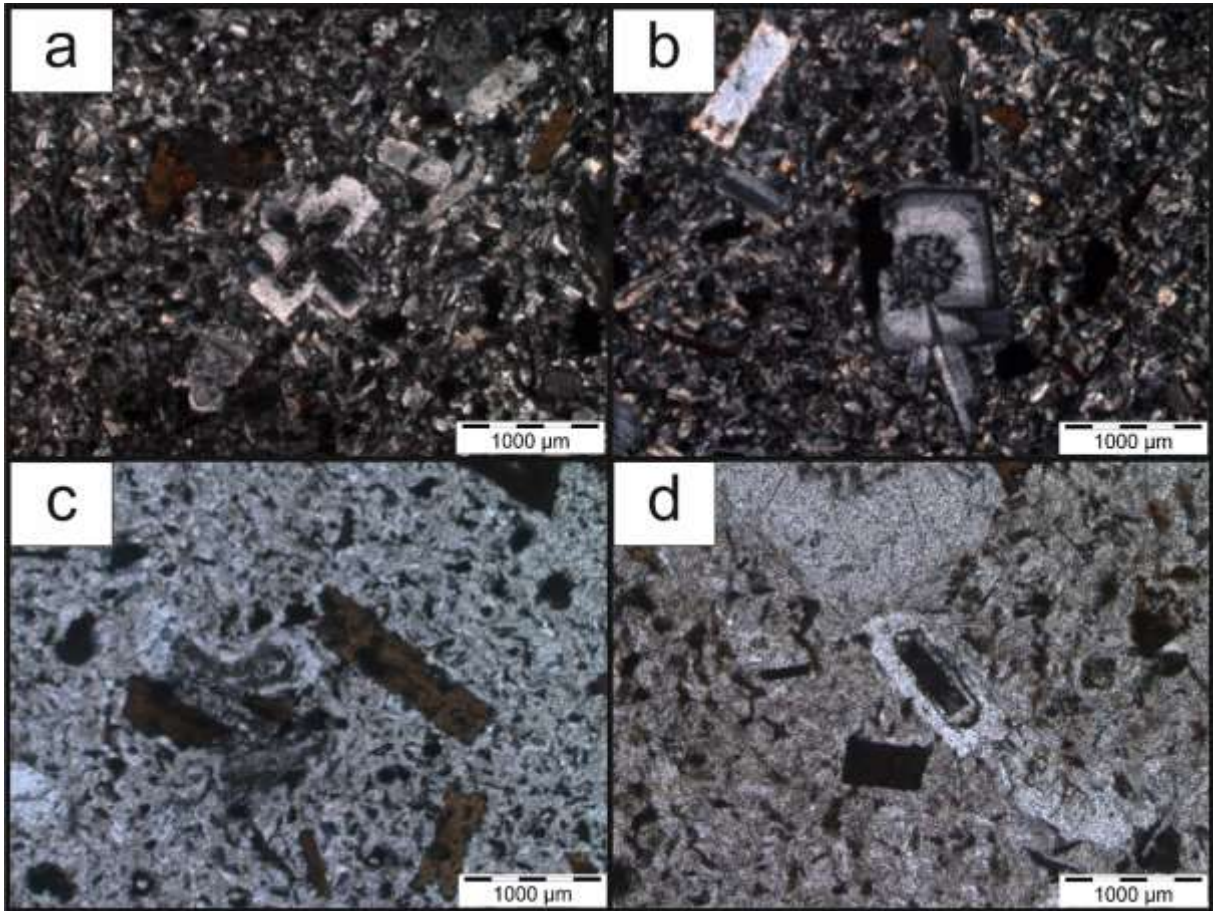
Figure 49: pictures of the thin section made from the "Schwarzer Stein"; a) A big Plagioclase cross in the middle of the sample. Furthermore, some Pyroxene and Biotite grains can be found in the siliciclastic matrix. Photo taken with crossed-polarized illumination b) A big Plagioclase grain with pronounced chemical zoning in the middle of the sample. Furthermore, some Plagioclase grains with typical twinnings. The photo was taken with crossed-polarized illumination. c) Some altered Pyroxene and Biotite grains with fretting grain boundaries. d) An altered Plagioclase grain in the siliciclastic matrix. Furthermore, some opaque phases.

## 11.2.4 RFA

A small piece of the sample was powdered and then melted to a fusion tablet with the TYP Vulcan XM, which was analyzed with the S4 Pioneer from Bruker AXS Inc. The results represent the whole rock composition (Fig.48). Some minor and trace elements like copper, Nickel and Uranium only appeared under the quantification limit, so they are irrelevant. The rock is mainly build up by $SiO_2$ (63.44 %), $Al_2O_3$ (16.18 %), $K_2O$ (4.91 %) and $Na_2O$ (3.68 %) (Fig. 50). Some trace Elements like Ba (1055.6ppm), Sr (444 ppm), Zr (305 ppm) and Rb (220 ppm) have relatively high content.

| $SiO_2$ | $Al_2O_3$ | $Fe_2O_3$ | MnO | MgO | CaO | $Na_2O$ |
|---|---|---|---|---|---|---|
| 88.1 KCps | 23.4 KCps | 65.2 KCps | 2.8 KCps | 2.9 KCps | 22.6 KCps | 3.3 KCps |
| 63.44 % | 16.18 % | 4.73 % | 0.078 % | 1.40 % | 2.97 % | 3.68 % |
| $K_2O$ | $TiO_2$ | $P_2O_5$ | Sum | | | |
| 38.2 KCps | 5.1 KCps | 1.4 KCps | | | LOI= 0.68 % | |
| 4.91 % | 0.58 % | 0.192 % | 99.19 % | | | |
| Ba | Ce | Cr | Cs | Ga | Nd | Pb |
| 0.5 KCps | 0.0 KCps | 0.5 KCps | 0.0 KCps | 0.6 KCps | 0.0 KCps | 0.6 KCps |
| 1055.6 ppm | 99 ppm | 27 ppm | 34 ppm | 25 ppm | 42 ppm | 64 ppm |
| Rb | Sr | Th | V | Zn | Zr | |
| 10.5 KCps | 23.5 KCps | 0.6 KCps | 0.2 KCps | 1.6 KCps | 4.2 KCps | |
| 220 ppm | 444 ppm | 38 ppm | 38 ppm | 39 ppm | 305 ppm | |

Figure 50: Whole rock composition of the "Schwarzer Stein".

### 11.2.5 Interpretation

The mineral and chemical composition and the structure point to a felsic volcanic or dyke rock. The plotted results of the RFA Analyses show that the rock has the whole rock composition of Trachyte (Fig. 49). The origin could be the nearer surrounding. To get a real idea about the reason of the color change much more analyses are necessary. This would get far beyond my work. But hopefully the future will bring clearness into this mystery.
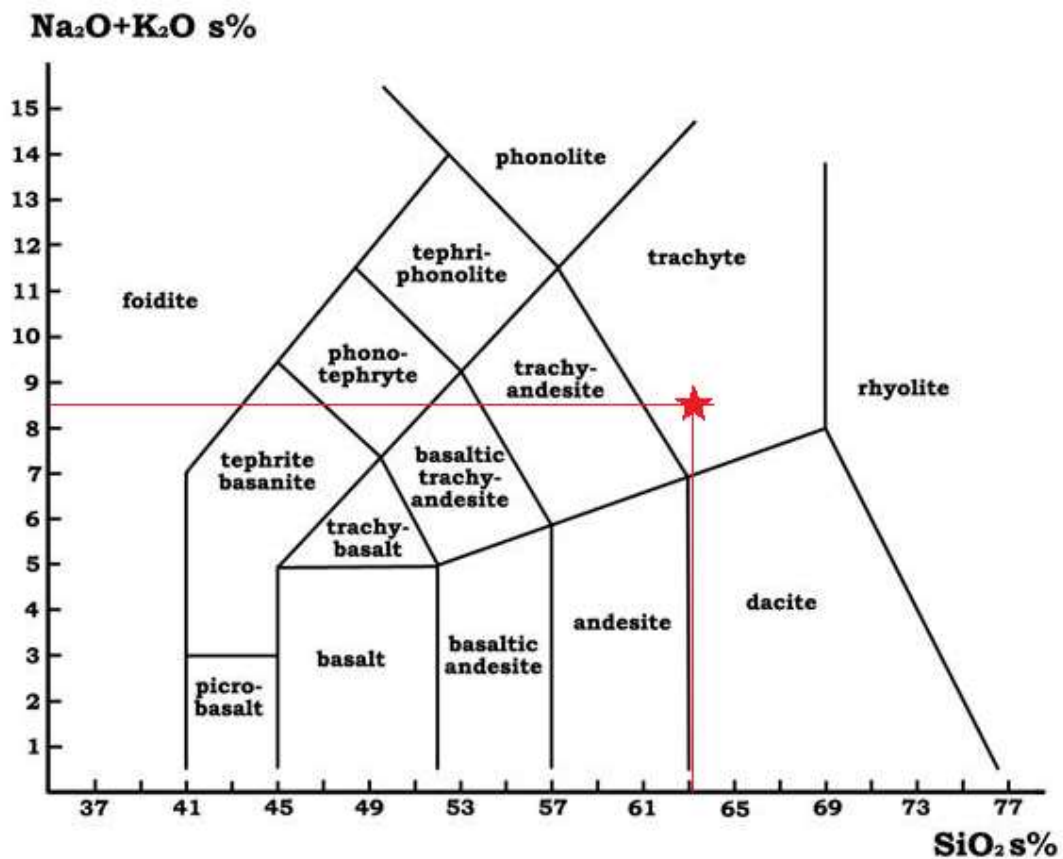


Figure 51: RFA result plotted into a TAS diagram; modified after
http://www.tankonyvtar.hu/hu/tartalom/tamop425/0038_foldrajz_mineralogy_Da/ch01s11.html.

## 11.3 Mineral Analyses

| Sample | Sample 2 | Sample 2 | Sample 2 | Sample 3 | Sample 3 | Sample 3 |
|---|---|---|---|---|---|---|
| Mineral | am1 | am2 | am3 | am1 | am2 | am3 |
| | | | | | | |
| SiO2 | 43.57 | 42.69 | 43.59 | 44.37 | 42.45 | 43.68 |
| TiO2 | 0.37 | 0.48 | 0.35 | 0.29 | 0.39 | 0.37 |
| Al2O3 | 15.39 | 15.06 | 14.25 | 13.17 | 15.68 | 14.51 |
| Cr2O3 | 0.00 | 0.00 | 0.00 | 0.00 | 0.00 | 0.00 |
| FeO | 16.74 | 16.58 | 16.40 | 15.53 | 15.90 | 15.35 |
| MnO | 0.09 | 0.15 | 0.17 | 0.06 | 0.13 | 0.09 |
| MgO | 7.66 | 7.85 | 7.83 | 9.11 | 8.39 | 7.87 |
| CaO | 9.56 | 9.76 | 9.53 | 9.75 | 10.26 | 9.89 |
| Na2O | 2.11 | 2.18 | 2.15 | 2.17 | 2.01 | 2.13 |
| K2O | 0.50 | 0.48 | 0.45 | 0.35 | 0.44 | 0.47 |
| F | 0.29 | 0.28 | 0.33 | 0.32 | 0.27 | 0.18 |
| Cl | 0.00 | 0.00 | 0.00 | 0.00 | 0.00 | 0.00 |
| **Total** | **96.28** | **95.51** | **95.05** | **95.12** | **95.92** | **94.54** |
| | | | | | | |
| Si per 23 O | 6.49 | 6.43 | 6.58 | 6.66 | 6.35 | 6.61 |
| Ti | 0.04 | 0.05 | 0.04 | 0.03 | 0.04 | 0.04 |
| Al | 2.70 | 2.67 | 2.54 | 2.33 | 2.76 | 2.59 |
| Cr | 0.00 | 0.00 | 0.00 | 0.00 | 0.00 | 0.00 |
| Fe3+ | 0.43 | 0.44 | 0.40 | 0.41 | 0.45 | 0.25 |
| Fe2+ | 1.66 | 1.65 | 1.68 | 1.54 | 1.54 | 1.70 |
| Mn | 0.01 | 0.02 | 0.02 | 0.01 | 0.02 | 0.01 |
| Mg | 1.70 | 1.76 | 1.76 | 2.04 | 1.87 | 1.78 |
| Ca | 1.53 | 1.58 | 1.54 | 1.57 | 1.64 | 1.60 |
| Na | 0.61 | 0.64 | 0.63 | 0.63 | 0.58 | 0.63 |
| K | 0.10 | 0.09 | 0.09 | 0.07 | 0.08 | 0.09 |
| F | 0.14 | 0.13 | 0.16 | 0.15 | 0.13 | 0.09 |
| Cl | 0.00 | 0.00 | 0.00 | 0.00 | 0.00 | 0.00 |
| **Cations** | **15.39** | **15.46** | **15.43** | **15.44** | **15.47** | **15.38** |

Figure 52: Mineral Analyses of amphiboles used for the geothermobarometry in chapter 6.2..

| Sample | Sample 2 | Sample 2 | Sample 2 | Sample 3 | Sample 3 | Sample 3 | Sample 4 | Sample 4 | Sample 4 |
|---|---|---|---|---|---|---|---|---|---|
| Mineral | bt1 | bt2 | bt3 | bt1 | bt2 | bt3 | bt1 | bt2 | bt3 |
| | | | | | | | | | |
| SiO2 | 49.45 | 49.46 | 48.83 | 49.31 | 47.57 | 47.70 | 48.66 | 47.28 | 47.25 |
| TiO2 | 0.45 | 0.58 | 0.53 | 0.42 | 0.53 | 0.57 | 0.57 | 0.50 | 0.61 |
| Al2O3 | 30.68 | 31.66 | 31.00 | 31.55 | 31.14 | 32.04 | 32.12 | 31.04 | 30.46 |
| Cr2O3 | 0.00 | 0.00 | 0.00 | 0.00 | 0.00 | 0.00 | 0.00 | 0.00 | 0.00 |
| FeO | 2.36 | 2.16 | 2.40 | 2.54 | 2.42 | 2.33 | 1.98 | 2.66 | 2.48 |
| MnO | 0.03 | 0.08 | 0.03 | 0.01 | 0.03 | 0.08 | 0.05 | 0.07 | 0.05 |
| MgO | 2.16 | 2.52 | 2.25 | 2.17 | 1.69 | 1.74 | 2.10 | 2.03 | 2.02 |
| CaO | 0.02 | 0.04 | 0.01 | 0.01 | 0.00 | 0.06 | 0.06 | 0.09 | 0.23 |
| BaO | 0.00 | 0.00 | 0.00 | 0.00 | 0.00 | 0.00 | 0.00 | 0.00 | 0.00 |
| Na2O | 0.46 | 0.45 | 0.58 | 0.79 | 0.65 | 0.65 | 0.61 | 0.70 | 0.83 |
| K2O | 9.66 | 9.45 | 9.53 | 10.53 | 10.42 | 10.67 | 10.61 | 10.09 | 9.69 |
| F | 0.10 | 0.13 | 0.24 | 0.20 | 0.18 | 0.18 | 0.14 | 0.06 | 0.24 |
| Cl | 0.00 | 0.00 | 0.00 | 0.00 | 0.00 | 0.00 | 0.00 | 0.00 | 0.00 |
| **Total** | **95.37** | **96.53** | **95.40** | **97.53** | **94.63** | **96.02** | **96.90** | **94.52** | **93.86** |
| | | | | | | | | | |
| Si per 11 O | 3.28 | 3.24 | 3.25 | 3.23 | 3.21 | 3.18 | 3.20 | 3.20 | 3.22 |
| Ti | 0.02 | 0.03 | 0.03 | 0.02 | 0.03 | 0.03 | 0.03 | 0.03 | 0.03 |
| Al | 2.40 | 2.45 | 2.43 | 2.44 | 2.48 | 2.52 | 2.49 | 2.47 | 2.44 |
| Cr | 0.00 | 0.00 | 0.00 | 0.00 | 0.00 | 0.00 | 0.00 | 0.00 | 0.00 |
| Fe3+ | 0.00 | 0.00 | 0.00 | 0.00 | 0.00 | 0.00 | 0.00 | 0.00 | 0.00 |
| Fe2+ | 0.13 | 0.12 | 0.13 | 0.14 | 0.14 | 0.13 | 0.11 | 0.15 | 0.14 |
| Mn | 0.00 | 0.00 | 0.00 | 0.00 | 0.00 | 0.01 | 0.00 | 0.00 | 0.00 |
| Mg | 0.21 | 0.25 | 0.22 | 0.21 | 0.17 | 0.17 | 0.21 | 0.21 | 0.21 |
| Ca | 0.00 | 0.00 | 0.00 | 0.00 | 0.00 | 0.00 | 0.00 | 0.01 | 0.02 |
| Ba | 0.00 | 0.00 | 0.00 | 0.00 | 0.00 | 0.00 | 0.00 | 0.00 | 0.00 |
| Na | 0.06 | 0.06 | 0.08 | 0.10 | 0.09 | 0.08 | 0.08 | 0.09 | 0.11 |
| K | 0.82 | 0.79 | 0.81 | 0.88 | 0.90 | 0.91 | 0.89 | 0.87 | 0.84 |
| F | 0.02 | 0.03 | 0.05 | 0.04 | 0.04 | 0.04 | 0.03 | 0.01 | 0.05 |
| Cl | 0.00 | 0.00 | 0.00 | 0.00 | 0.00 | 0.00 | 0.00 | 0.00 | 0.00 |
| **Cations** | **6.95** | **6.96** | **7.00** | **7.06** | **7.05** | **7.07** | **7.04** | **7.04** | **7.06** |
| | | | | | | | | | |
| XMg | 0.62 | 0.68 | 0.62 | 0.60 | 0.55 | 0.57 | 0.65 | 0.58 | 0.59 |

**Figure 53: Mineral Analyses of biotites used for the geothermobarometry in chapter 6.2..**

| Sample | Sample 2 | Sample 2 | Sample 2 | Sample 3 | Sample 3 | Sample 3 | Sample 4 | Sample 4 | Sample 4 |
|---|---|---|---|---|---|---|---|---|---|
| Mineral | gt1 | gt2 | gt3 | gt1 | gt2 | gt3 | gt1 | gt2 | gt3 |
| | | | | | | | | | |
| SiO2 | 36.65 | 36.45 | 36.50 | 37.79 | 37.69 | 37.50 | 36.92 | 37.40 | 37.43 |
| TiO2 | 0.08 | 0.10 | 0.07 | 0.03 | 0.03 | 0.01 | 0.05 | 0.05 | 0.00 |
| Al2O3 | 20.48 | 20.89 | 20.23 | 21.25 | 21.04 | 21.33 | 21.34 | 20.73 | 20.58 |
| FeO | 34.38 | 28.61 | 29.10 | 32.91 | 33.89 | 31.77 | 34.33 | 28.37 | 29.12 |
| MnO | 2.27 | 1.29 | 1.81 | 0.99 | 1.31 | 1.30 | 1.97 | 1.53 | 1.11 |
| MgO | 2.52 | 8.75 | 8.49 | 3.77 | 3.32 | 2.48 | 3.24 | 1.56 | 1.54 |
| CaO | 2.08 | 1.66 | 1.21 | 3.43 | 2.63 | 4.72 | 2.12 | 8.94 | 8.30 |
| **Total** | **98.49** | **97.82** | **97.46** | **100.23** | **99.98** | **99.15** | **99.99** | **98.62** | **98.10** |
| | | | | | | | | | |
| Si per 12 O | 3.01 | 2.98 | 2.99 | 3.01 | 3.02 | 3.02 | 2.97 | 3.02 | 3.04 |
| Ti | 0.00 | 0.00 | 0.00 | 0.00 | 0.00 | 0.00 | 0.00 | 0.00 | 0.00 |
| Al | 2.00 | 2.02 | 1.99 | 1.99 | 1.99 | 2.02 | 2.02 | 1.97 | 1.97 |
| Fe3+ | 0.00 | 0.00 | 0.02 | 0.00 | 0.00 | 0.00 | 0.05 | 0.00 | 0.00 |
| Fe2+ | 2.26 | 2.40 | 2.43 | 2.18 | 2.27 | 2.14 | 2.26 | 1.92 | 1.98 |
| Mn | 0.30 | 0.23 | 0.18 | 0.07 | 0.09 | 0.09 | 0.13 | 0.11 | 0.08 |
| Mg | 0.16 | 0.16 | 0.22 | 0.45 | 0.40 | 0.30 | 0.39 | 0.19 | 0.19 |
| Ca | 0.27 | 0.19 | 0.16 | 0.29 | 0.23 | 0.41 | 0.18 | 0.77 | 0.72 |
| **Cations** | **7.99** | **7.97** | **7.99** | **7.99** | **7.98** | **7.97** | **8.00** | **7.98** | **7.97** |
| | | | | | | | | | |
| Xgrs | 0.05 | 0.05 | 0.07 | 0.15 | 0.13 | 0.10 | 0.13 | 0.06 | 0.06 |
| Xalm | 0.76 | 0.81 | 0.81 | 0.73 | 0.76 | 0.73 | 0.76 | 0.64 | 0.67 |
| Xsps | 0.10 | 0.08 | 0.06 | 0.02 | 0.03 | 0.03 | 0.05 | 0.04 | 0.03 |
| Xprp | 0.09 | 0.06 | 0.05 | 0.10 | 0.08 | 0.14 | 0.06 | 0.26 | 0.24 |
| XFe | 0.89 | 0.93 | 0.94 | 0.88 | 0.91 | 0.84 | 0.93 | 0.71 | 0.73 |

Figure 54: Mineral Analyses of garnets used for the geothermobarometry in chapter 6.2..

| Sample | Sample 2 | Sample 2 | Sample 2 | Sample 3 | Sample 3 | Sample 3 | Sample 4 | Sample 4 | Sample 4 |
|---|---|---|---|---|---|---|---|---|---|
| Mineral | pl1 | pl2 | pl3 | pl1 | pl2 | pl3 | pl1 | pl2 | pl3 |
| | | | | | | | | | |
| SiO2 | 69.89 | 69.73 | 70.46 | 70.20 | 69.08 | 67.69 | 69.24 | 70.47 | 70.51 |
| TiO2 | 0.01 | 0.02 | 0.08 | 0.01 | 0.06 | 0.00 | 0.03 | 0.03 | 0.07 |
| Al2O3 | 19.81 | 19.75 | 20.40 | 20.11 | 20.08 | 19.40 | 20.34 | 20.39 | 20.69 |
| Fe2O3 | 0.23 | 0.22 | 0.06 | 0.38 | 0.31 | 0.27 | 0.28 | 0.26 | 0.15 |
| MnO | 0.05 | 0.03 | 0.01 | 0.02 | 0.08 | 0.02 | 0.00 | 0.04 | 0.01 |
| MgO | 0.00 | 0.26 | 0.13 | 0.34 | 0.25 | 0.24 | 0.09 | 0.12 | 0.13 |
| CaO | 0.25 | 0.30 | 0.17 | 0.37 | 0.25 | 0.28 | 0.50 | 0.25 | 0.35 |
| Na2O | 10.32 | 10.40 | 10.40 | 11.32 | 11.92 | 11.56 | 11.67 | 11.79 | 11.49 |
| K2O | 0.03 | 0.06 | 0.06 | 0.12 | 0.06 | 0.09 | 0.07 | 0.02 | 0.07 |
| **Total** | **100.67** | **100.82** | **101.91** | **102.87** | **102.09** | **99.55** | **102.22** | **103.37** | **103.47** |
| | | | | | | | | | |
| Si per 8/12.5 O | 3.02 | 3.01 | 3.00 | 2.98 | 2.97 | 2.98 | 2.97 | 2.98 | 2.98 |
| Ti | 0.00 | 0.00 | 0.00 | 0.00 | 0.00 | 0.00 | 0.00 | 0.00 | 0.00 |
| Al | 1.01 | 1.00 | 1.03 | 1.01 | 1.02 | 1.01 | 1.03 | 1.02 | 1.03 |
| Fe3+ | 0.01 | 0.01 | 0.00 | 0.01 | 0.01 | 0.01 | 0.01 | 0.01 | 0.01 |
| Mn | 0.00 | 0.00 | 0.00 | 0.00 | 0.00 | 0.00 | 0.00 | 0.00 | 0.00 |
| Mg | 0.00 | 0.02 | 0.01 | 0.02 | 0.02 | 0.02 | 0.01 | 0.01 | 0.01 |
| Ca | 0.01 | 0.01 | 0.01 | 0.02 | 0.01 | 0.01 | 0.02 | 0.01 | 0.02 |
| Na | 0.86 | 0.87 | 0.86 | 0.93 | 0.99 | 0.99 | 0.97 | 0.97 | 0.94 |
| K | 0.00 | 0.00 | 0.00 | 0.01 | 0.00 | 0.01 | 0.00 | 0.00 | 0.00 |
| **Cations** | **4.91** | **4.92** | **4.91** | **4.98** | **5.02** | **5.01** | **5.00** | **4.99** | **4.98** |
| | | | | | | | | | |
| Xab | 0.46 | 0.46 | 0.46 | 0.48 | 0.49 | 0.49 | 0.48 | 0.49 | 0.48 |
| Xan | 0.54 | 0.53 | 0.54 | 0.52 | 0.51 | 0.50 | 0.51 | 0.51 | 0.52 |
| Xkfs | 0.00 | 0.00 | 0.00 | 0.00 | 0.00 | 0.00 | 0.00 | 0.00 | 0.00 |

Figure 55: Mineral Analyses of plagioclases used for the geothermobarometry in chapter 6.2..